Contents of issue 3 vol. LVI

Engineering Transactions, T. **LVI**, nr 3, str. 185–308, Warszawa 2008

ENGINEERING TRANSACTIONS • *Engng. Trans.* • **56**, 3, 187–200, 2008
Polish Academy of Sciences • Institute of Fundamental Technological Research

VIBRATIONS OF TIMOSHENKO BEAMS ON TWO-PARAMETER ELASTIC SOIL

N. M. A u c i e l l o

Department of Structural Engineering
University of Basilicata
Via dell'Ateneo Lucano, 10 – 85100, Potenza, Italy

In this paper the influence of the two-parameter elastic soil on the dynamic behaviour of a beam with variable cross-section is examined, in the presence of conservative axial loads. The beams are assumed to follow the well-known Timoshenko hypotheses, in order to take into account both the rotary inertia and shear deformation effect. The Rayleigh–Ritz approach is used and Boundary Characteristic Orthogonal Polynomials are chosen as trial functions; (BCOPs method [2]). The theory is concisely presented in a matrix form, so that the contribution of the rotary inertia and of the soil can be easily recognized. Various examples and comparisons are illustrated, in order to emphasize the influence of the soil properties and of the beam taper ratio. Finally, the results are also compared with the results given by other authors, using exact and approximate approaches.

Notations

H	depth of soil,
A, A_o	cross-sectional area of beam; cross-sectional area of beam in $x_1 = 0$,
$\mathbf{K}_U$, $\mathbf{K}_w$, $\mathbf{K}_G$	matrices in Eqs. (3.7), (3.8), (3.9),
E, G	Young's modulus; shear modulus of beam,
I, I_o	area moment of inertia; area moment of inertia in $x_1 = 0$,
k	shear factor,
k_w, k_G	Winkler, first coefficient of the elastic soil; second coefficient,
$\mathbf{K}$, $\mathbf{M}$	stiffness matrix; mass matrix,
L	length of the beam,
N, P	axial force; non-dimensional parameter,
P_c	critical buckling load parameter,
$\mathbf{q}_1$, $\mathbf{q}_2$	vector coefficients of trial function in Eqs. (3.1), (3.2),
r	radius of inertia of the beam, Eq. (4.4),
$\mathbf{v}$, $\mathbf{R}$	vectors Eq. (2.8),
U, U_P	strain energy; energy of axial force,
u_1, u_2, u_3	displacements of beam,
Ω_i	i-th non-dimensional eigenfrequency of beam; Eq. (4.4),
$\mathbf{\Phi}$, $\mathbf{\Psi}$	shape functions,
α	thickness ratio; Eq. (4.1),
φ	rotation of the cross-section,
γ_S	shear deformation,

γ parameter of foundation; Eq. (2.13),
$\boldsymbol{\sigma}$, $\boldsymbol{\varepsilon}$ stress and strain vectors,
υ_S Poisson's coefficient,
ρ mass density,
λ_w, λ_G non-dimensional parameters of soil; Eq. (4.3),
ω_i natural frequency.

1. Introduction

Various engineering problems can be traced back to the dynamic analysis of beams on elastic soil, and quite frequently the soil behaviour is approximated by the well-known Winkler model, according to which the soil is viewed as a distribution of mutually independent axial springs, thus neglecting the shear-contributed load causing constant displacements, and consequently – no bending of the beam. This drawback can be eliminated by adopting more refined two-parameter elastic models, which take into account the shear properties of the soil. Both the classical Filonenko and Pasternak models define an additional soil parameter in order to simulate an interaction between the springs, whereas Vlasov [8] aims to consider the influence of the elastic medium depth. According to this theory, Vallabhan and Das [9] proposed a variational procedure, which leads to a simplified form of the second elastic soil parameter.

Most contributions to the dynamic analysis of beams on a two-parameter elastic soil refer to slender beams, so that the classical Euler–Bernoulli hypotheses are usually accepted. Quite recently, a finite element procedure for the free vibration frequencies of slender beams on the Vlasov soil has been proposed by Franciosi and Masi [6].

If the beam cannot considered to be slender, it is convenient to adopt the Timoshenko theory, which takes into account both the shear deformations and the rotary inertia of the beam, and what nevertheless leads to a manageable differential problem. An exact solution for stiffness matrix for a Timoshenko beam on Winkler soil has been given by Chen and Panteldes [3], taking into account the effects of the axial forces, whereas De Rosa [5] has given the free vibration frequencies of Timoshenko beams with constant cross-section, resting on a two-parameter elastic soil, using two different models of the second soil parameter.

Semi-analytical and numerical approaches are obviously not limited to beams with constant cross-section. In the finite element context, a four-node element has been proposed by Yokoyama [10], for Rayleigh and Timoshenko beams, and the same author, in a later paper [11], considered the effects of axial forces and different boundary conditions. Finally, a refined cubic-quintic element has been implemented by Bruno *et al.* [4].

A different approach has been used by Filipich and Rosales [7], according to which the Rayleigh quotient is optimized and the fundamental frequency can

be detected with great precision. On the other hand, the higher frequencies cannot be found whit sufficient accuracy.

In this paper we aim at a general method for estimation of the free vibration frequencies of Timoshenko beams with varying cross-section and non-classical boundary conditions, resting on varying two-parameter elastic soil. The analysis uses a variational Rayleigh-Ritz approach and sets of modified orthogonal polynomials, which can cope with different approximation degrees of displacements and rotations [2].

2. Formulation of the problem

Let us consider an isotropic beam with varying cross-section, resting on two-parameter elastic soil and subjected to a conservative axial load at the end. A Cartesian reference frame is x_1, x_2, x_3, such that x_1 becomes the beam axis, whereas x_2, x_3, are assumed to be the principal axes of the cross-section. If the Timoshenko model is assumed to be valid, then the displacements can be written as:

$$u_1 = -x_2\varphi(x_1,t), \qquad u_2 = u_2(x_1,t), \qquad u_3 = 0, \tag{2.1}$$

where $\varphi(x_1,t)$ is the rotation of the cross-section, which turns out to be different from the rotation θ of the neutral axis, so that the difference

$$\gamma_S = \frac{\partial u_2}{\partial x_1} - \varphi \tag{2.2}$$

gives the additional rotation due to the shear deformation.

According to (2.1), the strain components are given by:

$$\boldsymbol{\varepsilon} = \begin{bmatrix} -x_2 \dfrac{d\varphi}{dx_1} \\ \dfrac{du_2}{dx_1} - \varphi \end{bmatrix}. \tag{2.3}$$

If the derivative with respect to x_1 is written as an apex, the Hooke's law for isotropic material gives the corresponding stress components:

$$\boldsymbol{\sigma} = \mathbf{D}\boldsymbol{\varepsilon} = \begin{bmatrix} EI & 0 \\ 0 & GA \end{bmatrix} \begin{bmatrix} -x_2\varphi' \\ u_2' - \varphi \end{bmatrix} = \begin{bmatrix} -EI\, x_2\varphi' \\ kGA\,(u_2' - \varphi) \end{bmatrix}, \tag{2.4}$$

where A is the cross-sectional area, I is the moment of inertia, E is the Young's modulus, G is the shear modulus, and k is the shear factor.

The strain energy can be written as:

$$U = \frac{1}{2}\int_V \boldsymbol{\sigma}^T\boldsymbol{\varepsilon}\,dx_1 = \frac{1}{2}\int_V \boldsymbol{\varepsilon}^T\mathbf{D}\boldsymbol{\varepsilon}\,dx_1, \tag{2.5}$$

and using (2.3) and (2.4):

$$U = \frac{1}{2}\int_0^L \begin{bmatrix} -EI\varphi' \\ kGA(u_2' - \varphi) \end{bmatrix}^T \begin{bmatrix} -x_2\varphi' \\ u_2' - \varphi \end{bmatrix} dx_1 \tag{2.6}$$

$$= \frac{1}{2}\int_0^L \left[EI(\varphi')^2 + kGA(u_2' - \varphi)\right] dx_1,$$

after integration with respect to the cross-sectional area A.

The potential energy of the axial force N at the end is a quadratic function of the displacements, which can be written as:

$$U_P = \frac{N}{2}\int_0^L u_2' dx_1. \tag{2.7}$$

Finally, the kinetic energy of the system is equal to:

$$T = \frac{1}{2}\int_0^L \dot{\mathbf{v}}^T \mathbf{R}\, \dot{\mathbf{v}}\, dx_1, \tag{2.8}$$

where $\mathbf{v}$ and $\mathbf{R}$ are given by:

$$\mathbf{v} = \begin{bmatrix} u_2 \\ \varphi \end{bmatrix}, \tag{2.9}$$

$$\mathbf{R} = \begin{bmatrix} \rho A & 0 \\ 0 & \rho I \end{bmatrix}, \tag{2.10}$$

respectively, where ρ is the mass density of the beam.

From (2.8) it is possible to separate the variables, and the kinetic energy becomes

$$T = \frac{\omega^2}{2}\int_0^L \rho(u_2^2\, A + \varphi^2\, I)\, dx_1. \tag{2.11}$$

According to Winkler, the pressure at the generic point is linearly proportional to the corresponding displacement, but quite often this Winkler hypothesis cannot be considered to be valid and more refined pressure-displacement relationships must be accepted, as for example:

$$p(x_1) = k_w\, u_2 - k_G \frac{d^2 u_2}{dx_1^2}, \tag{2.12}$$

where the physical interpretation of the second parameter k_G varies according to the different model proposed. For example, the Filonenko–Borodich soil parameter k_G is the tensile force of an ideal membrane connecting the Winkler spring, whereas Pasternak assumes that the second parameter is equal to the shear force between the foundation and the soil.

A more refined model is considered by Vlasov, assuming that the foundation rests on an elastic half-plane, and some simplifying hypothesis allow us to express the second soil parameter as:

$$k_G = \gamma \frac{E_S}{(1+\upsilon_S)}, \tag{2.13}$$

where E_S is the elastic modulus of the soil, υ_S is the Poisson coefficient, and γ is a coefficient which depends on the foundation geometry. If E_S and υ_S are assumed to vary linearly with the depth H, a variational procedure, as suggested by Vallabhan and Das [9], gives a simple expression for the elastic soil parameters.

In any case, the strain energy of the soil can be calculated by using (2.12), and regardless of the particular model, it can be written as:

$$U_S = \int_0^L \left[k_w\, u_2^2 + k_G \left(\frac{d^2 u_2}{dx_1^2} \right)^2 \right] dx_1. \tag{2.14}$$

3. Approximate analytical solution

An approximate solution for the problem at hand can be obtained by assuming that the displacements u_2 and the rotations ϕ can be expressed as

$$\hat{u}_2(x_1) = \sum_{i=1}^{n} a_i \Phi_i = \mathbf{\Phi}^T \mathbf{q}_1, \tag{3.1}$$

$$\hat{\varphi}(x_1) = \sum_{i=1}^{n} b_i \Psi_i = \mathbf{\Psi}^T \mathbf{q}_2, \tag{3.2}$$

where $\mathbf{q}_1$ and $\mathbf{q}_2$ play the role of generalized coordinates, whereas Φ_i and Ψ_i are the shape functions which must obey the only geometric boundary conditions. If this expression are inserted into the strain energy formulae, then a discrete structural system is obtained, with a finite number of degrees of freedom. The strain energy (2.6) becomes:

$$U = \frac{1}{2}\int_0^L EI(\mathbf{q}_2^T \boldsymbol{\Psi}' \boldsymbol{\Psi}'^T \mathbf{q}_2) dx_1 = \frac{1}{2}\int_0^L kGA \left[\boldsymbol{\Phi}'^T \mathbf{q}_1 - \boldsymbol{\Psi}^T \mathbf{q}_2\right]^T \left[\boldsymbol{\Phi}'^T \mathbf{q}_1 - \boldsymbol{\Psi}^T \mathbf{q}_2\right] dx_1, \tag{3.3}$$

where the strain energy (2.14) due to the elastic soil is given by

$$U_S = \frac{1}{2}\int_0^L k_w \left(\boldsymbol{\Phi}^T \mathbf{q}_1\right)^T \left(\boldsymbol{\Phi}^T \mathbf{q}_1\right) dx_1 = \frac{1}{2}\int_0^L k_G \left(\boldsymbol{\Phi}'^T \mathbf{q}_1\right)^T \left(\boldsymbol{\Phi}'^T \mathbf{q}_1\right) dx_1 \tag{3.4}$$

and the potential energy of the axial load (2.7) transform as follows:

$$U_P = \frac{N}{2}\int_0^L \mathbf{q}_1 \boldsymbol{\Phi}' \boldsymbol{\Phi}'^T \mathbf{q}_1 dx_1. \tag{3.5}$$

If the elastic soil parameters k_w and k_G are assumed to be constant along the beam axis, then the total potential energy of the system can be written as

$$U_t = \frac{1}{2}\mathbf{q}^T \left[\mathbf{K}_U + k_w \mathbf{K}_w + (k_G - N)\,\mathbf{K}_G\right] \mathbf{q} = \frac{1}{2}\mathbf{q}^T \mathbf{K} \mathbf{q}, \tag{3.6}$$

where the coordinates have been substituted into the column vector $\mathbf{q} = [\mathbf{q}_1\ \mathbf{q}_2]^T$ and:

$$\mathbf{K}_U = kG\int_0^L A \begin{bmatrix} \boldsymbol{\Phi}'\boldsymbol{\Phi}'^T & -\boldsymbol{\Psi}\boldsymbol{\Phi}'^T \\ -\boldsymbol{\Psi}\boldsymbol{\Psi}'^T & \boldsymbol{\Psi}\boldsymbol{\Psi}^T \end{bmatrix} dx_1 + E\int_0^L I \begin{bmatrix} 0 & 0 \\ 0 & \boldsymbol{\Psi}'\boldsymbol{\Psi}'^T \end{bmatrix} dx_1, \tag{3.7}$$

$$\mathbf{K}_w = \int_0^L \begin{bmatrix} \boldsymbol{\Phi}\boldsymbol{\Phi}^T & 0 \\ 0 & 0 \end{bmatrix} dx_1, \tag{3.8}$$

$$\mathbf{K}_G = \int_0^L \begin{bmatrix} \boldsymbol{\Phi}'\boldsymbol{\Phi}'^T & 0 \\ 0 & 0 \end{bmatrix} dx_1. \tag{3.9}$$

The $\mathbf{K}_U$ matrix is the sum of the bending and shear stiffness matrices, whereas $\mathbf{K}_w$ is the Winkler soil stiffness matrix. The stiffening effect of the second soil parameter is clearly indicated in (3.6), because k_G and the axial force N both multiply the same geometric stiffness matrix $\mathbf{K}_G$.

Finally, if the mass density is assumed to be constant along the beam, then the assumptions (3.1) and (3.2) lead to the following matrix form of the kinetic energy (2.11):

$$T = \frac{\omega^2}{2} \int_0^L \rho \left[A \left(\mathbf{q}_1 \mathbf{\Phi} \mathbf{\Phi}^T \mathbf{q}_1 \right) + I \left(\mathbf{q}_2 \mathbf{\Psi} \mathbf{\Psi}^T \mathbf{q}_2 \right) \right] dx_1 = \frac{\omega^2}{2} \mathbf{q}^T \mathbf{M} \mathbf{q}, \tag{3.10}$$

where

$$\mathbf{M} = \int_0^L \rho \begin{bmatrix} A\mathbf{\Phi}\mathbf{\Phi}^T & 0 \\ 0 & I\mathbf{\Psi}\mathbf{\Psi}^T \end{bmatrix} dx_1. \tag{3.11}$$

The mass matrix $\mathbf{M}$ can be divided into the mass matrix due to the transverse displacements and the mass matrix due to the rotary inertia. A trivial application of the well-known Hamilton principle leads to the following eigenvalue problem:

$$(\mathbf{K} - \omega^2 \mathbf{M})\mathbf{q} = 0, \tag{3.12}$$

which in turn leads to the frequency equation

$$\det(\mathbf{K} - \omega^2 \mathbf{M}) = 0. \tag{3.13}$$

It has been already mentioned that the shape functions must obey only the geometric boundary conditions, so that it will be possible to write:

$$\Phi_1(x_1) = \sum_{j=0}^{n_u} a_j x_1^j, \tag{3.14}$$

$$\Psi_1(x_1) = \sum_{j=0}^{n_\varphi} b_j x_1^j, \tag{3.15}$$

where n_u and n_φ are the geometric conditions which must be imposed on the vertical displacements and rotations, respectively. The coefficients a_i and b_i can be determined imposing the boundary conditions, whereas the higher-order functions can be sought by means of the *Gram–Schmidt* [12] iterative method.

The geometric boundary conditions at the ends of the beam can be written as follows:

Pinned–Pinned:

$$x_1 = 0, \qquad x_1 = L \Rightarrow u_1 = 0\,; \tag{3.16}$$

Pinned–Clamped:

$$x_1 = 0 \Rightarrow u_1 = 0, \qquad x_1 = L \Rightarrow \left[\begin{array}{c} u_1 = 0 \\ u_{1,1} = 0 \end{array} \right. ; \tag{3.17}$$

Clamped–Free:

$$x_1 = 0 \Rightarrow \left[\begin{array}{c} u_1 = 0 \\ u_{1,1} = 0 \end{array} \right. , \qquad x_1 = L \Rightarrow \left[\begin{array}{c} u_1 \neq 0 \\ u_{1,1} \neq 0 \end{array} \right. . \tag{3.18}$$

4. Numerical examples

In order to test the method suggested above, some numerical examples have been performed, for a beam with arbitrarily varying cross-section, with the area and moment of inertia given by the general relationships:

$$A(x_1) = A_0 \left[1 + \alpha \frac{x_1}{L} \right], \tag{4.1}$$

$$I(x_1) = I_0 \left[1 + \alpha \frac{x_1}{L} \right]^3, \tag{4.2}$$

where A_0 and I_0 are the cross-sectional area and moment of at the abscissa $x_1 = 0$. It is also usual to introduce the following non-dimensional parameters:

$$P = \frac{NL^2}{\pi^2 E I_0}, \qquad \lambda_w = \frac{k_w L^2}{E I_0}, \qquad \lambda_G = \frac{k_G L^4}{\pi^2 E I_0}, \tag{4.3}$$

whereas the free vibration frequencies are usually written as:

$$\Omega_i^2 = \omega_i^2 L^4 \frac{\rho A_0}{E I_0}, \qquad r^2 = \frac{I_0}{A_0}. \tag{4.4}$$

As the first comparison, let us consider the beams with constant cross-section, subjected to axial forces as studies by Yokoyama [11] by means of a finite element approach. The Poisson coefficient is equal to 0.25, $E/G = 2.5$, the cross-section is assumed to be rectangular, and consequently, the shear factor is given by $k = 2/3$. In the following we have used 5 polynomial trial function in order to approximate both the displacements and rotations, so that the resulting problem has 10 degrees of freedom. The first three frequency coefficients Ω_i have been calculated for pinned-pinned (P-P) beam and for an pinned-clamped (P-C) beam. The results are given in Table 1 together with the free frequencies as given in [11] for a finite element mesh with 16 elements. The full agreement with the exact frequencies is quite evident, small discrepancies can be noticed only for the higher frequencies, but the error turns out to be smaller than 0.2%.

Table 1. First three non-dimensional frequencies for beams (constant cross-section).

P	λ_W	λ_G	P-P			P-C		
			Exact	Present	[11]	Exact	Present	[11]
0	0	0	8.210	8.214	8.220	10.630	10.626	10.630
			24.230	24.228	24.310	25.620	25.616	25.710
			41.540	41.545	41.960	42.030	42.035	42.460
0.6			3.470	3.466	3.470	7.320	7.323	7.330
			19.220	19.280	19.310	20.930	20.931	21.030
			35.080	35.352	35.480	35.700	35.750	36.160
	0.6 π^4		8.210	8.214	8.220	10.460	10.481	10.490
			20.590	20.645	20.670	22.200	22.207	22.300
			35.860	36.126	36.250	36.500	36.508	36.900
		1		12.638	12.640		14.419	14.420
				28.075	28.100		29.248	29.340
				46.191	46.340		46.281	46.710

In order to study the influence of the soil parameters, let us consider, as a first example, the pinned-pinned beam and the clamped-free (C-F) beam with constant cross-section in the absence of axial forces. The first two frequency parameters are given in Figs. 1, 2 and in Figs. 3, 4 for the (P-P) beam and for the cantilever beam, respectively, where the solid lines refer to Ω_1 and the dashed

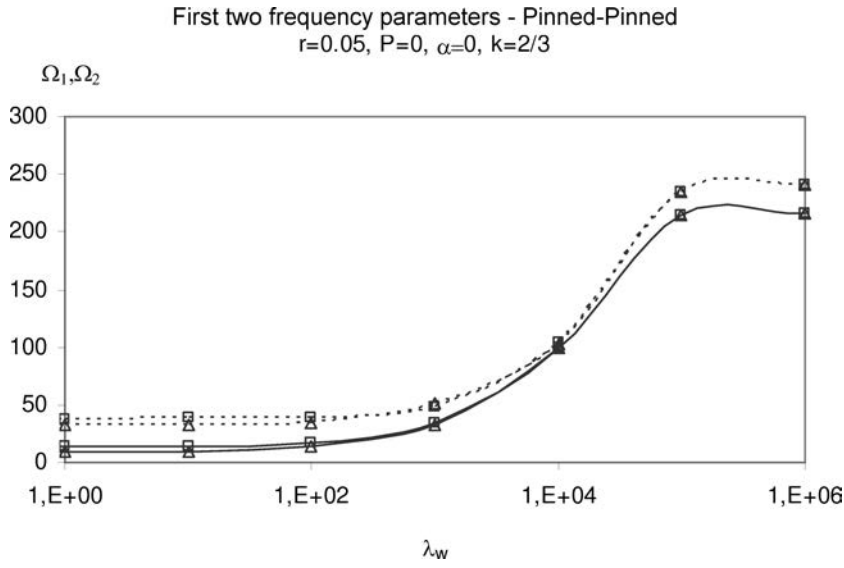

Fig. 1.

lines refer to Ω_2. Two different λ_G values have been considered, i.e. $\lambda_G = 0$ ($\triangle$) and $\lambda_G = 1$ ($\square$). It is worth noting that, regardless of the r value, the influence of λ_G is reduced as λ_w increases, and the stiffening effect for large λ_w values causes the coalescence of the first two vibration frequencies.

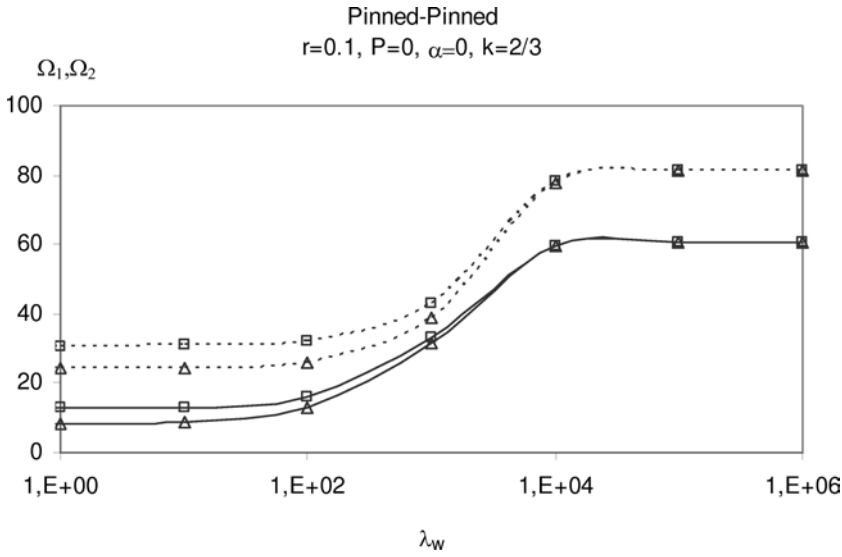

FIG. 2.

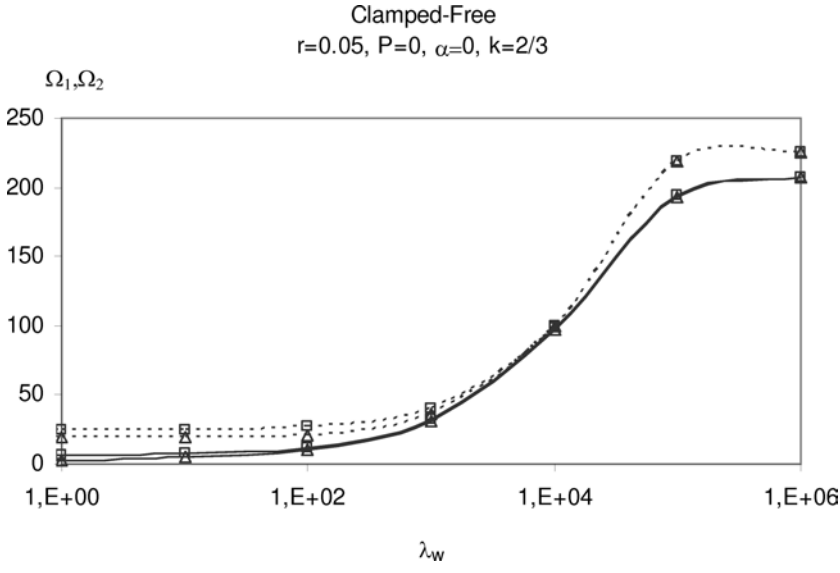

FIG. 3.

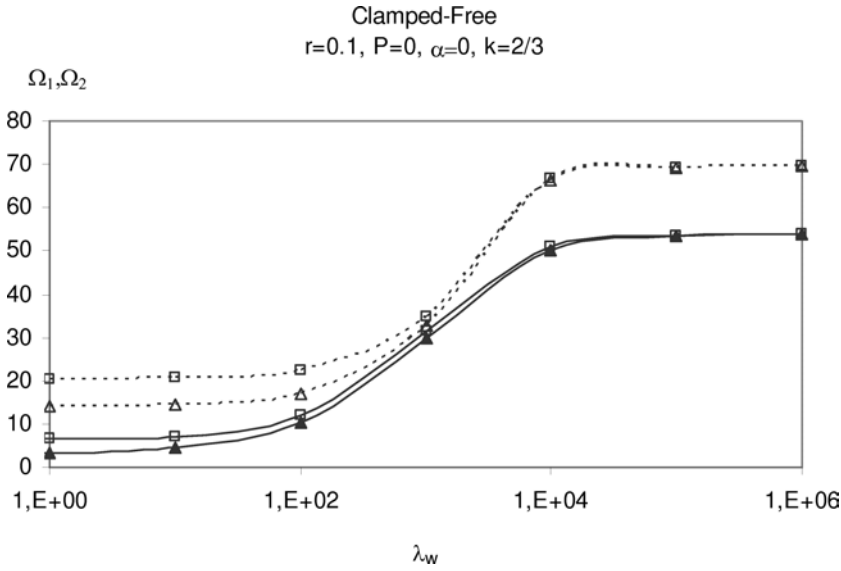

FIG. 4.

The influence of axial load and of the taper ratio (α) on the fundamental frequencies is illustrated by the graphs in Figs. 5–7. For all the boundary conditions the frequency parameter Ω goes to zero as $P/P_c \to -1$. Finally, the influence of the taper ratio α seems to be relevant for the cantilever beam, whereas it is less important for simply-supported beam and pinned-clamped beam. In Table 2 the non-dimensional critical loads are given, which have been used to obtain the previous pictures.

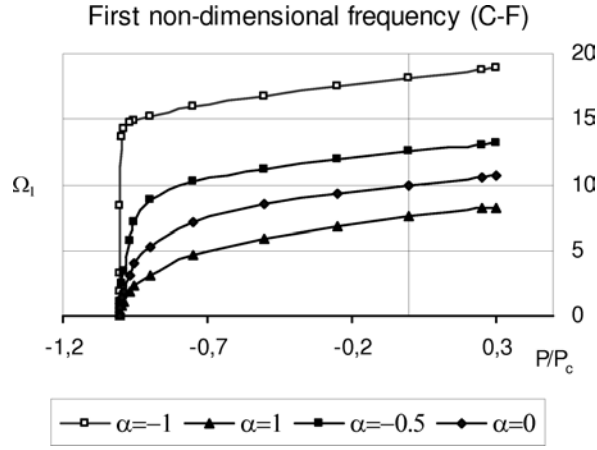

FIG. 5.

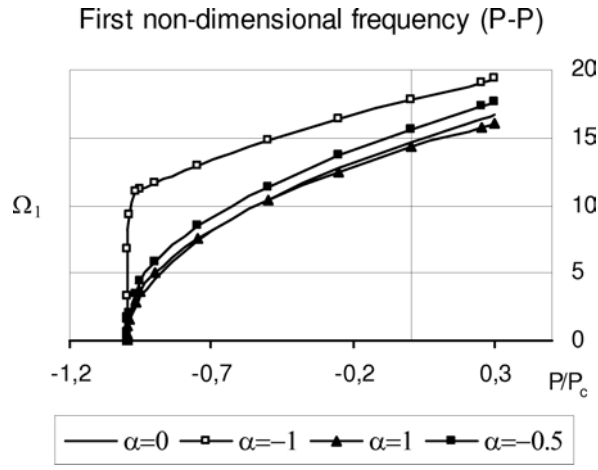

FIG. 6.

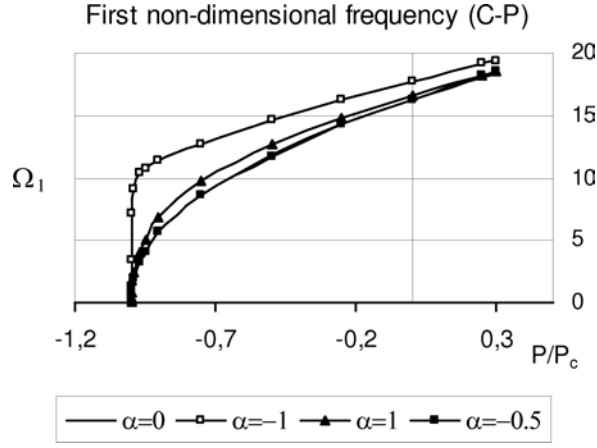

FIG. 7.

Table 2. Critical parameter (P_c) for different boundary conditions.

$r = 0.1$ $\lambda_G = 1$ $\lambda_W = 0.6\ \pi^4$ $k = 2/3$										
α	-1	-0.9	-0.75	-0.5	0	0.25	0.5	0.75	1	1.25
C-F	1.0255	1.0643	1.178	1.373	1.7415	1.904	2.056	2.19	2.323	2.434
P-F	1.0254	1.0665	1.1779	1.362	1.7269	1.894	2.045	2.177	2.289	2.382
P-P	1.0612	1.1463	1.3946	1.785	2.3298	2.546	2.749	2.935	3.104	3.253
P-C	1.1467	1.3443	1.5951	2.036	2.5908	2.827	3.031	3.204	3.359	3.464

The use of BCOPs method to calculate free vibration frequencies and critical load is always influenced by trial functions, and a careful choice leads to well approximated results. In turn, the trial functions depend on the boundary conditions, so that it seems to be convenient to use polynomials.

5. Conclusion

In this paper, a powerful version of the Rayleigh–Ritz variational method has been applied to the vibration analysis of Timoshenko beams on a two-parameter elastic soil. The influence of various structural parameters on the behaviour of the free vibration frequencies has been illustrated in various numerical examples.

The proposed approach belongs to the so-called semi-analytical methods (SAN methods), and as such it can be considered as a useful tool in purely numerical approaches (finite element methods, differential quadrature methods etc.), in which all the parameters must be defined from the very beginning.

The numerical examples show the reliability of the method, and the particular efficiency of the chosen trial functions.

References

1. M. Hetenyi, *Beams on elastic foundation*, Ann. Arbor, University of Michigan Press, 1961.
2. S. Chakraverty, R. B. Bhat, I. Stiharu, *Recent reserch on vibration of structures using Boundary Characteristic Orthogonal Polynomials in the Rayleigh-Ritz method*, The Shock and Vibration Digest, **31**, 3, 187–194, 1999.
3. F. Y. Chen, C. P. Pantelides, *Dynamic Timoshenko beam-columns on elastic media*, ASCE J. Struct. Engng., **114,** 1524–1550, 1988.
4. M. C. Bruno, V. Di Capua and C. Franciosi, *New interpolation functions in eigenfrequency analysis of Timoshenko beams on two-parameter elastic soil*, Engng. Trans., **44**, 2, 283–294,1996.
5. M. A. De Rosa, *Free vibration of Timoshenko beams on two-parameter elastic foundation*, Comput. & Struct., **57**, 151–156, 1995.
6. C. Franciosi, A. Masi, *Free vibration of foundation beams on two-parameter elastic soil*, Comput. & Struct., **47**, 419–426, 1993.
7. C. P. Filipich, M. B. Rosales, *A variant of Rayleigh's method applied to Timoshenko beams embedded in a Winkler-Pasternak medium*, J. Sound and Vibr., **124**, 443–451, 1988.
8. V. Z. Vlasov, U. N. Leontiev, *Beams, plates and shells on elastic foundation. Jerusalem*, Israel Program for Scientific Translations.
9. G. V. C. Vallabhan, K. R. Das, *A refined model for beams on elastic foundation*, Int. J. Solid Structures, **27**, 629–637, 1991.
10. T. Yokoyama, *Vibration and transiet response of Timoshenko beams resting on elastic foundations*, Ingenieur Archiv, **57**, 81–90, 1987.

11. T. Yokoyama, *Vibration analysis of Timoshenko beam-columns on two-parameter elastic foundations*, Comput. & Struct., **61**, 995–1007, 1996.

12. K. Rektorys, *Variational methods in mathematics, science and engineering*, D. Reidel Publishing Comp., Boston 1977.

Received April 12, 2007; revised version November 26, 2007.

ENGINEERING TRANSACTIONS • *Engng. Trans.* • **56**, 3, 201–225, 2008
Polish Academy of Sciences • Institute of Fundamental Technological Research

MATERIAL DESIGN OF ANISOTROPIC ELASTIC CELLULAR BODIES WITH RESPECT TO CONTACT PROBLEM

D. Jasińska, M. Janus–Michalska

Institute of Structural Mechanics
Cracow University of Technology
Warszawska 24, 31-155 Kraków, Poland

Two-dimensional contact problem formulated for anisotropic, elastic bodies is considered. As an example of anisotropic medium, the cellular material is taken. The idea of two-scale modeling is adopted for formulation of an equivalent continuum, on the basis of which elastic properties can be obtained [2, 3]. Typical cellular microstructures with various types of symmetries are considered. Special attention is paid to cell structures giving negative Poisson's ratio in some directions (re-entrant cells). Application of the energy-based criterion for equivalent continuum gives macroscopic yield condition [2, 5]. Condition for the energy coefficient defined as a sum of weighted energies stored in elastic eigenstates ensures that the material works in elastic state. Unilateral frictional contact problem is analyzed using FEM. Calculations are performed for rough contact of square block subjected to normal load. Numerical solutions show differences in deformation type and contact stress distributions for different types of microstructures of the analyzed medium. The study enables the optimal choice of material structure topology, which ensures the reduction of peak contact pressure and friction stress, and applicability of anisotropic material to the given problem.

Key words: contact, friction, cellular anisotropic materials, negative Poisson's ratio.

1. Introduction

Cellular materials, with their variety of microstructures and types of material symmetries, adopted for contact problems, provide interesting topics for research. Two-scale modeling let us calculate the elastic properties of equivalent continuum on the basis of unit cell analysis. Some cell structures lead to negative Poisson's ratio in some directions. Materials with negative Poisson's ratio are called auxetic due to increasing cross-section in tension. They may be useful for a variety of applications. Among their important mechanical properties the reduction of stress concentration in contact problems shows a new area of applications. Such problem was investigated for auxetic isotropic foam [11, 12] and the results show essential differences compared with the solutions for conventional foams. For three-dimensional isotropic body limits of acceptable Poisson's ratio hold $-1 \leq \nu \leq 0.5$ as a result of thermodynamical considerations [7, 10].

For anisotropic materials these bounds are wider, theoreticaly they can reach infinity. The existence of directions with auxetic behaviour in cellular materials is connected with high anisotropy.

2. Formulation of the contact problem

For the unilateral static contact problem of anisotropic linear elastic body with stiff and rough obstacle, the following system of equations must be fulfilled [3]:

$$\sigma_{ij,j} + f_i = 0, \qquad \sigma_{ij} = S_{ijkl}\varepsilon_{kl}, \qquad \varepsilon_{ij} = \frac{1}{2}(u_{i,j} + u_{j,i}) \quad \text{in} \quad \Omega \tag{2.1}$$

completed with boundary conditions

$$u_i = \hat{u}_i \qquad \text{on} \qquad \Gamma_{D,} \qquad \sigma_{ij} \cdot n_j = t_i \qquad \text{on} \qquad \Gamma_{F,} \tag{2.2}$$

contact conditions on Γ_C

$$\sigma_n \cdot (u_n - g) = 0, \qquad \sigma_n \leq 0, \qquad u_n - g \leq 0 \tag{2.3}$$

and friction conditions on Γ_C

$$|\boldsymbol{\sigma}_T| < \mu\,|\sigma_n| \Rightarrow \Delta\mathbf{u}_T = 0, \quad |\boldsymbol{\sigma}_T| = \mu\,|\sigma_n| \Rightarrow \exists\lambda > 0; \quad \Delta\mathbf{u}_T = -\lambda\boldsymbol{\sigma}_T, \tag{2.4}$$

where σ_{ij} – Cauchy stress tensor, ε_{ij} – small strain tensor, S_{ijkl} – anisotropic elastic stiffness matrix, u_i – displacement vector, f_i – body forces, $\hat{u}_i$ – prescribed displacements on Γ_D, t_i – forces acting on Γ_F, n_i – unit normal vector, $\Gamma_D \cup \Gamma_F \cup \Gamma_C$ – boundary of the domain Ω, g – initial gap, $\sigma_n = \sigma_{ij}n_in_j$ – contact pressure, $u_n = \mathbf{u} \circ \mathbf{n}$ – displacement normal to the boundary, $\sigma_{Ti} = \sigma_{ij} \cdot n_j - \sigma_n \cdot n_i$ – tangential contact force, and $\Delta\mathbf{u}_T = \Delta(\mathbf{u} - u_n \cdot \mathbf{n})$ – increment of tangential displacement.

To solve the boundary value problem formulated above (nonlinear due to conditions (2.3) and (2.4)), the FEM approach is used.

3. Cellular microstructure

Cellular materials, due to a variety of material structure topology, reveal different anisotropic properties. Microstructure of material is modeled by idealized regular repeating pattern of unit cells. A skeleton of a cell is modeled as an elastic beam structure with stiff joints. The following cellular plane structures are analyzed: a) square cell structure, b) 'honeycomb' structure, c) equilateral triangular structure, d) 'reentrant' structure (giving auxetic material).

These structures represent a unit thickness layer cut from 3-dimensional material working in plane strain state. Figure 1 shows the structures mentioned above and their representative unit cells.

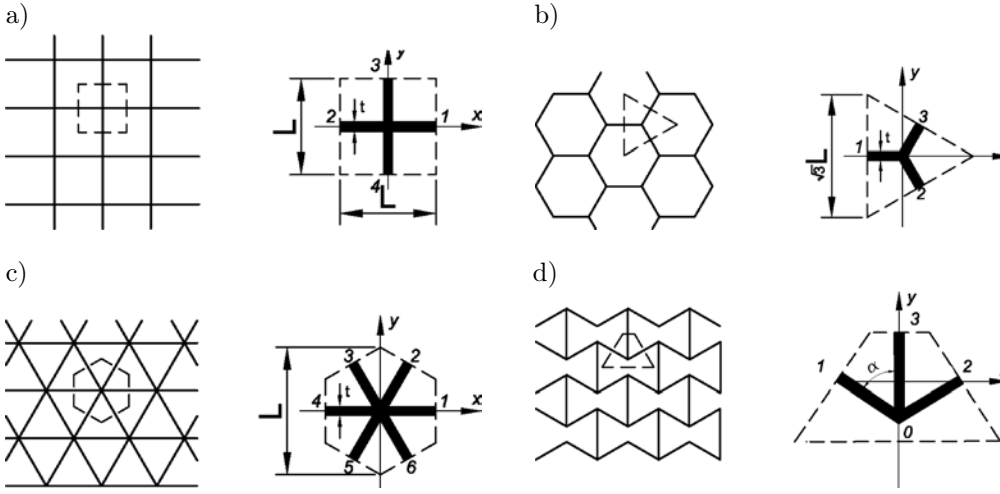

FIG. 1. Regular cellular plane structures, and their representative unit cells: a) square cell structure, square unit cell, b) 'honeycomb' structure, triangle unit cell, c) equilateral triangular structure, hexagonal unit cell, d) 'reentrant' structure, trapezoid unit cell.

Geometry of a representative unit cell can be described by midpoint position vectors: $\mathbf{b}_i^0$, where $\left|\mathbf{b}_1^0\right| = h/2$, $\left|\mathbf{b}_i^0\right| = L/2$, $i = 1, 2, ...n$. L, h, t, γ – geometric structural parameters (for a), b), c) structures $L = h$). Skeleton material parameters are: Young's modulus – E_s, Poisson's ratio – ν_s, limit of linear elasticity – R_e.

3.1. Stiffness matrices

A framework of micromechanical modeling [2, 3, 5] is used to obtain stiffness matrices of an elastic anisotropic equivalent continuum. It starts with analyzing uniform macrostrains over the unit cell defined as follows:

$$\boldsymbol{\varepsilon} = \langle \boldsymbol{\varepsilon}^s \rangle_V = \frac{1}{V} \sum_{A_i} \operatorname{sym} (\mathbf{n}_i \otimes \mathbf{u}_i)\, dS, \tag{3.1}$$

where $\mathbf{u}_i$ – midpoint displacement vector, $\mathbf{n}_i$ – unit normal to the cell boundary, V – volume of the representative cell, A_i – area of cell wall perpendicular to i beam.

The model assumes that macrostrains of equivalent continuum are defined by midpoint displacements of the skeleton structure. In terms of 6-D space (Kelvin notation), plane strain tensor is represented by vector $\boldsymbol{\varepsilon} = \left(\varepsilon_x, \varepsilon_y, \sqrt{2}\varepsilon_{xy}\right)$ and stiffness tensor representation is a 3×3 matrix.

Given uniform unit strain fields ${}^K\tilde{\varepsilon}$, $K = 1, 2, 3$ on the unit cell, as written below:

$$(3.2)_1 \qquad {}^1\tilde{\varepsilon} = (1,0,0)\,, \qquad {}^2\tilde{\varepsilon} = (0,1,0)\,, \qquad {}^3\tilde{\varepsilon} = \left(0,0,\sqrt{2}\right),$$

the displacements for the midpoints $i = 1, 2, ...n$ in skeleton structure can be found:

$$(3.2)_2 \qquad \boldsymbol{\Delta}_i = \boldsymbol{\Delta}_i({}^K\tilde{\varepsilon}), \qquad i = 1, 2, ...n, \qquad K = 1, 2, 3.$$

Next the forces normal ${}^K\tilde{F}_{in}$ and tangential ${}^K\tilde{F}_{i\tau}$ to each skeleton beam are obtained with the use of the Timoshenko beam theory. For structures a), b), and c) these are analytical solutions. For a reentrant structure d) forces are calculated numerically (using FEM ANSYS code). These forces produce stress field on macroscale (in equivalent continuum) $\tilde{\boldsymbol{\sigma}}$, and on microscale (in skeleton material) $\tilde{\boldsymbol{\sigma}}^s$.

For arbitrary uniform strain state represented by vector $\boldsymbol{\varepsilon} = \left({}^1\varepsilon, {}^2\varepsilon, {}^3\varepsilon\right)$, the forces can be calculated as linear combination of previous solutions as follows:

$$(3.3) \qquad F_{in}(\boldsymbol{\varepsilon}) = \sum_{K=1}^{3} {}^K\varepsilon\, {}^K\tilde{F}_{in}, \qquad F_{i\tau}(\boldsymbol{\varepsilon}) = \sum_{K=1}^{3} {}^K\varepsilon\, {}^K\tilde{F}_{i\tau}.$$

The definition of effective continuum assumed here is based on equivalence of the strain potential for the discrete structure and the strain potential of an equivalent continuum. It refers to averaging the strain energy density as written below:

$$(3.4) \qquad \Phi_E = \langle {}^s\Phi_E \rangle_V = \frac{1}{V} \int\limits_{V_s} ({}^s\Phi_E)\, dV_s,$$

where strain potential of the beam skeleton may be obtained using the following formula:

$$(3.5) \quad U = \int\limits_{V_s} ({}^s\Phi_E)\, dV_s = \sum_{i=1}^{3} \left(\int\limits_0^{l_i} \frac{(F_{ni})^2\, d\xi_i}{2E_s A_s} + \mu \int\limits_0^{l_i} \frac{(F_{\tau i})^2\, d\xi_i}{2G_s A_s} + \int\limits_0^{l_i} \frac{(F_{\tau i}(l_i - \xi_i))^2\, d\xi_i}{2E_s J} \right),$$

where E_s, G_s – Young and shear modulus for the skeleton material, A_s, J – beam cross-sectional area and moment of inertia, μ – energy cross-sectional coefficient (for rectangular cross-section $\mu = 1.2$).

Due to linearity of the stress-strain relationship, the strain energy density function is represented by the following quadratic form:

$$\Phi_E = \frac{1}{2}\boldsymbol{\varepsilon} : \mathbf{S} : \boldsymbol{\varepsilon}. \tag{3.6}$$

Introducing relation (3.3) to the expression of strain potential and differentiating it with respect to macrostrain components as follows:

$$S_{IJ} = \frac{1}{V}\left(\int\limits_{V_S} \frac{\partial^2 \left({}^S\Phi_E\right)}{\partial \left({}^I\varepsilon\right) \partial \left({}^J\varepsilon\right)} dV_S\right), \tag{3.7}$$

one obtains the formula for stiffness matrix components of an anisotropic equivalent continuum.

These components can be obtained as a result of a procedure based on Eqs. (3.1)–(3.4) and (3.6)–(3.7) [2].

3.2. Poisson's ratio and other material properties

Typical cellular structures with honeycomb and triangular shape of skeleton give always positive Poisson's ratio values in each direction in plane since they represent transversal symmetry. For isotropy in two-dimensional problems, limits of acceptable Poisson's ratio become $-1 \leq \nu \leq 1$ due to thermodynamical considerations [9]. The honeycomb structure is more compliant and Poisson's ratio can attain greater value, but limited by relation $\nu \leq 1$. The triangular structure shape is stiff and gives lower Poisson's ratio. The value of Poisson's ratio for the symmetries mentioned above is constant; it means that it is independent of the direction of tension. This constant is dependent on geometric and material microstructural parameters as given in Appendix B. Square structure gives anisotropic material with zero Poisson's ratio in symmetry axis. In other directions the value is limited by relation $0 \leq \nu \leq 1$. Generally for greater cellular material density of fixed microstructure type, the Poisson's ratio value is lower than for lower density. Some skeleton geometries lead to nonpositive Poisson's ratio. For instance, a honeycomb with inverted hexagonal cells leads to negative Poisson's ratio in some directions. This unusual characteristics is achieved by forming the cells into re-entrant shape, which bulges inwards and which unfolds under tension resulting in a lateral expansion [6]. Detailed study of directional properties of cellular material with re-entrant honeycomb structure in dependence on microstructural parameters is given in [2].

Graphical representation of chosen material properties for material structures a), b), c), d) with geometric and skeleton material data used for numerical examples are given in Appendix B.

Evaluation of cellular material properties decides on the applicability of the material to the given problem.

3.3. Assessment of elastic range

Majority of cellular materials reveal nonlinear behavior. Although linear analysis gives only estimation of elastic limits, it enables to predict applicability of chosen microstructure to material design.

Matrix representation of stiffness tensor for plane structures in Kelvin's notation in 6-D space is as follows:

$$\mathbf{S} = \begin{bmatrix} S_{11} & S_{12} & S_{13} \\ S_{12} & S_{22} & S_{23} \\ S_{13} & S_{23} & S_{33} \end{bmatrix}. \tag{3.8}$$

In general this matrix has three eigenvalues: λ_{I}, λ_{II}, λ_{III}, and the corresponding stiffness matrix eigenstrains:

$${}^{\mathrm{I}}\tilde{\boldsymbol{\varepsilon}} = \left({}^{\mathrm{I}}\tilde{\varepsilon}_x, {}^{\mathrm{I}}\tilde{\varepsilon}_y, {}^{\mathrm{I}}\tilde{\varepsilon}_{xy}\right), \quad {}^{\mathrm{II}}\tilde{\boldsymbol{\varepsilon}} = \left({}^{\mathrm{II}}\tilde{\varepsilon}_x, {}^{\mathrm{II}}\tilde{\varepsilon}_y, {}^{\mathrm{II}}\tilde{\varepsilon}_{xy}\right), \quad {}^{\mathrm{III}}\tilde{\boldsymbol{\varepsilon}} = \left({}^{\mathrm{III}}\tilde{\varepsilon}_x, {}^{\mathrm{III}}\tilde{\varepsilon}_y, {}^{\mathrm{III}}\tilde{\varepsilon}_{xy}\right)$$

or stiffness matrix eigenstresses:

$${}^{\mathrm{I}}\tilde{\boldsymbol{\sigma}} = \lambda_{\mathrm{I}}{}^{\mathrm{I}}\tilde{\boldsymbol{\varepsilon}}, \qquad {}^{\mathrm{II}}\tilde{\boldsymbol{\sigma}} = \lambda_{\mathrm{II}}{}^{\mathrm{II}}\tilde{\boldsymbol{\varepsilon}}, \qquad {}^{\mathrm{III}}\tilde{\boldsymbol{\sigma}} = \lambda_{\mathrm{III}}{}^{\mathrm{III}}\tilde{\boldsymbol{\varepsilon}}. \tag{3.9}$$

Equations (3.1)–(3.4) enable to calculate the forces in skeleton structure for strain eigenstates and to formulate the limit condition for bending and tension in the skeleton in the form:

$$\max_i \left({}^{\alpha}\sigma_x^s\right) = R_e, \qquad \alpha = \mathrm{I},\ \mathrm{II},\ \mathrm{III}, \qquad i = 1, 2, ...n. \tag{3.10}$$

The coefficients defined as follows:

$$k_\alpha := \frac{R_e}{{}^{\alpha}\tilde{\sigma}_x^s} \qquad \alpha = \mathrm{I},\ \mathrm{II},\ \mathrm{III} \tag{3.11}$$

are obtained as a result of analytical considerations or numerical calculations. Analytical formulae for these coefficients depending on geometric structural and skeleton material parameters for structures a), b), c) are given in Appendix A. For structure d) these coefficient are obtained as a result of numerical calculations.

Limit eigenstrains and eigenstresses are as follows:

$${}^{\alpha}\boldsymbol{\varepsilon}^{\mathrm{gr}} = k_\alpha{}^{\alpha}\tilde{\boldsymbol{\varepsilon}}, \qquad {}^{\alpha}\sigma^{\mathrm{gr}} = \lambda_\alpha{}^{\alpha}\boldsymbol{\varepsilon}^{\mathrm{gr}}, \qquad \alpha = \mathrm{I},\ \mathrm{II},\ \mathrm{III}. \tag{3.12}$$

The analysis presented above lets us also predict deformability of the given material in elastic range. It can be described as maximum elongation in the x, y direction or shear angle in the xy plane, which reads as follows:

$$\max|\varepsilon_x| = \sum_{\alpha=1}^{\mathrm{III}} |{}^{\alpha}\varepsilon_x^{\mathrm{gr}}|, \quad \max|\varepsilon_y| = \sum_{\alpha=1}^{\mathrm{III}} \left|{}^{\alpha}\varepsilon_y^{\mathrm{gr}}\right|, \quad \max|\varepsilon_{xy}| = \sum_{\alpha=1}^{\mathrm{III}} \left|{}^{\alpha}\varepsilon_{xy}^{\mathrm{gr}}\right|. \tag{3.13}$$

3.4. Energy-based yield criterion for anisotropic continuum

For an arbitrary anisotropic solid, the energy-based Rychlewski criterion [13] is formulated in the form of a sum of weighted energies stored in eigenstates of anisotropy stiffness tensor as follows:

$$\sum_{\alpha=1}^{\mathrm{III}} \frac{{}^{\alpha}\Phi_E}{{}^{\alpha}\Phi_E^{\mathrm{gr}}} = 1, \tag{3.14}$$

where ${}^{\alpha}\Phi_E^{\mathrm{gr}}$ is the critical energy for α state, $\alpha = \mathrm{I}, \mathrm{II}, \mathrm{III}$.

Energy-based yield criterion is a type of energy hypothesis for cellular material. The subject of investigation is the limit state of linear elasticity which corresponds to the first yield point in the skeleton structure. Such an approach was successively adopted to a cellular 3D structured material [3, 5] and foams. It shows a good agreement with experimental data [5].

Critical energies in Eq. (3.14) can be calculated by means of the formula:

$${}^{\alpha}\Phi_E^{\mathrm{gr}} = \frac{1}{2}\,{}^{\alpha}\boldsymbol{\sigma}^{\mathrm{gr}} \cdot {}^{\alpha}\boldsymbol{\varepsilon}^{\mathrm{gr}} = \frac{1}{2}\lambda_{\alpha} k_{\alpha}^2\, {}^{\alpha}\tilde{\boldsymbol{\varepsilon}}^2. \tag{3.15}$$

The criterion presented above gives macroscopic yield condition for arbitrary stress state, in particular for uniaxial tension, which is important due to the fact that it can be compared with experimental results. For the considered structures a), b), c), the formulae depending on skeleton material parameters and geometric parameters of skeleton structures are given in Appendix A. For structure d) these energies are obtained numerically.

The elastic stiffness matrix (3.8), yield stresses and limit strains (3.12), (3.13) describing deformability in the elastic range, depend on material properties of a solid phase of the cell and topological arrangement of its structure. Detailed study of material properties depending on structural parameters is given in [2, 3].

3.5. Material strength in arbitrary plane stress state

The considered contact problem is linearly elastic. To conform this requirement it is necessary to introduce a measure of material strength in arbitrary

point of the material and give the range of this measure for elasticity. The consequence of the adopted form of yield criterion is the choice of energy coefficient defined as a sum of weighted energies stored in subsequent eigenstates as written below:

$$\varphi = \sum_{\alpha=1}^{\mathrm{III}} \frac{{}^{\alpha}\Phi_E}{{}^{\alpha}\Phi_E^{\mathrm{gr}}}. \tag{3.16}$$

In the limit state the coefficient reaches its maximum value $\varphi = 1$. Critical energies can be defined as structural parameters of the material strength.

For generality of considerations we assume arbitrary orientation of cellular x, y axes with respect to global X, Y coordinate axes in which the contact problem is described. This orientation is given by angle β, as shown in Fig 2.

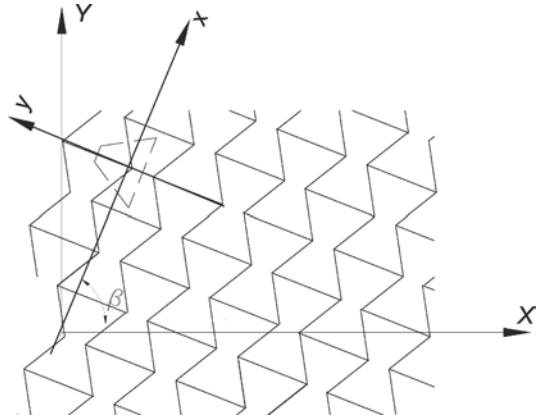

FIG. 2. Material orientation with respect to the global coordinate system.

To evaluate the energy coefficient in arbitrary point M with stress vector:

$$\boldsymbol{\sigma}^{(M)} = \left(\sigma_X^{(M)},\, \sigma_Y^{(M)},\, \sqrt{2}\sigma_{XY}^{(M)}\right) \tag{3.17}$$

it is necessary to decompose it into stress eigenstates. As a result, the stress vector for point M can be expressed as a linear combination of limit eigenstresses as written below:

$$\boldsymbol{\sigma}^{(M)} = A^{\mathrm{I}}\boldsymbol{\sigma}^{\mathrm{gr}} + B^{\mathrm{II}}\boldsymbol{\sigma}^{\mathrm{gr}} + C^{\mathrm{III}}\boldsymbol{\sigma}^{\mathrm{gr}}, \tag{3.18}$$

where coefficients of this combination are as follows:

$$A = \frac{\sigma_X^{(M)}\,{}^{\mathrm{II}}\sigma_Y^{\mathrm{gr}} - \sigma_Y^{(M)}\,{}^{\mathrm{II}}\sigma_X^{\mathrm{gr}}}{{}^{\mathrm{I}}\sigma_X^{\mathrm{gr}}\,{}^{\mathrm{II}}\sigma_Y^{\mathrm{gr}} - {}^{\mathrm{II}}\sigma_X^{\mathrm{gr}}\,{}^{\mathrm{I}}\sigma_Y^{\mathrm{gr}}}, \qquad B = \frac{\sigma_Y^{(M)}\,{}^{\mathrm{I}}\sigma_X^{\mathrm{gr}} - \sigma_X^{(M)}\,{}^{\mathrm{I}}\sigma_Y^{\mathrm{gr}}}{{}^{\mathrm{I}}\sigma_X^{\mathrm{gr}}\,{}^{\mathrm{II}}\sigma_Y^{\mathrm{gr}} - {}^{\mathrm{II}}\sigma_X^{\mathrm{gr}}\,{}^{\mathrm{I}}\sigma_Y^{\mathrm{gr}}},$$
$$C = \frac{\sigma_{XY}^{(M)}}{{}^{\mathrm{III}}\sigma_{XY}^{\mathrm{gr}}}. \tag{3.19}$$

The energy coefficient is expressed by relation:

$$\varphi = A^2 + B^2 + C^2 \leq 1$$

which gives the following condition:

$$\varphi = d_1 \left(\sigma_X^{(M)}\right)^2 + d_2 \left(\sigma_Y^{(M)}\right)^2 + d_3 \left(\sigma_{XY}^{(M)}\right)^2 + d_4 \left(\sigma_X^{(M)} \sigma_Y^{(M)}\right) + d_5 \left(\sigma_X^{(M)} \sigma_{XY}^{(M)}\right) + d_6 \left(\sigma_Y^{(M)} \sigma_{XY}^{(M)}\right) \leq 1, \tag{3.20}$$

where:

$$d_1 = 0.25 \left[\left(\frac{1}{m_1}\right)^2 + \left(\frac{\cos 2\beta}{m_2}\right)^2 + \left(\frac{\sin 2\beta}{m_3}\right)^2\right], \qquad d_2 = d_1,$$

$$d_3 = \left[\left(\frac{\sin 2\beta}{m_2}\right)^2 + \left(\frac{\cos 2\beta}{m_3}\right)^2\right],$$

$$d_4 = 0.5 \left[\left(\frac{1}{m_1}\right)^2 - \left(\frac{\cos 2\beta}{m_2}\right)^2 - \left(\frac{\sin 2\beta}{m_3}\right)^2\right],$$

$$d_5 = 0.5 \sin 4\beta \left[\left(\frac{1}{m_2}\right)^2 + \left(\frac{1}{m_3}\right)^2\right], \qquad d_6 = -d_5,$$

$$m_1 = \lambda_1 k_1, \qquad m_2 = \lambda_2 k_2, \qquad m_3 = \lambda_3 k_3 \Big/ \sqrt{2}$$

and β is the angle shown in Fig. 2.

4. Numerical analysis

Calculations of stiffness matrices and energy strength coefficients (material parameters) for the considered anisotropic materials are performed independently on a microstructural level by considering the strain-stress relations for a unit cell. Analytical formulae for stiffness matrices coefficients and critical energies for structures a), b), c) are obtained with application of symbolic operations provided by the Mathcad program. For structure d) the relevant description can be obtained numerically by means of FEM system.

Subsequently, those parameters were used in the FEM analysis (with ANSYS software) of numerical examples presented below.

All examples deal with a rectangular prism in plane state of strain, in rough contact with stiff flat foundation. Simple geometry and load enable to analyze the influence of microstructure type on the deformation, contact stresses and distribution of material strength coefficient.

4.1. Square block made of material with different cell types under pressure

A square block of dimensions B*H=1*1 m in contact with a stiff foundation is analysed. The contact is rough with coefficient of friction $\mu = 0.3$. Pressure $p = 25$ kN/m is applied to upper edge of the block (see Fig. 3).

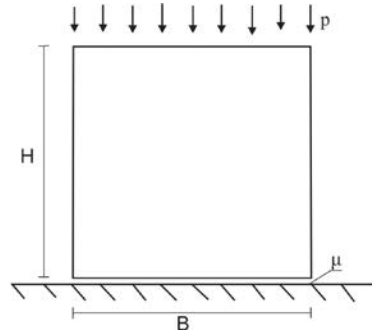

FIG. 3. Geometry and load for numerical examples.

Materials of all the types of microstructure presented above are considered. The skeleton material data are: $E_S = 10$ GPa, $\nu_S = 0.3$, $R_e = 10$ MPa and the geometric parameters are chosen to obtain the same relative material density $\rho = 0.1154$ of anisotropic cellular media in all cases. Table 1 shows specification of geometrical parameters for unit cells. Notation of the types of microstructures are the same as in Fig. 1.

Table 1. Specification of unit cells.

Structure type	Geometric parameters of skeleton [mm]	Skeleton beam thickness t [mm]
a)	$L_{01} = L_{02} = L_{03} = L_{04} = 2.6$	0.15
b)	$L_{01} = L_{02} = L_{03} = L_{04} = L_{05} = L_{06} = 1.5$	0.15
c)	$L_{01} = L_{02} = L_{03} = 4.5$	0.15
d)	$L_{01} = L_{02} = L_{03} = 3.15 \;\; \gamma = 70^0$	0.15

Resultant macroscopic material constants are given in Table 2.

Table 2. Anisotropic material constants for cellular materials of different cell types.

Structure type	E_X [MPa]	E_Y [MPa]	ν_{XY}	ν_{YX}
a) $\beta = 0$	576.92	576.92	0.0	0.0
b)	21.87	21.87	0.96	0.96
c)	385.47	385.47	0.33	0.33
d) $\beta = 90^\circ$	0.13	1.95	−0.26	−3.85

Analysis of Table 2 leads to the conclusion that macroscopic material constants depend on the type of cellular structure. Resultant Young's moduli are the greatest for structures a) and c), smaller for honeycomb structure b) and by several orders smaller for the re-entrant structure d). Materials of structures b) and c) are isotropic and have positive Poisson's ratio. Material of structure a) has zero Poisson's ratios and structure d) produces negative Poisson's ratios, when unit cell axis are placed parallel to the coordinate frame.

The contact problem with application to the described cellular solids is solved. Figure 4 shows deformations of a square block for different materials.

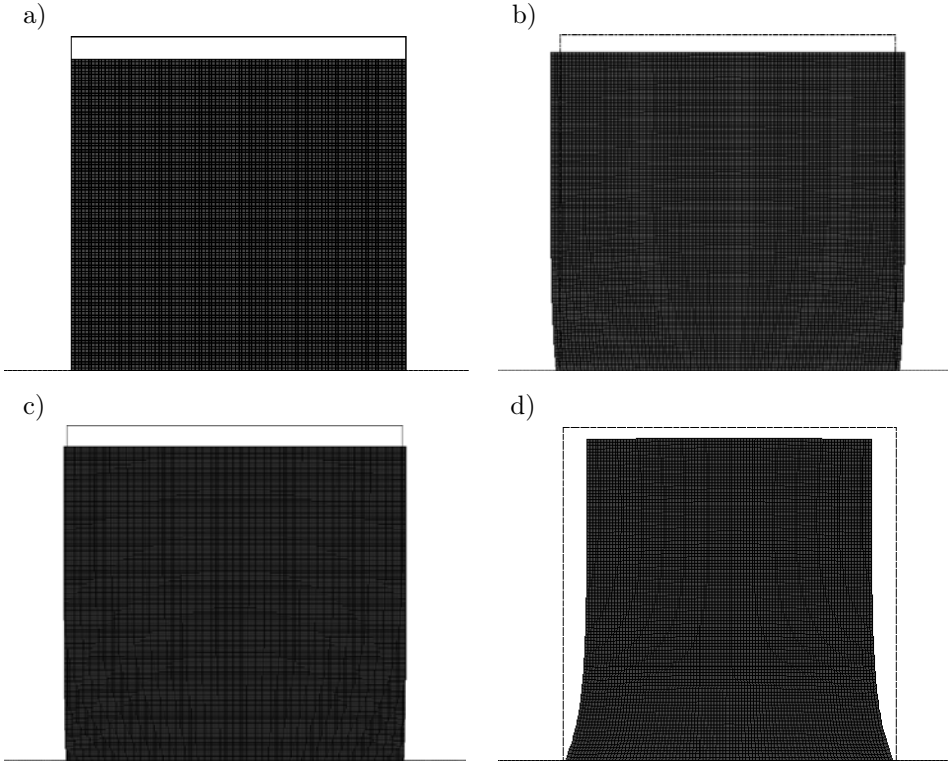

FIG. 4. Deformation of a square block of cellular material: a) square cell (material a) displacement scale 1500, b) honeycomb cell (material b) displacement scale 50, c) triangle (material c) displacement scale 1000, d) re-entrant (material d) displacement scale 3.

Differences in deformation types for structures with positive, zero, and negative Poisson's ratios can be observed.

Figures 5 and 6, show the relative contact pressure, friction stress distribution and contact status along the contact line.

It can be clearly seen from Fig. 5 that the most advantageous contact stress distributions correspond to a material with nonpositive Poisson's ratio. For material a) characterized by $\nu_{XY} = 0$, contact pressure is constant and friction

stress vanishes. For structure d) with $\nu_{XY} < 0$ contact pressure is homogenous in the centre of contact zone, and decreasing near the edges. Friction stress maximum appears at the point where slip begins. Figure 6 shows contact separation at the corners for this material. Structures b) and c), characterized by positive, constant ν, show the well-known pick contact pressure and friction force at the corners of the contact zone. This concentration is much greater for structure b) with ν equal to 0.96 in comparison to material with c) structure where ν attains the value 0.3.

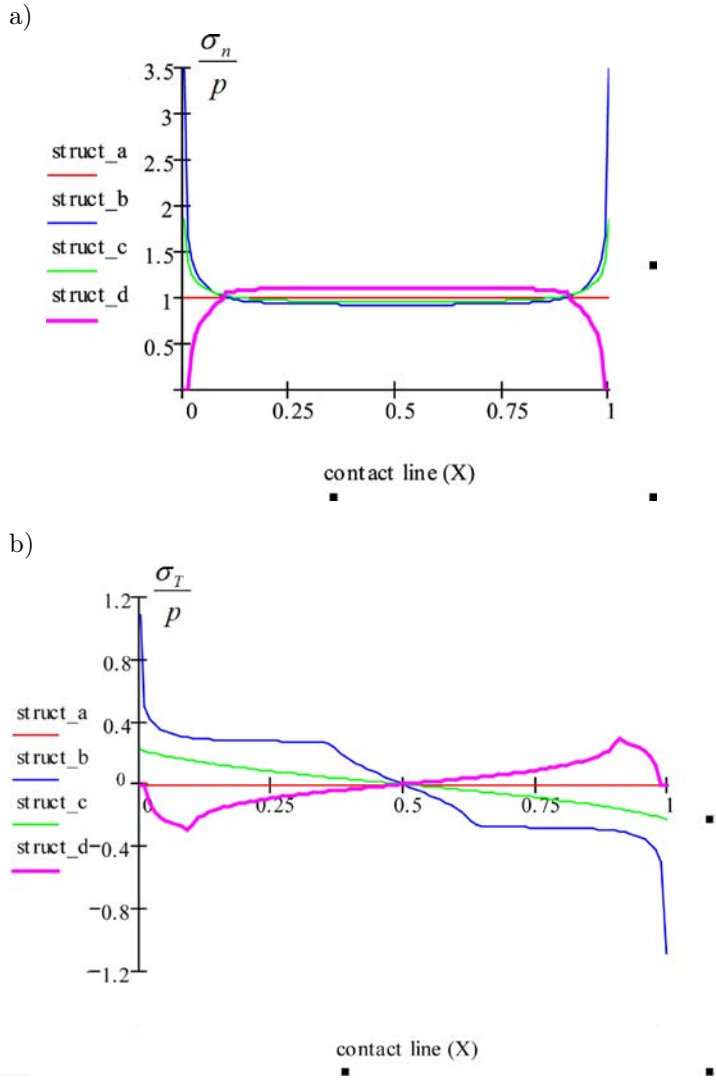

FIG. 5. Contact pressure and friction stress distribution along the contact line for different cell types.

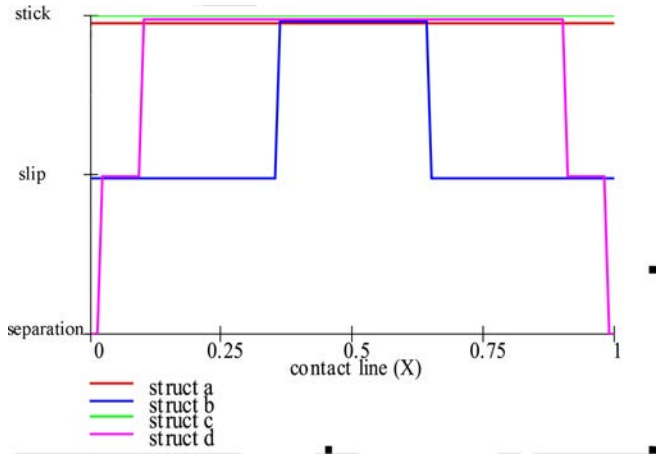

FIG. 6. Contact status (stick slip and separation zones) for different cell types.

During calculations, the energy-based yield criterion (3.20) is checked to ensure work in elastic range. Distribution of material strength coefficient for materials with structures b), c), and d) are shown in Fig. 7. For material with structure a) the value of this coefficient is constant ($\varphi = 1.0\text{E-}5$). Vanishing of

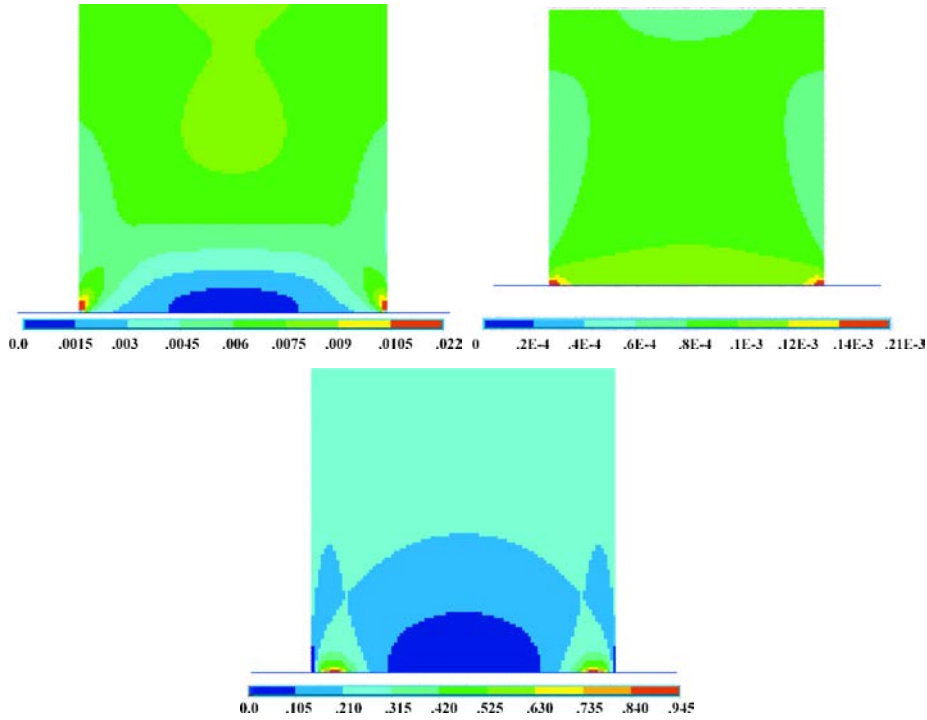

FIG. 7. Distribution of the material strength coefficient for material of structures b), c), d).

Poisson's ratio results in the lack of friction in this loading case. For structures with positive Poisson's ratio, the material strength coefficient reaches maximum in the corners of contact surface as a result of peak contact pressure. Points with maximum coefficient for structure d) correspond with maximum friction force. Reduction of the material strength in the center of contact area for structures b) and d) can be explained by energy considerations in microscale.

For the considered cellular materials, the results of numerical calculations are summarised in Table 3. The last column of this table presents the ratio of applied pressure to the admissible vertical load in nonfrictional case ($p_{y\,\max}$) for estimation of applicability of the chosen material to the given contact problem.

Table 3. Results for different cell types

Structure type	$\sigma_{n\,\max}/p$	$\sigma_{t\,\max}/p$	$\varphi_{\max}$	$p/p_{y\,\max}$
a)	1	0	0.00001	0.004
b)	3.6	1.08	0.022	0.083
c)	1.85	0.23	0.0002	0.009
d)	1.09	0.28	0.95	0.492

4.2. Square block made of re-entrant cellular material with different location of cell axis with respect to the contact line

Square block with geometry and contact data as in Example 4.1 with pressure $p = 4$ kN/m applied to its upper edge is analyzed. The block is made of re-entrant cell structure d) with skeleton material data and geometry of the unit cell as in Table 1, but with different placing of the cell symmetry axis with respect to the global coordinate system (and subsequently to body geometry, load and contact line). Calculations were made for three chosen angle values: 0, 45, and 90 degrees (see Fig. 2). Macroscopic, anisotropic material constants for those cases are presented in Table 4.

Table 4. Anisotropic material constants for different β angles.

β	E_X [MPa]	E_Y [MPa]	ν_{XY}	ν_{YX}	$p/p_{y\,\max}$
0	1.954	0.128	−3.85	−0.26	0.31
45	0.104	0.104	0.365	0.365	0.38
90	0.128	1.954	−0.26	−3.85	0.08

Numerical results are visualized in Figs. 8–11. The greatest vertical load capacity and the smallest Poisson's ratio $\nu_{YX} = -3.85$ correspond to the angle 90 degrees. It causes the reduction of contact pressure, and hence of the friction stress near the ends of contact line with separation at the corners. A more

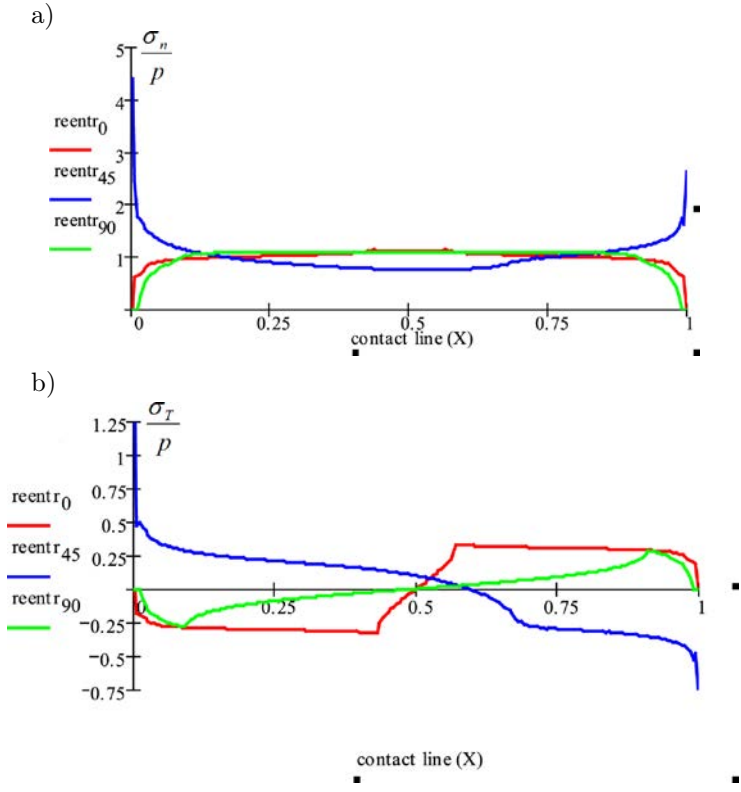

FIG. 8. Contact pressure and friction stress distribution along contact line for different reentrant cell orientation.

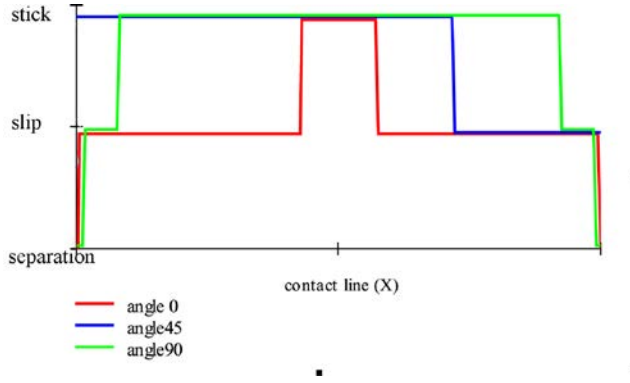

FIG. 9. Contact status (stick, slip, and separation zones) for different re-entrant cell orientation.

uniform contact pressure distribution appears for the angle of 0 degrees, with negative, but smaller absolute value of Poisson's ratio $\nu_{XY} = -0.26$. The skew placement of the cell results in positive Poisson's ratio, peak contact stresses at

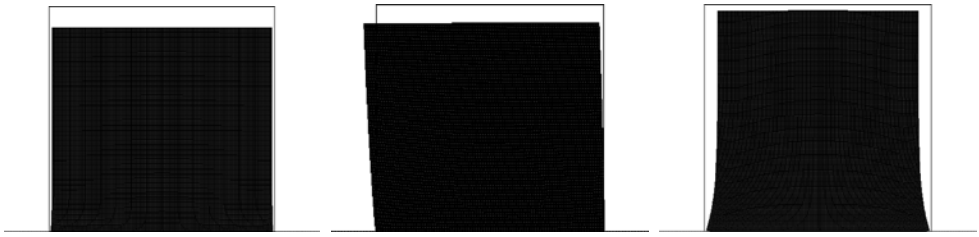

FIG. 10. Deformation of a square block made of reentrant cell microstructure for different cell orientations: $\beta = 0$ deformation scale 3, $\beta = 45$ deformation scale 2, and $\beta = 90$ deformation scale 15.

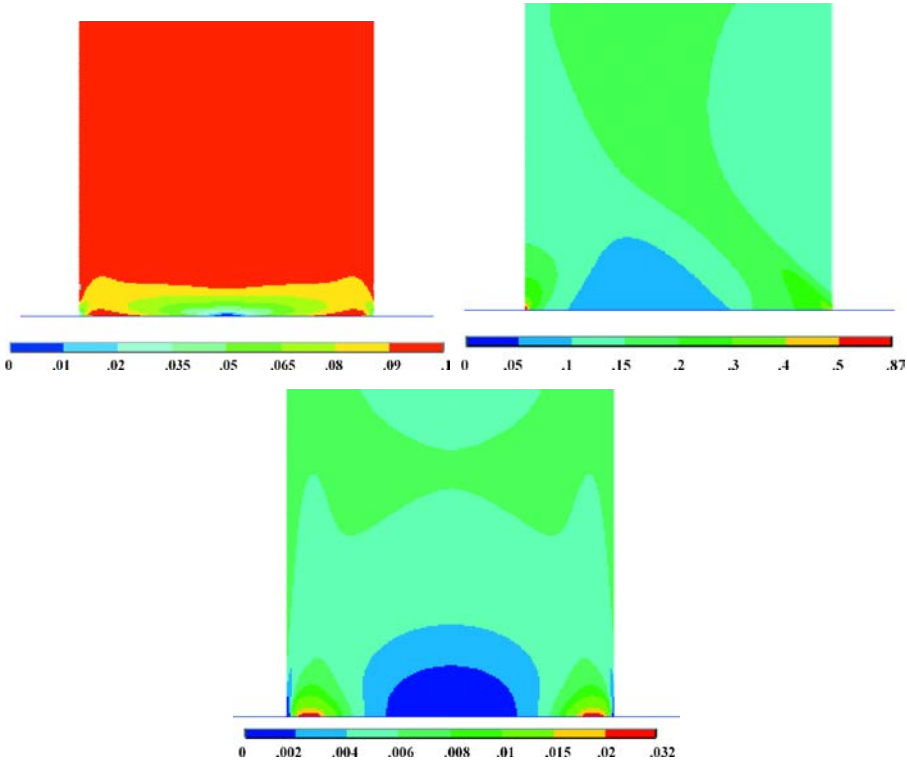

FIG. 11. Distribution of material strength coefficient for different reentrant microstructure orientation: β=0, β=45, and β=90.

the corners, and unsymmetric deformation despite the symmetric boundary conditions, due to lack of symmetry in microstructure. For 90 degrees angle, despite the smallest $\nu_{YX} = -3.85$, the stick area dominates in contact zone (Fig. 9). It is caused by domination of the resultant shear modulus over the bulk modulus. Directional proportion G/K reveals dilatational properties of the considered material and determines the relation of shear and dilatational deformation. For 0 degrees, a more uniform deformation (Fig. 10), and predominance of slip in

contact area (Fig. 9) is observed. Distributions of material strength coefficient are presented in Fig. 11. In all cases the reduction of material strength can be noticed in the center of contact zone. It can be explained by considerations on a microscale level.

4.3. Square block made of material of square cells with different locations of cell axis with respect to contact line

For comparison with the previous example, a block with the same geometry, load and boundary conditions, but made of material with structure a) (square cell) with different orientations of the cell symmetry axis with respect to global coordinate system is considered. The chosen angle values are: 0 and 45 degrees (due to structure symmetry the results for 0 and 90 degrees agree).

Material constants are given in Table 5.

Table 5. Anisotropic material constants for different β angles.

β	E_X [MPa]	E_Y [MPa]	ν_{XY}	ν_{YX}	$p_y/p_{y\,\max}$
0	576.92	576.92	0	0	0.0005
45	3.795	3.795	0.99	0.99	0.018

Figures 12–15 present the results of numerical calculations.

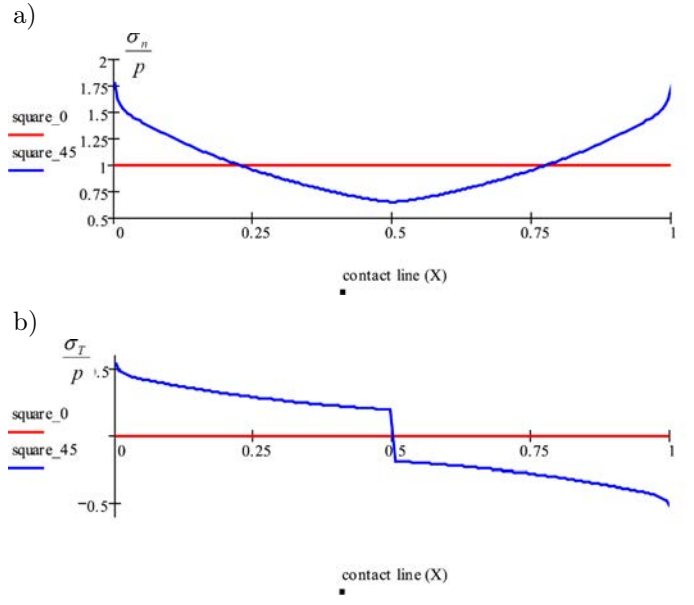

FIG. 12. Relative contact pressure and friction stresses distribution along the contact line for different square cell orientations.

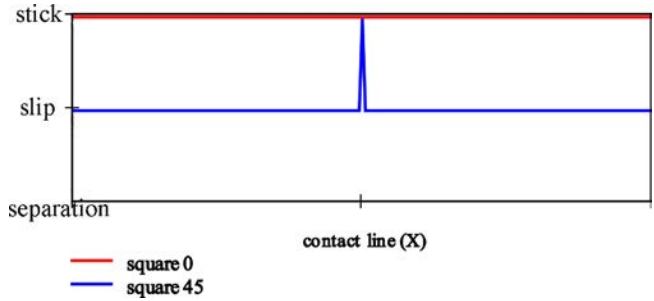

FIG. 13. Contact status (stick, slip, and separation zones) for different square cell orientations.

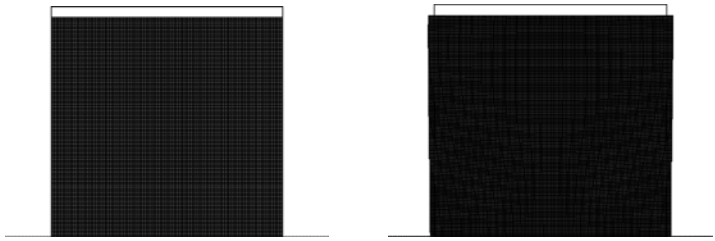

FIG. 14. Deformation of the body for different square cell orientations: $\beta = 0$ deformation scale 10000, $\beta = 45$ deformation scale 50.

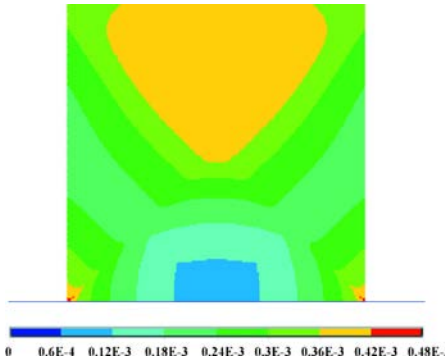

FIG. 15. Distribution of the material strength coefficient for square cell structure with orientation: $\beta = 45$.

Skew placement of the cell ($\beta = 45$) resulting in high positive Poisson's ratio leads to peaks of normal and tangential contact stresses (Figs. 12, 13), and concentration of the material strength (Fig. 15) in the corners of the contact line. Directions of reduction of the material strength coefficient for this case correspond with the maximum stiffness directions (see Appendix B). Unlike the re-entrant cell, in Example 4.2, deformation in this case is symmetrical, due to square structure symmetry for 45 degrees. For material orientation given by $\beta = 0$ ($\nu_{XY} = \nu_{YX} = 0$), the contact pressure is constant, friction stress equals

zero, and the material strength is uniform. The value of the material strength coefficient is $\varphi = 2.5\text{E-}7$.

Detailed comparison of results of the numerical examples presented above shows that stress field and contact status depend on macroscopic material properties, especially on Poisson's ratio. This ratio for cellular materials depends mainly on the topology of microstructure. The analysed structures of types b) and c) give isotropic material with positive Poisson's ratio and hence high peak contact pressure and friction stresses.

Structure d) (re-entrant) gives a compliant material with negative Poisson's ratios for a broad range of angles ($\beta \in (-18°, 18°) \cup (72°, 108°)$) (see Appendix B, point d). So the assumption that deformation at small strains does not influence the material properties can be adopted in this case. Such a material with proper placement with respect to the contact line can produce advantageous contact pressure distributions with reductions in the corners of the contact area.

Structure a), with cell symmetry axis parallel to contact line, gives a very stiff material with zero Poisson's ratio. It might seem to be most advantageous for the class of contact problems presented above (with loads perpendicular to the contact line and hence without global sliding), because it produces uniform contact pressure and zero friction stress. However it is worth to notice that material of structure a) has zero Poisson's ratio, only for unit cell placed exactly parallel to the coordinate frame. Graph of dependence of ν_{XY} on the angle of cell orientation shows that for all angles other than 0 and 90, the Poisson's ratio is positive and can reach high values, even in the close neighbourhood of 0 and 90 (see Appendix B, point a). The assumption, typical for linear analysis, that initial configuration of the structure is the reference configuration may be inappropriate in this case. It may cause that advantageous properties of the material can be overestimated. Real contact properties, especially for materials with Poisson's ratio very sensitive to cell orientation, should be obtained as a result of full nonlinear analysis, in which anisotropic effective properties of material are dependent on local configuration of the deformed body.

5. Conclusions

An analysis of static contact of cellular solid with rough stiff foundation is undertaken. Micromechanical model of cellular material is applied to predict mechanical properties on a macroscale. The study is focused on prediction of the stress distribution in contact zone and the material strength in the elastic range. Cellular materials, due to a variety of structure topology, what results in different types of material symmetry and macroscopic properties, can be tailored to special demands of the given problem. The example of contact shows that differences in behaviour can be essential and clearly visible. Special attention is paid to materi-

als with anisotropic properties, especially to materials with re-entrant structure, which give negative Poisson's ratio in a certain range of directions. Proper choice of microstructural geometrical parameters can determine the expected elastic properties. These properties and the orientation of material symmetry axis with respect to the load direction can significantly influence the contact stress distribution and may play an important role in reducing the contact peak pressure. Comparison of a material with square cells with a material of re-entrant structure allows to point out a more advantageous type of microstructure by discussion of the influence of directional material properties on the results of given example.

The contact mechanics of cellular materials is important for their friction and wear behaviour and also, under static conditions, in applications as antivibrating supports. The first topic requires consideration on a microscale and with the two-scale modelling approach can be promising area for research. The second topic requires analysis on a macro scale. The work on this problem started in this paper can be developed.

Appendix A.
Stiffness matrices, Kelvin moduli, eigenstates and critical energies

Notation: $\mathbf{S}$ – stiffness matrix, λ_α – eigenvalues of $\mathbf{S}$, ${}^{\alpha}\tilde{\boldsymbol{\varepsilon}}$ – strain eigenstates, k_α – scalar multiplier for critical eigenstate, ${}^{\alpha}\Phi_E^{\mathrm{gr}}$ – critical energies in eigenstates, $\alpha = \mathrm{I}, \mathrm{II}, \mathrm{III}$. L, h, t, γ – microstructural parameters (Fig. 1), E_s, v_s, R_e – skeleton material parameters.

a) Square cell structure

$$\mathbf{S} = \begin{bmatrix} \dfrac{E_s t}{L} & 0 & 0 \\ 0 & \dfrac{E_s t}{L} & 0 \\ 0 & 0 & \dfrac{E_s t^3}{L^3} \end{bmatrix},$$

$$\lambda_{\mathrm{I}} = \frac{E_s t}{2l_i}, \qquad \lambda_{\mathrm{II}} = \frac{E_s t}{2l_i}, \qquad \lambda_{\mathrm{III}} = \frac{E_s t^3}{8l_i^3},$$

$${}^{\mathrm{I}}\tilde{\boldsymbol{\varepsilon}} = (1,\, 1,\, 0)\,, \qquad {}^{\mathrm{II}}\tilde{\boldsymbol{\varepsilon}} = (1,\, -1,\, 0)\,, \qquad {}^{\mathrm{III}}\tilde{\boldsymbol{\varepsilon}} = (0,\, 0,\, 1)\,,$$

$$k_{\mathrm{I}} = \frac{R_e}{E_s}, \qquad k_{\mathrm{II}} = \frac{R_e}{E_s}, \qquad k_{\mathrm{III}} = \frac{R_e}{E_s}\frac{2\sqrt{2}l_i}{3t},$$

$${}^{\mathrm{I}}\Phi_E^{\mathrm{gr}} = \frac{R_e^2}{E_s}\frac{t}{2l_i}, \qquad {}^{\mathrm{II}}\Phi_E^{\mathrm{gr}} = \frac{R_e^2}{E_s}\frac{t}{2l_i}, \qquad {}^{\mathrm{III}}\Phi_E^{\mathrm{gr}} = \frac{R_e^2}{E_s}\frac{t}{9l_i},$$

$$2l_i = L,$$

b) honeycomb structure

$$\mathbf{S} = \begin{bmatrix} \frac{\sqrt{3}E_s t}{6L}\frac{\left(L^2+3t^2\right)}{\left(L^2+t^2\right)} & \frac{\sqrt{3}E_s t}{6L}\frac{\left(L^2-t^2\right)}{\left(L^2+t^2\right)} & 0 \\ \frac{\sqrt{3}E_s t}{6L}\frac{\left(L^2-t^2\right)}{\left(L^2+t^2\right)} & \frac{\sqrt{3}E_s t}{6L}\frac{\left(L^2+3t^2\right)}{\left(L^2+t^2\right)} & 0 \\ 0 & 0 & \frac{\sqrt{3}E_s t^3}{3L\left(L^2+t^2\right)} \end{bmatrix},$$

$$\lambda_{\mathrm{I}} = \frac{\sqrt{3}}{6}\frac{E_s t}{l_i}, \qquad \lambda_{\mathrm{II}} = \lambda_{\mathrm{III}} = \frac{\sqrt{3}}{3}\frac{E_s t^3}{l_i\left(4l_i^2+t^2\right)},$$

$${}^{\mathrm{I}}\tilde{\boldsymbol{\varepsilon}} = (1,\,1,\,0)\,, \qquad {}^{\mathrm{II}}\tilde{\boldsymbol{\varepsilon}} = (1,\,-1,\,0)\,, \qquad {}^{\mathrm{III}}\tilde{\boldsymbol{\varepsilon}} = (0,\,0,\,1)\,,$$

$$k_{\mathrm{I}} = \frac{R_e}{E_s}, \qquad k_{\mathrm{II}} = \frac{R_e}{E_s}\frac{\left(4l_i^2+t^2\right)}{\left(2l_i^2+t^2+3\sqrt{3}tl_i\right)}, \qquad k_{\mathrm{III}} = \frac{R_e}{E_s}\frac{\sqrt{2}\left(4l_i^2+t^2\right)}{(6l+t)\,t},$$

$${}^{\mathrm{I}}\Phi_E^{\mathrm{gr}} = \frac{R_e^2}{E_s}\frac{\sqrt{3}t}{12l_i}, \qquad {}^{\mathrm{II}}\Phi_E^{\mathrm{gr}} = \frac{R_e^2}{E_s}\frac{\sqrt{3}\left(4l_i^2+t^2\right)t^3}{6l_i\left(2l_i+t^2+3\sqrt{3}l_i t\right)^2},$$

$${}^{\mathrm{III}}\Phi_E^{\mathrm{gr}} = \frac{R_e^2}{E_s}\frac{\sqrt{3}t}{3l_i}\frac{\left(4l_i^2+t^2\right)}{\left(6l_i+t\right)^2},$$

c) equilateral triangular structure

$$\mathbf{S} = \begin{bmatrix} \frac{\sqrt{3}E_s t\left(3L^2+2t^2\right)}{4L^3} & \frac{\sqrt{3}E_s t\left(L^2-t^2\right)}{4L^3} & 0 \\ \frac{\sqrt{3}E_s t\left(L^2-t^2\right)}{4L^3} & \frac{\sqrt{3}E_s t\left(3L^2+2t^2\right)}{4L^3} & 0 \\ 0 & 0 & \frac{\sqrt{3}E_s t}{4L} \end{bmatrix},$$

$$\lambda_{\mathrm{I}} = \frac{\sqrt{3}}{6}\frac{E_s t}{l_i}, \qquad \lambda_{\mathrm{II}} = \lambda_{\mathrm{III}} = \frac{\sqrt{3}}{3}\frac{E_s t^3}{l_i\left(4l_i^2+t^2\right)},$$

$$^{\mathrm{I}}\tilde{\boldsymbol{\varepsilon}} = (1,\, 1,\, 0)\,, \qquad ^{\mathrm{II}}\tilde{\boldsymbol{\varepsilon}} = \left(1,\, -1,\, ^{0}\right), \qquad ^{\mathrm{III}}\tilde{\boldsymbol{\varepsilon}} = (0,\, 0,\, 1)\,,$$

$$k_{\mathrm{I}} = \frac{R_e}{E_s}, \qquad k_{\mathrm{II}} = \frac{R_e}{E_s}\frac{\left(4l_i^2 + t^2\right)}{\left(2l_i^2 + t^2 + 3\sqrt{3}tl_i\right)}, \qquad k_{\mathrm{III}} = \frac{R_e}{E_s}\frac{\sqrt{2}\left(4l_i^2 + t^2\right)}{(6l + t)\,t},$$

$$^{\mathrm{I}}\Phi_E^{\mathrm{gr}} = \frac{R_e^2}{E_s}\frac{\sqrt{3}\left(4l_i^2 + t^2\right)t}{64l_i^3}, \qquad ^{\mathrm{II}}\Phi_E^{\mathrm{gr}} = \frac{R_e^2}{E_s}\frac{2\sqrt{3}l_i t}{\left(2l_i + 3\sqrt{3}t\right)^2}, \qquad ^{\mathrm{III}}\Phi_E^{\mathrm{gr}} = \frac{R_e^2}{E_s}\frac{\sqrt{3}l_i}{96t},$$

d) Inverted honeycomb, re-entrant structure.

$$\mathbf{S} = \begin{bmatrix} s_{1111} & s_{1122} & 0 \\ s_{1122} & s_{2222} & 0 \\ 0 & 0 & 2s_{1212} \end{bmatrix},$$

$$\lambda_{\mathrm{I}} = \frac{1}{2}\left(s_{1111} + s_{2222} - \sqrt{\left(s_{1111} - s_{2222}\right)^2 + 4s_{1122}^2}\right),$$

$$\lambda_{\mathrm{II}} = \frac{1}{2}\left(s_{1111} + s_{2222} + \sqrt{\left(s_{1111} - s_{2222}\right)^2 + 4s_{1122}^2}\right),$$

$$\lambda_{\mathrm{III}} = 2s_{1212},$$

$$^{\mathrm{I}}\tilde{\varepsilon}_x = 1.0, \qquad ^{\mathrm{I}}\tilde{\varepsilon}_y = \frac{\left(s_{2222} - s_{1111} - \sqrt{\left(s_{1111} - s_{2222}\right)^2 + 4s_{1122}^2}\right)}{2s_{1122}},$$

$$^{\mathrm{I}}\tilde{\varepsilon}_{xy} = 0,$$

$$^{\mathrm{II}}\tilde{\varepsilon}_x = 1.0, \qquad ^{\mathrm{II}}\tilde{\varepsilon}_y = \frac{\left(s_{2222} - s_{1111} + \sqrt{\left(s_{1111} - s_{2222}\right)^2 + 4s_{1122}^2}\right)}{2s_{1122}},$$

$$^{\mathrm{II}}\tilde{\varepsilon}_{xy} = 0,$$

$$^{\mathrm{III}}\tilde{\varepsilon}_x = 0, \qquad ^{\mathrm{III}}\tilde{\varepsilon}_y = 0, \qquad ^{\mathrm{I}}\tilde{\varepsilon}_{xy} = 1.0.$$

$\mathbf{S}$, k_α, $^{\alpha}\Phi_E^{\mathrm{gr}}$ – obtained numerically.

Appendix B.

Macroscopic material parameters and admissible vertical pressure in uniaxial tension in dependence on the angle of tension direction

Skeleton material data: $E_S = 10$ GPa, $\nu_S = 0.3$, $R_e = 10$ MPa.
Geometrical parameters of microstructures as given in Table 1.

a) Square cell structure (anisotropic material)
analytical formula:

$$E = \frac{E_s t^3}{L\left[t^2\left(1-\sin^2 2\alpha\right)+L^2\right]}, \qquad \nu = \frac{\left(L^2-t^2\right)\sin^2 2\alpha}{\left[t^2\cos^2 2\alpha + L^2\right]},$$

$$E_{\min} = E\left(\alpha = \frac{\pi}{4}\right) = \frac{E_s t^3}{L^3}, \qquad \nu_{\max} = \nu\left(\alpha = \frac{\pi}{4}\right) = \frac{\left(L^2-t^2\right)}{L^2},$$

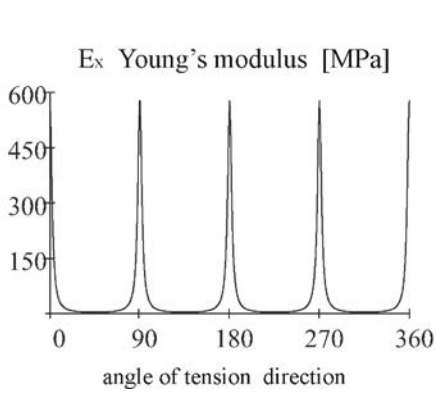

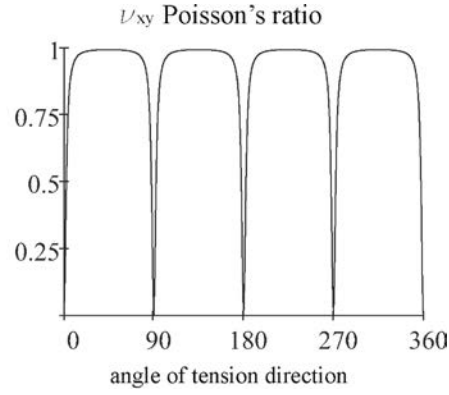

analytical formula:

$$p_{\max} = \frac{4R_e t^2}{L\left[4t^2\left(1+\cos^2 2\beta\right)+18L^2\sin^2 2\beta\right]^{1/2}}.$$

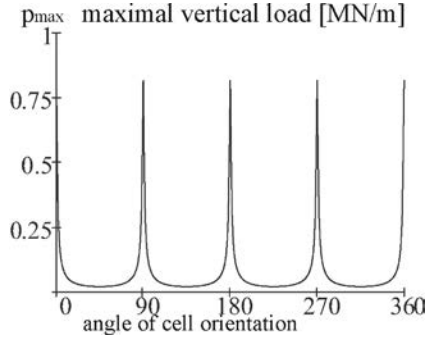

b) Honeycomb structure (isotropic material)
analytical formulae:

$$E = \frac{4E_s t^3}{\sqrt{3}L\left[3t^2+L^2\right]} = 21.87 \text{ MPa},$$

$$\nu = \frac{\left(L^2 - t^2\right)}{L^2 + 3t^2} = 0.96, \qquad \nu_{\max} = \nu\left(\frac{t}{L} \to 0\right) = 1,$$

$p_{\max} = 0.3$ MN/m.

c) Equilateral triangle cell structure (isotropic material)
analytical formulae:

$$E = \frac{\sqrt{3}E_s t\left(4L^2 + t^2\right)\left(2L^2 + t^2\right)}{4L^3\left[2t^2 + 3L^2\right]} = 385.47 \text{ MPa},$$

$$\nu = \frac{L^2 - t^2}{3L^2 + 2t^2} = 0.33, \qquad \nu_{\max} = \nu\left(\frac{t}{L} \to 0\right) = 0.333,$$

$p_{\max} = 2.77$ MN/m.

d) Re-entrant structure (anisotropic material)

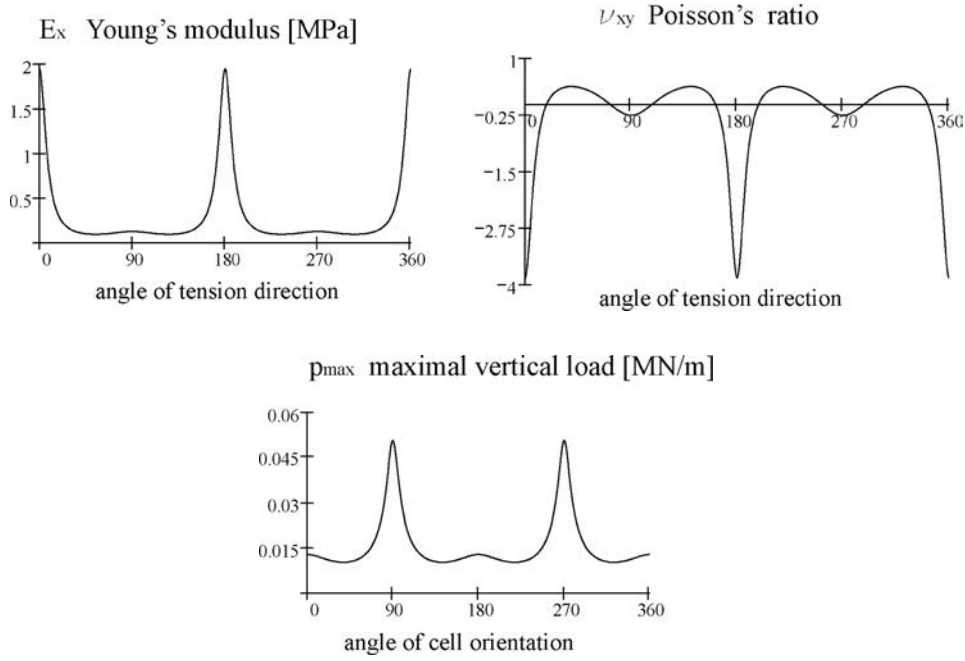

References

1. ANSYS 10.0 manual
2. M. Janus–Michalska, *Micromechanical model of auxetic cellular materials,* submitted for publication in Archives of Metallurgy and Materials.
3. M. Janus–Michalska, *Effective models describing elastic behaviour of cellular materials*, Archives of Metallurgy and Materials, **50**, 3, 595–608, 2005.

4. N. Kikuchi, J. T. Oden, *Contact problems in elasticity: a study of variational ineqalitiees and finite element methods*, SIAM, Philadelphia 1988.

5. P. Kordzikowski, M. Janus–Michalska, R. B. Pęcherski, *Specification of energy – based criterion of elastic limit states for cellular materials*, Archives of Metallurgy and Materials, **50**, 3, 621–634, 2005.

6. R. S. Lakes, *Foam structures with a negative Poisson's ratio*, Science, **235**, 1038–1040, 1987.

7. R. S. Lakes, *Design considerations for materials with negative Poisson's ratios*, Trans. ASME J. Mech., **115**, 696–700, 1993.

8. D. W. Overaker, A. M. Cuitino, N. A. Langrana, *Elastoplastic micromechanical modeling of two-dimensional irregular convex and nonconvex (re-entrant) hexagonal foams*, Transactions of ASME, **65**, 1998.

9. A. Scalia, *Contact Problem for porous elastic half-plane*, J. Elasticity, **60**, 91–102, 2000.

10. G. E. Stavroulakis, *Auxetic behavior: appearance and engineering applications*, Physica Status Solidi, **3**, 710–720, 2005.

11. G. Szefer, D. Kędzior, *Contact of elastic bodies with negative poisson's ratio*, Springer V., 2002.

12. Y. Wang, R. Lakes, *Analytical parametric analysis of the contact problem of human buttocks and negative Poisson's ratio foam cushions*, Int. J. Sol. Struc., **39**, 4825–38, 2002.

13. J. Rychlewski, *Unconventional approach to linear elasticity*, Arch. Mech., **47**, 149–171, 1995.

Received May 14, 2007; revised version February 11, 2008.

ENGINEERING TRANSACTIONS • *Engng. Trans.* • **56**, 3, 227–245, 2008
Polish Academy of Sciences • Institute of Fundamental Technological Research

CHANGES OF THE YIELD CONDITION DUE TO ACCUMULATION OF DAMAGE OF METAL ALLOYS

G. S o c h a

Materials and Structures Research Centre
Institute of Aviation
Al. Krakowska 110/114, 02-256 Warszawa, Poland

The results of the experimental investigations of fatigue damage accumulation and redistribution of residual stresses are reported in this paper. Local measurements of the inelastic response under constant stress amplitude were used to observe two phenomena for selected alloys. It was found that fatigue damage accumulation and redistribution of residual stress affect the yield condition for the investigated materials. Yield condition with damage parameter and the parameter representing residual stress state are proposed. The damage parameter is calculated, basing on the definition given in the author's previous paper. It was also found that the yield condition and damage parameters are different for dynamic (cyclic loading) and for static (for unloaded material) conditions. Physical interpretation for the observed experimental results is given in this paper. Fatigue damage accumulation is divided into three phases: cyclic stabilisation, local increase of crystal defects density, formation and propagation of the crack. Local methods of strain measurements, together with dynamic measurements of damage parameter, were found to be crucial for proper observation of fatigue damage accumulation.

Key words: fatigue damage accumulation, yield condition, residual stress.

1. Introduction

It is widely accepted that accumulation of the fatigue damage affects mechanical properties of elastic-plastic materials. Since local damage of crystal structure and formation of material discontinuities (cracks) underlie this process, progress of damage should be manifested by changes of the yield condition. These changes are usually described by hardening rules. Among the parameters of this rule, there should be at least one related to the progress of damage. If this is the case, using well-known techniques of yield locus determination we should be able to investigate accumulation of the fatigue damage due to service loads.

Many theoretical models have been proposed to describe the damage-introduced changes of the yield condition. Most of them assume that due to damage accumulation, the plastic anisotropy is introduced into material. Damage-introduced plastic anisotropy is a very complex phenomenon, general form of the

equation describing yield condition of anisotropic material consists of 21 constants [14]. Determination of all the constants is impossible in experimental manner using uniaxial tests like those of tension, compression or shear. Sophisticated complex-stress testing techniques have to be used to determine the yield locus of anisotropic material. For this reason, simplified models of plastic anisotropy, describing results of experiments with satisfactory accuracy are still searched. However many propositions, usually based on nonlocal yield condition of Drucker–Prager type, can be found in literature [15, 16] and [17], most of them lack any experimental verification. In a few cases such verification can be also found [18, 19] and [20]. In this paper, simple form of the yield condition taking into account the damage-induced plastic anisotropy is proposed. Such simple, physically motivated yield condition should be useful for investigation of damage accumulation, quantifying damage and estimation fatigue life of engineering materials subject to complex stress states and complicated loading histories. Moreover, anisotropy parameters used in this model are easy to determine with the use of simple tests (tension, compression or shear tests).

Many researchers still intensively investigate accumulation of the fatigue damage due to service loads for elastic-plastic materials such as metal alloys. Basic concepts like the SN curve and Linear Damage Rule (LDR) were formulated long time ago ([1–3]), but the use of such a simple method for prediction of the fatigue life can lead to enormous over- or underestimation. There are many reasons for such a situation. The most important is the fact that traditional testing technique is not suitable for observation of the damage progress during the test. Usually, the number of cycles to failure at a given amplitude of test controlling parameter (stress, strain or others) is the only result of such a test. Having no data concerning the damage progress, one can only assume a damage model (the manner, in which accumulation of the fatigue damage progresses). In the engineering practice, fatigue life prediction is in most cases (more than 90%) based on the Palmgren-Miner concept of linear damage rule (LDR); in a very few cases more complex theories are used (double-linear [4], non-linear [5]). Experimental verification of the applied damage model is crucial for obtaining accurate and credible fatigue life prediction. Any observation of the damage progress requires a definition of the measurable damage parameter. Changes of this parameter during the fatigue test can be plotted as a function of the load cycle number or cycle ratio. Such an experimentally determined plot, usually described as the damage curve, uniquely determines the proper damage model to be applied.

In publications, many definitions of the damage parameters can be found. A good review of the state-of-the art was given in [6]. A brief summary of the most popular damage quantifying parameters is shown in Table 1. Those parameters are divided into three groups: mechanical, physical and metallurgical. Mechanical parameters are usually measured in the strength laboratory. Some of

them, such as the elasticity modulus, strain or stress amplitude changes under constant stress or strain amplitude, inelastic strain or strain energy, can be measured during the fatigue tests. Many attempts to investigate the fatigue damage accumulation have been made, but consistent, sufficiently accurate and credible data were not collected. The reason for such a situation lies in the measurement technique and it will be discussed later. Other mechanical parameters: fatigue limit, tensile strength, ductility, hardness, must be measured with the use of the destructive test (e.g. static tension), so on-line observation of the damage progress during the fatigue test using such parameters is not possible.

Table 1. Damage parameters.

Mechanical	Physical	Metallurgical
Elastic modulus	Velocity or attenuation of ultrasonic waves	Number of dislocations
Stress amplitude	Magnetic properties	Diameter of the dislocation cell
Strain amplitude	Electric potential	Shear band spacing
Inelastic strain amplitude	Temperature	Surface density of shear bands
Strain energy	Acoustic Emission	Crack front length
Others: fatigue limit, tensile strength, ductility, hardness	Others: density, X-ray diffraction, positron annihilation	Crack area

However, changes of mechanical properties are undoubtedly related to the damage progress, for most of them the damage-induced changes are very small. Some of them are influenced by other phenomena such as strain-hardening or residual stress redistribution. An additional disadvantage of the above-mentioned mechanical damage parameters is that they cannot be used for inspections of real construction components as non-destructive inspection techniques (NDI). Such inspection techniques are usually based on measurements of physical properties. Measurement of: velocity or attenuation of ultrasonic wave, magnetic properties [21], electric conductivity, temperature, acoustic emission, density, X-ray diffraction or positron annihilation, is widely used for detection of material physical discontinuities. There have also been attempts to use such techniques for detection of damage accumulation in the phase preceding formation of physical discontinuities in the investigated material ([22] and [23]). If such an indirect damage detection technique could be considered to be credible, one has to prove that the changes of the physical property in question are related to the fatigue

damage accumulation. This can be achieved only by performing calibration of this technique with the use of a set of the calibration specimens (specimens with a known amount of damage introduced in laboratory environment). For the preparation of such specimens it is necessary to define measurable and physically based damage parameter, allowing accurate measurements of the accumulated fatigue damage.

Since it is well known that accumulation of the damage results in structural changes, direct methods of damage measurements can be based on structural observations [24]. Among the propositions of metallurgical damage parameters the best known are: the number of dislocations, diameter of the dislocation cell, shear band spacing, surface density of shear bands, crack front length or summary crack area. Some of those parameters correspond to the phenomenon of initial phase of the fatigue damage process (dislocations, shear bands) and the remaining ones characterize physical discontinuities (cracks) propagating in the material. However, crack is the most obvious and measurable effect of the fatigue damage process, but it can be detected only in the final phase of the process and sometimes it is too late to avoid disaster. Damage parameters based on the crack size measurements are well known; probably the most popular is Kachanow's definition [7]. His proposition: the surface density of cracks, was well received by theoreticians and was later developed by Murakami [8] into a second-rank tensor representing damage of the material. From the practical point of view, this proposition has two serious disadvantages: first of all, the use of this definition is limited only to the final phase of the process, so it is useless for early damage measurements and, what is even more important in engineering practice, it is not measurable before the final failure of the construction component takes place.

It is well known that the stress concentration zone forms around the crack tip under load. For the elastic-plastic material such stress concentration results in formation of a plastic zone, even if the bulk of undamaged material is still stressed below the yield limit. It means that for the load which should give us theoretically an elastic response of the material, due to the local yielding at the crack tip, this response starts to be non-linear. This phenomenon can also be macroscopically observed as the decrease of the yield limit. For a constant stress amplitude cyclic loading, nucleation and growth of the micro-cracks should in this case produce the increase of local inelastic strain amplitude (hysteresis loop width).

If the crystal structure defect such as dislocation is generated, it increases locally the Stacking Fault Energy and lowers the energy necessary to activate (move) the slip system. This effect can be also macroscopically observed as decrease of the yield stress. It is well known, that theoretical yield stress calculated for a perfect crystal on the basis of elastic constants and geometry of the crystal cell, is several times greater than the one observed in the case of real materials.

This is because real materials always possess some defects of their crystal structure (under cyclic load it leads to stress-strain hysteresis, even if the maximum stress is below the yield stress). Generation of new defects under cyclic load must then result in a decrease of macroscopically measured yield stress. If the yield stress for the investigated material decreases, increase of the inelastic response (amplitude) is observed under a constant stress amplitude.

As it was mentioned before, there are two kinds of structural changes revealed in the material due to the progress of the damage: defects of crystal structure and physical discontinuities. A physically based damage parameter should be sensitive to the increase of both the number of defects and propagation of physical discontinuities. Proposition of such a parameter was given in author's paper [9]. This proposition is based on the assumption, that both the mentioned kinds of damage-induced defects result in the local decrease of yield stress. For real materials, yielding is a continuous process, it may start locally much earlier than yielding of the material bulk takes place. Although different definitions of the yield stress are available (offset yield limit, upper or lower yield limit), none of them is to be regarded as the stress state separating purely elastic deformation and material yielding. This makes accurate measurements of yielding onset very difficult. A much better technique is based on the application of the constant amplitude cyclic stress, with simultaneous measurement of inelastic strain amplitude. Increase of such an inelastic response is related to changes of the yield stress and reflects redistribution of residual stress and progress of damage.

It is very important that the same result can be expected due to the generation of crystal defects and formation of physical discontinuities. This result – increase of inelastic response under constant load amplitude - was successfully detected and observed using experimental technique described in paper [10]. The definition of damage parameter, based on analysis of the obtained data is given below:

$$D = \frac{\Delta\varepsilon^i - \Delta\varepsilon_0^i}{\Delta\varepsilon_f^i - \Delta\varepsilon_0^i}, \tag{1.1}$$

where $\Delta\varepsilon^i$ denotes the value of inelastic strain range for the load cycle under consideration, $\Delta\varepsilon_0^i$ stands for the initial value of inelastic strain range at the considered stress amplitude and the final value $\Delta\varepsilon_f^i$ corresponds to the instant of material damage. It is crucial that all the parameters included in the Eq. (1.1) must be determined with the use of local methods of strain measurements. Application of the traditional methods requires uniform stress and strain distribution in the specimens gauge part. If this distribution is not homogeneous, such methods fail and production of consistent results regarding damage accumulation is impossible.

2. Fatigue damage of elastic-plastic material as a three-phase process

Physical phenomena underlying accumulation of the fatigue damage are nowadays well recognized. Structural observations carried out by many researchers allowed to conclude that in early stages, the fatigue damage results from slipping of crystal defects. As it was mentioned in the last paragraph, even if the global stress is below the yield limit, zones of stress concentration can be found in polycrystalline materials. In this zone, a local slip of crystal defects can be observed. As the result of that local slip, new crystal defects are generated and the Stacking Fault Energy increases locally. This process can finally lead to a situation in which maximum principal service stress is greater than the local decohesion stress. As a result, crack starter in the form of physical discontinuity is formed. This process was observed in paper [10], with the use of inelastic response measurements performed during the fatigue test. It must be recalled at this point, that the performed tests were stress-controlled with constant amplitude. Fully reversible stress cycle ($R = -1$) was applied to avoid any ratchetting behaviour. All tests were performed in ambient temperature, the load oscillation frequency was 20 Hz. Specimen designed according to ASTM requirements is shown in Fig. 1. Hourglass design was used to concentrate the stress in the narrowest cross-section. For this cross-section, the fatigue damage accumulation rate was assumed to be the highest. Transversal extensometer was used to measure the change of the specimen diameter. Local transversal strain ε_{22} was calculated for the narrowest cross-section, and using the well-known formula:

$$\varepsilon_{11} = -\frac{\varepsilon_{22}}{\nu}, \tag{2.1}$$

axial strain ε_{11} was calculated. The value of Poisson's ratio ν was assumed to be -0.33 for the elastic range and -0.5 for the plastic range. The recorded data

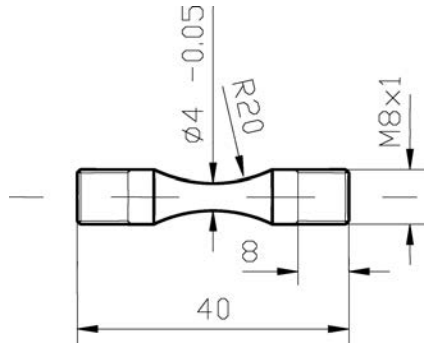

Fig. 1. Design of the specimen. Dimensions in mm.

(axial strain and stress) were used to plot the hysteresis loop shown in Fig. 2. Width of such a hysteresis loop $\Delta\varepsilon^i$ shown in this figure, called further the local inelastic response, was recorded for selected load cycles. Local inelastic response was plotted in a double logarithmic frame as a function of the load cycle number. As a result, the plot illustrating fatigue damage accumulation was obtained.

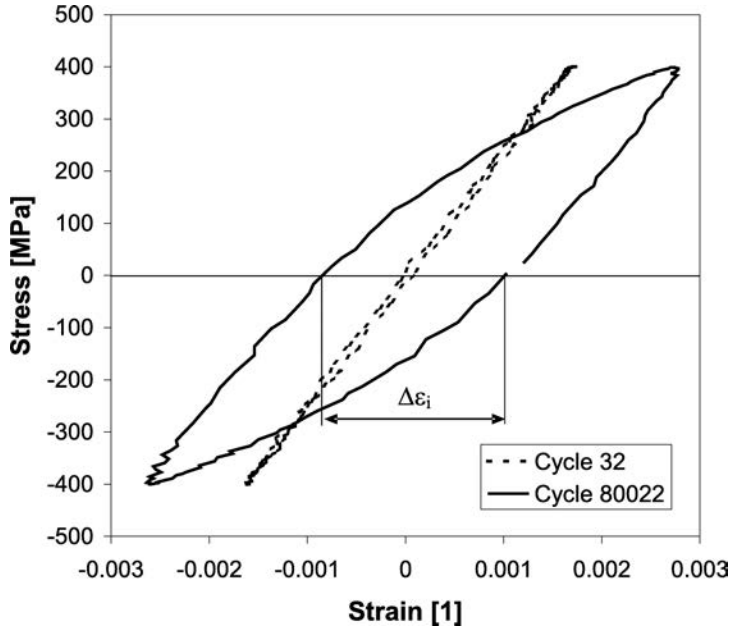

FIG. 2. Example of hysteresis loop recorded for selected cycles of load with indicated inelastic response for 80022 load cycle.

Examples of the recorded data are shown in Fig. 3 for the steel A 336 GR5 and in Fig. 4 for A 387 GR22. In both figures, one of the data sets represents a typical HCF test: for A 336 GR5 the stress amplitude 350 MPa is slightly above the endurance limit (342 MPa) and similarly, for A 387 GR22 the stress amplitude was set to 475 MPa (endurance limit 462 MPa). For such a small stress amplitude, the process of fatigue damage accumulation can be divided into three phases differing in the rate of inelastic response increase. During the first phase, no progress of damage can be observed, response of the material is quasi-elastic with constant width of the hysteresis loop – inelastic strain range for a cycle of load remains constant. At the end of the first phase, due to local increase of the Stacking Fault Energy new defects of crystal structure begin to be generated. This phenomenon, the local increase of crystal defects density, continues during the second phase of the fatigue damage process occupying about 80% of the fatigue life. As the local density of defects reaches the critical value,

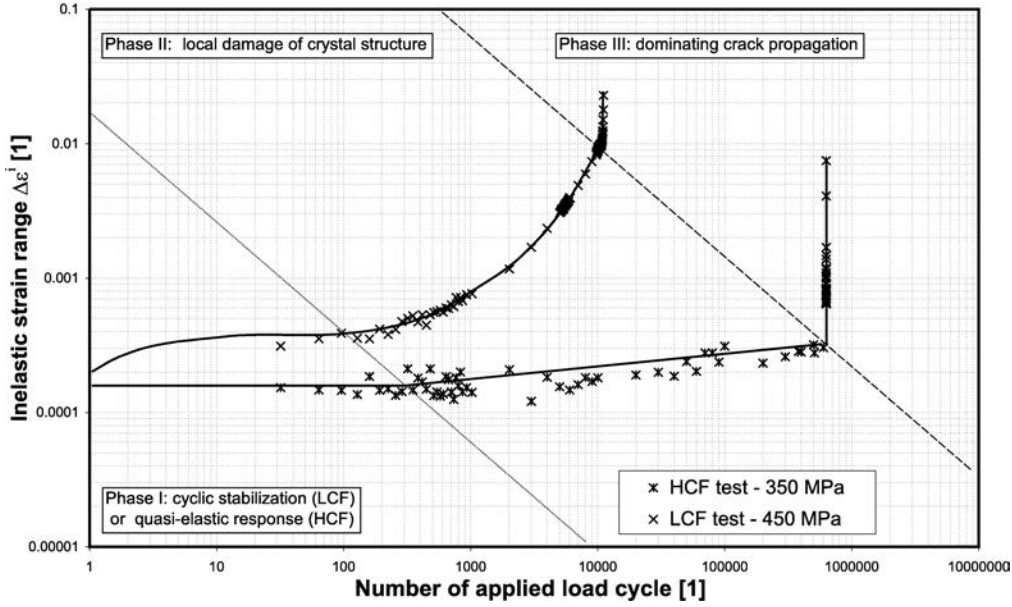

FIG. 3. Inelastic response as a function of the applied load cycle number for HCF and LCF test – A336 GR5 steel.

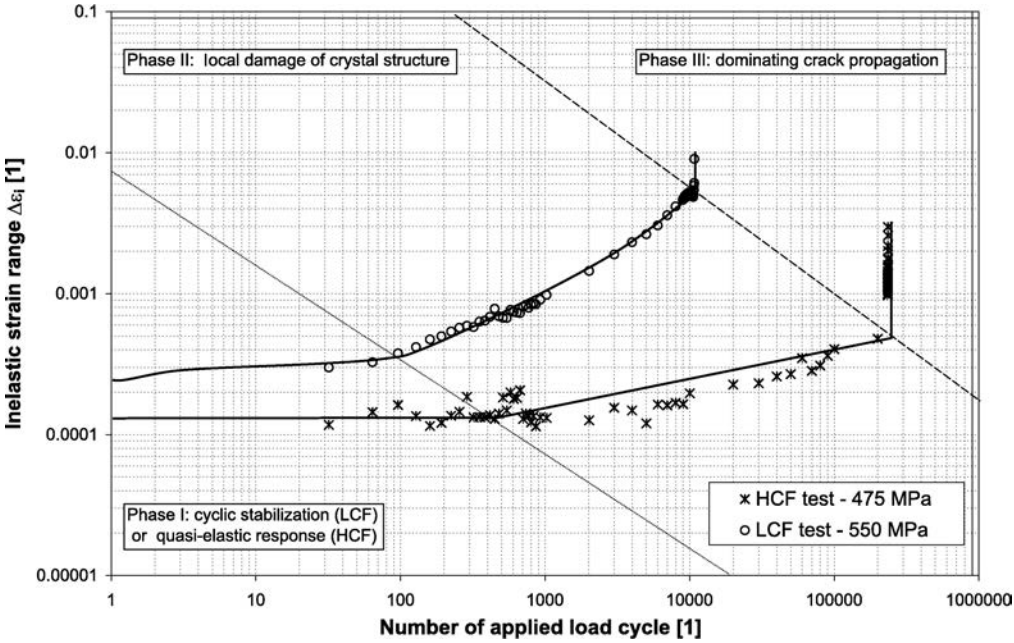

FIG. 4. Inelastic response as a function of the applied load cycle number for HCF and LCF test – A387 GR22 steel.

the Stacking Fault Energy can be locally so high that service stress may exceed the decohesion stress, discontinuity of the material is formed and the second phase of the process ends. At the beginning of the third phase, coalescence of few micro-discontinuities leads to formation of the dominant crack. This crack propagates during that phase until it reaches the critical size, when under the service load unstable propagation of the crack is triggered (critical value of the stress intensity factor K_c is exceeded) and final failure of construction component takes place.

For the HCF test, the defects generation and increase of defects density is strongly localised and the possibility of dislocation movement is limited. That situation is different in the case of a LCF test, when the bulk of material yields and the dislocation can move. This movement leads to redistribution of residual stress. Redistribution of residual stress can be macroscopically observed as a transient stabilization of the material response (saturation of the hysteresis loop). However, due to technical limitations, the initial hysteresis loops were not recorded in the case of tests shown in Figs. 3 and 4, special tests were performed to investigate redistribution of residual stress manifested by cyclic stabilisation. Results of those tests will be reported in the following Sec. 3.

3. Dynamic and static balance of defected crystal structure

The test program shown in Fig. 5, was in this case simple. Constant stress amplitude tests were performed in ambient temperature with the frequency of 1 Hz. The initially applied amplitude was selected below the endurance limit to obtain a quasi-elastic behaviour. After 50 load cycles with continuous recording of the stress and strain, loading was stopped for about 5 minutes, stress amplitude was increased by 25 MPa in case of A336 GR5 steel (50 MPa in case of A387 GR22) and cycling was restarted with cycle counter set to zero. All tests were performed in a sequence, higher amplitude following the lower one after 5 minutes pause. Strain measurement technique was described in the previous section. This procedure was repeated until the stress amplitude almost reached the yield limit. For each recorded stress-strain loop, the inelastic strain range was calculated. Results of the tests are shown in Figs. 6 and 7 for A336 GR5 and A387 GR22 steel respectively.

It can be seen in both figures that for low stress amplitudes (close to the endurance limit), the material response is stable. Width of the hysteresis loop (inelastic strain) remains almost constant. We can assume that there is no damage progress at this amplitude. For higher stress amplitudes, inelastic response starts to increase with the applied load cycles. Two phases of the process can be observed. During the first phase, rate of this process is higher and during the second phase, the decrease of inelastic response rate can be observed. This phe-

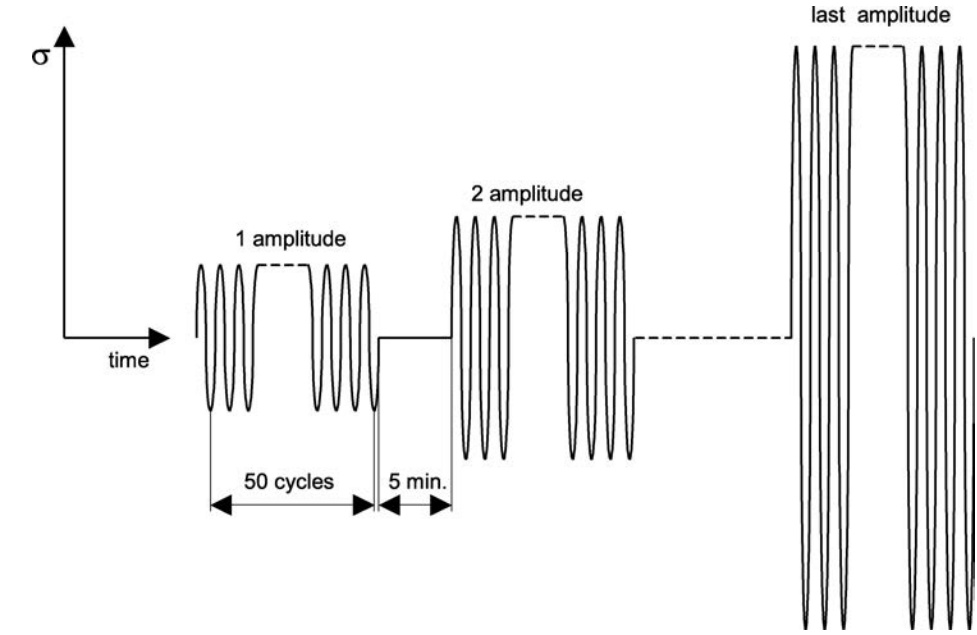

FIG. 5. Test program – cyclic stabilisation and redistribution of residual stress.

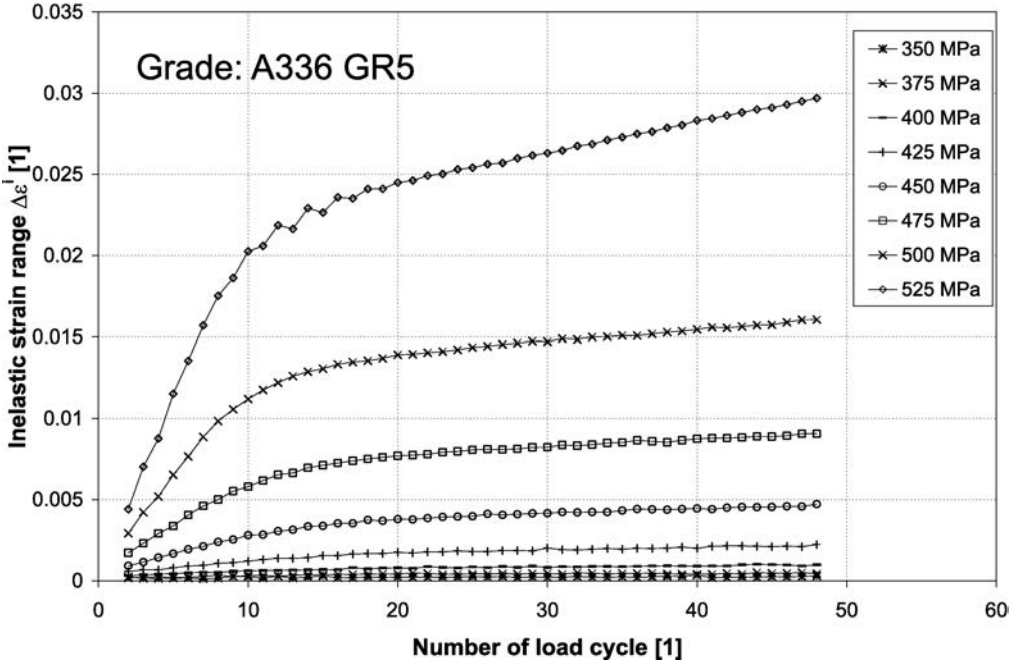

FIG. 6. Inelastic response as a function of the applied load cycle number for A336 GR5 steel.

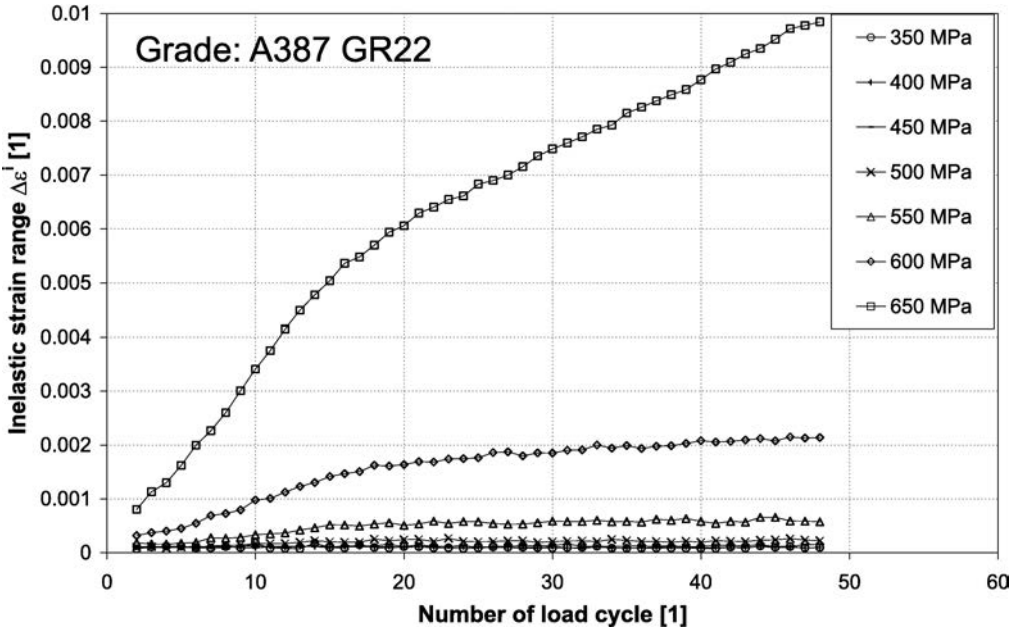

FIG. 7. Inelastic response as a function of the applied load cycle number for A387 GR22 steel.

nomenon can be explained as follows: during the first phase, the dislocations can move on a relatively long distance and this leads to redistribution of the residual stress. Movement of the dislocations leads to their mutual locking and finally, a certain quasi-stable state is achieved. Using the traditional testing method, this phenomenon would be observed as the stabilisation of the hysteresis loop. However, if the material response is observed locally, as in the case of the investigation presented, no saturation of the hysteresis loop (stabilisation of inelastic response) can be detected. This is because the fatigue damage accumulation is a localised phenomenon, and a proper (local) method of observation has to be used to obtain credible results. If there is no cyclic stabilisation, we can assume that the fatigue damage process in case of a LCF test starts immediately. During the first phase of the process, those two phenomena: redistribution of residual stress and accumulation of the fatigue damage overlap. This phase ends when the possibility of dislocation movement is strongly limited due to their mutual locking. Further increment of the inelastic response can be attributed to local generation of new defects appearing in agglomeration of dislocations – the rate of the process slows down and stabilizes.

It has to be emphasized, that each time when loading starts after a 5 minutes pause, that kind of dynamic balance between the redistributed residual stress and the locally increased damage of the material has to be achieved. In Figs. 6 and 7 one can observe that at the end of each LCF test, inelastic strain amplitude

reaches some value. After a short pause (approximately 5 minutes), this value decreases significantly – static balance between the residual stress and local damage of the material is achieved due to diffusion of the defects. If loading of the material is resumed with a higher stress amplitude, dynamic balance (cyclic saturation) is achieved again.

Transition between dynamic and static balance of local damage and residual stress was observed in one of the author's papers [11] for aluminium alloy, called PA6 according to Polish Standard. Simple test was repeated for a specimen cut out from one rod of the material. The test program is shown in Fig. 8. After stretching the specimen to 0.04 mm/mm of axial strain, direction of load was reversed by 180 degrees in the stress space (transition to compression). Tensile yield stress, measured for plastic offset 0.00001, 0.0001, 0.001, 0.01 mm/mm was 235.83, 236.85, 237.21 and 247.35 MPa, respectively. Subsequent compressive loading was performed after different intervals of time elapsed from the moment when 0.04 mm/mm of tensile strain was achieved: 0.25, 0.5, 2 and 380 hours. In Fig. 9 change of the yield limit under compressive load is plotted as a function of time. It can be seen that for a small offset, the yield limit changes with time. These changes can be attributed to diffusion of defects that results in redistribution of residual stress and leads to a new state of balance achieved with time. This balance is different than the state before prestraining, because during plastic flow of the material some of the defects moved to new positions. What is even more important, new defects were generated during this process. Movement and generation of new defects should affect the yield condition of the

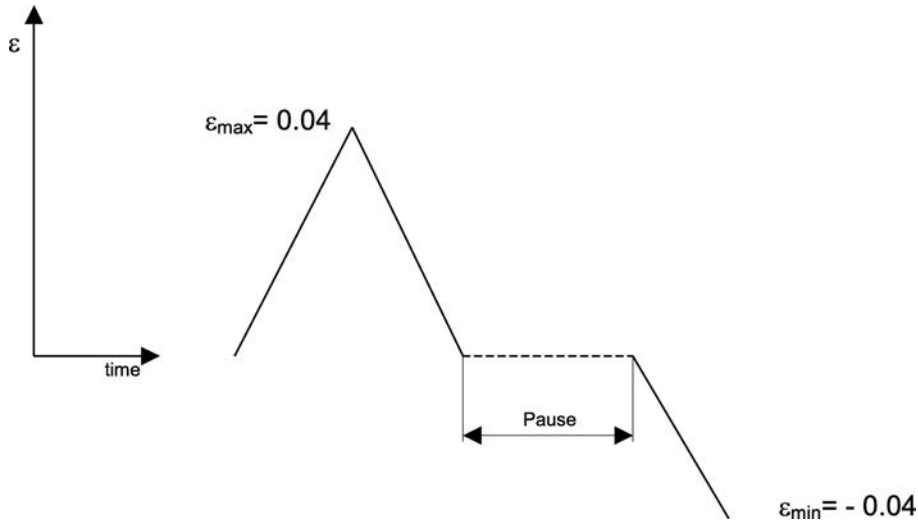

FIG. 8. Test program – material recovery.

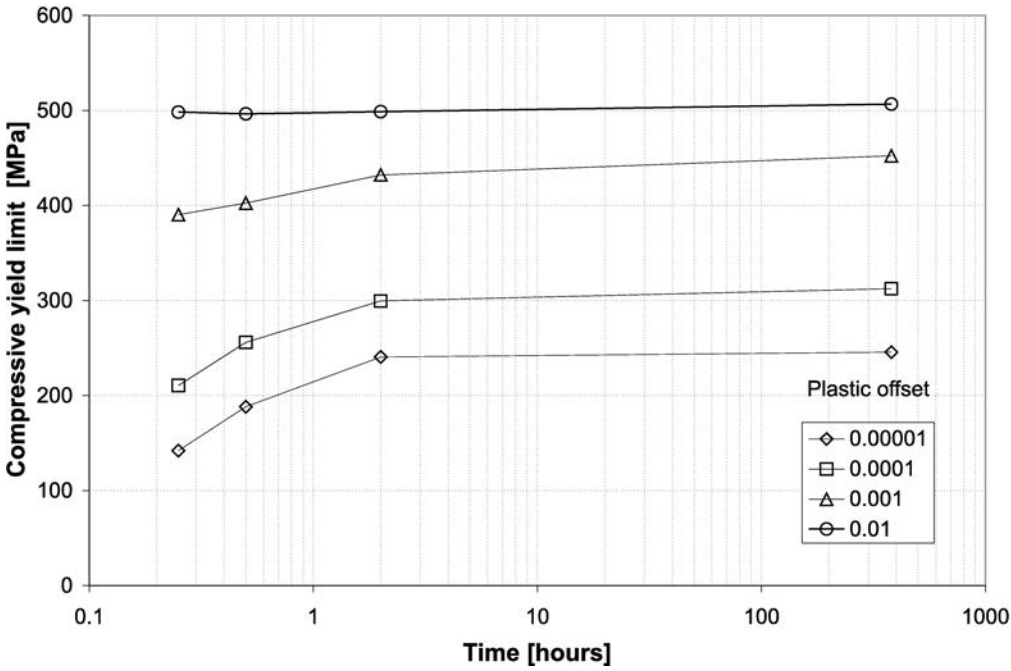

FIG. 9. Changes of the compressive yield limit as a function of the time elapsed after initial tensile prestrainig for PA6 aluminium alloy.

material in question. That change should be manifested by plastic anisotropy (directional dependence of the yield limit). In a general case, for complex stress states the yield condition is given by the following equation [12, 13]:

$$F\left(\sigma_{ik} - \alpha_{ik}\right) = k^2, \tag{3.1}$$

where two anisotropy parameters α_{ik} and k correspond to kinematic and isotropic strain hardening. First of them, α_{ik}, is usually identified as a tensor representing the residual stress state. We can assume that its changes should reflect redistribution of this residual stress caused by movement of the defects. The second anisotropy parameter k, represents increase (hardening) or decrease (softening) of the yield surface. Generation of new defects should be in this case manifested by the decrease of that parameter (yield limit should be smaller for all the loading paths in the stress space). Of course, it will also be affected by annihilation and diffusion of defects after unloading.

At this point we can assume (disregarding other effects such as element segregation, grain boundary diffusion of phase transformations) that these two mentioned anisotropy parameters are related to two phenomena: redistribution of residual stresses and accumulation of damage. For a simple case of uniaxial loading (tension – compression) we can easily determine the changes of para-

meters in question, with the use of tensile and compressive tests. In paper [11] the yield condition (3.1) for uniaxial stress states was simplified to the following form:

$$\sigma_{11} - \alpha_{11} = \pm\sqrt{3} \cdot k, \tag{3.2}$$

where k denotes the yield stress in shear. If Y_{11} denotes the tensile yield stress and Z_{11} denotes the compressive yield stress, we can determine the values of anisotropy coefficients in the following form:

$$\alpha_{11} = \frac{Y_{11} - Z_{11}}{2}, \qquad k = \frac{Y_{11} + Z_{11}}{2\sqrt{3}}. \tag{3.3}$$

Time changes of the anisotropy parameters after 0.04 mm/mm prestraining in tension and unloading are shown in Figs. 10 and 11.

In Fig. 10 the parameter α_{11} representing residual stress is shown as a function of time after prestraining. As it was mentioned, yield limit in tension and compression was determined for four values of the plastic offset. It can be seen that, immediately after deformation, value of residual stress is the highest for

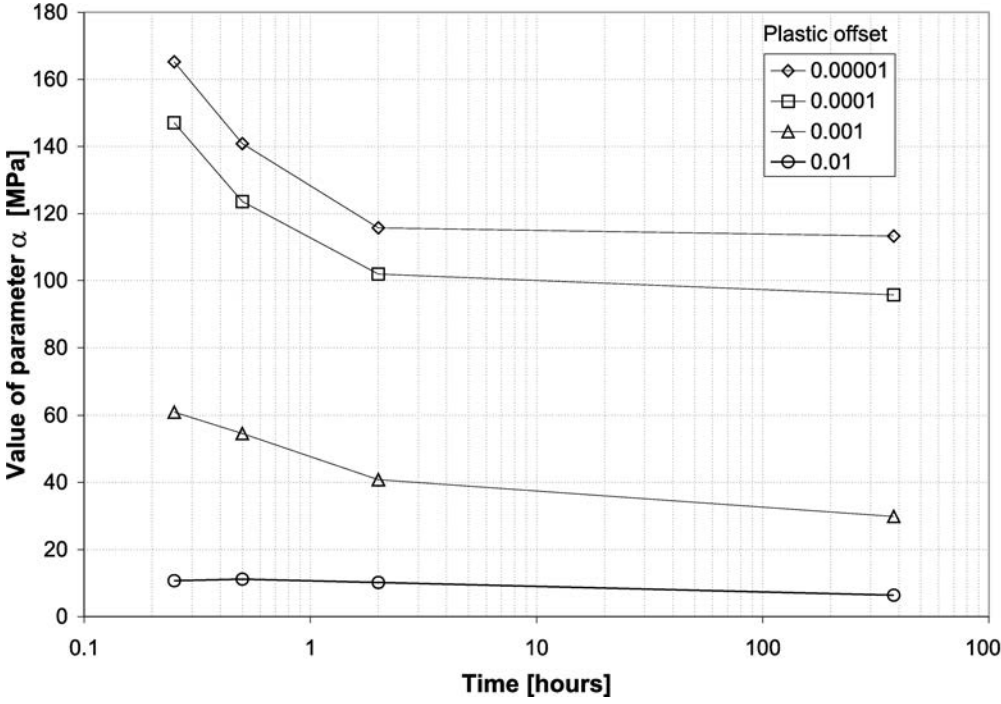

FIG. 10. Anisotropy parameter α representing residual stress as a function of the time elapsed after prestraining.

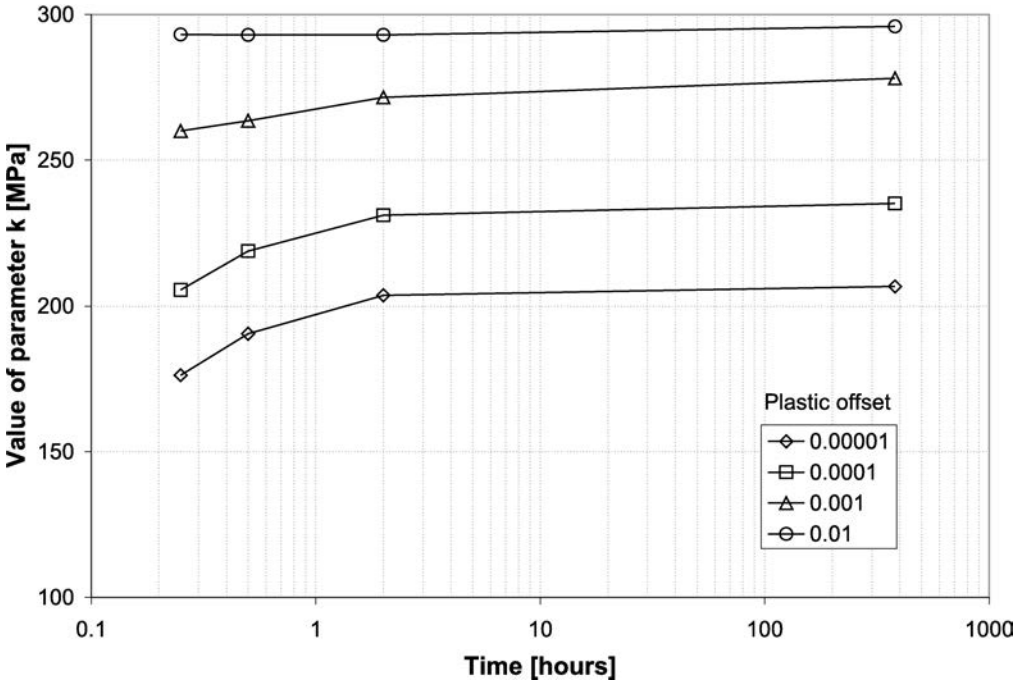

FIG. 11. Anisotropy parameter k representing damage accumulation as a function of the time elapsed after prestraining.

all the offset definitions. It decreases with time due to recovery of the material. That recovery is performed by diffusion of defects in the field of the residual stress. After approximately 2 hours, static balance of material is achieved.

The second one of the above-mentioned parameters k representing accumulation of the damage also undergoes similar changes shown in Fig. 11. In this case, increase of the value can be observed indicating transition from dynamic to static balance of the material. It has to be mentioned that, in contrast with cyclic loading, where significant amount of damage was introduced to the material, in the case of static prestraining, mainly slips of the crystal defects took place. This means that in case of static balance, the value of k after prestraining was close to the one before loading. Time changes of parameter k shown in Fig. 11 can be attributed mainly to transition from the dynamic to static balance of crystal structure. This effect is consistent with the results obtained for A336 GR5 steel. For dynamic balance, the observed inelastic strain was much greater than the static one. It means that yield limit for static conditions is greater than that for dynamic conditions. To observe the progress of damage, we shall compare static or dynamic anisotropy parameters. However, we should be careful to avoid mixing the static and dynamic parameters since in this case the inconsistent picture of the damage accumulation would be obtained.

4. Distribution of residual stress and local character of damage accumulation

As it was suggested in the previous section two anisotropy parameters: α and k can be identified with the residual stress state and with the accumulated damage. The problem is that both phenomena are not uniformly distributed in the investigated bulk of the material. This makes the measurements of the accumulated damage extremely difficult. Traditional material testing technique assumes that strain measurement is performed in the bulk of material with uniform strain distribution – gauge part of the specimen. Using an extensometer it is possible to measure the displacement between two points of the specimen's gauge part and dividing it by the extensometer gauge length (measurement base), one can obtain the value of strain for the stressed material. This works well if the gauge part of the specimen is uniformly deformed. Measurements of elastic constants like Young's modulus or Poisson's ratio are typical examples of such measurements. Moreover, initial yielding (before deformation localisation onset) exhibits tendency to homogenise the strain field due to mutual interaction of dislocations. Therefore, the yield limit can be properly determined using the traditional material testing technique. Since stress is usually determined as the load divided by the area of gauge part cross-section, we can consider all the above-mentioned parameters as credible. The homogeneity of stress and strain distribution cannot be assumed in case of damage accumulation. This process reveals a tendency to localisation: if it starts at some spot of the material, it develops there. High Stocking Fault Energy for a such spot of material facilitates generation of new defects. It is very difficult to estimate the size of damaged area but strain distribution is obviously not uniform in the gauge part of the specimen. Additional complication is that residual stress distribution is related to damage distribution. Balance between the two phenomena is different for static and dynamic conditions. If we want to obtain a consistent picture of damage accumulation, all the measurements of anisotropy parameters should be performed in a static or dynamic manner.

Assuming that the two mentioned damage parameters were measured for static conditions, the progress of damage would be hardly observable. For this reason in paper [9] and [10] the value of damage parameter was measured for dynamic conditions. In this case we can postulate the following form of the yield condition:

$$F\left(\sigma_{ik}-\alpha_{ik}\right)=\left[\left(1-\beta D\right)k_0\right]^2, \tag{4.1}$$

where D stands for the damage parameter and β is a coefficient representing reduction of the yield limit. This coefficient can be defined as follows:

$$\beta=\frac{k_f}{k_0}, \tag{4.2}$$

where k_f stands for the yield stress in shear at material failure (formation of crack) and k_0 stands for the yield stress in shear corresponding to the virgin (undamaged) material assuming isotropy. It has to be stressed once more that there are two conditions necessary to obtain credible measurements results: all the parameters have to be measured locally and mixing of static and dynamic measurements must be avoided.

5. Conclusions

The following conclusions can be drawn from this study:

- Changes of plastic anisotropy are related to accumulation of damage and residual stress redistribution.
- Accumulation of damage and residual stress are local phenomena. Assuming uniform distribution of stress and strain in a Representative Volume Element of the material in order to use traditional material testing techniques, can result in inconsistent picture of the investigated phenomenon.
- State of plastic anisotropy is different for static and dynamic conditions. Transition from dynamic to static balance is achieved after load removal. Transition from static to dynamic balance is usually observed for cyclic loading as stabilisation of the hysteresis loop after the initial load cycles. In case of local measurements of material inelastic response, decrease of inelastic strain changes rate was observed instead of cyclic stabilisation.
- To observe accumulation of damage and distribution of residual stress, local methods of inelastic strain measurements are necessary. Such methods nowadays exist and can be applied in material testing. Using traditional material testing techniques (assuming uniform stress and strain distribution for the gauge part of the specimen), results in obtaining inconsistent picture of damage accumulation.
- To obtain consistent picture of damage accumulation, measurement of anisotropy parameters should be performed in static or dynamic manner. Mixing of the two kinds of measurements can lead to many misunderstandings.
- To describe the damage progress, yield condition in the form given in this paper can be used. Such condition represents local state of the material. Measurements performed on the Representative Volume Element (RVE) can be regarded as the averaged result. Result of such measurements depend on the measurement technique (measurement base and position of extensometer, stress distribution etc.).

References

1. A. Wöhler, *Versuche über die Festigkeit der Eisenbahnwagenachsen*, Zeitschrift für Bauwesen, 1860.
2. A. Palmgren, *Die Lebensdauer von Kugellagern*, Verfahrenstechnik, Berlin, **68**, 339–341 1924.
3. M.A. Miner, *Cumulative damage in fatigue*, Journal of Applied Mechanics, **67**, A159–A164, 1945.
4. B.F. Langer, *Fatigue failure from stress cycles of varying amplitude*, ASME Journal of Applied Mechanics, **59**, A160–A167, 1937.
5. S.M. Marco, W.L. Starkey, *A concept of fatigue damage*, Trans. of ASME, **76**, 627–632, 1954.
6. L. Yang, A. Fatemi, *Cumulative Fatigue Damage Mechanisms and Quqntifying Parameters: A Literature Review*, J. of Testing and Evaluation, **26**, 2, 89–100, 1998.
7. L.M. Kachanov, *Introduction to Continuum Damage Mechanics*, Martinus Nijhoff, The Netherlands, 1986.
8. S. Murakami, *Progress of continuum damage mechanics*, JSME Int. J., **30**, 701–10, 1987.
9. G. Socha, *Prediction of the Fatigue Life on the Basis of Damage Progress Rate Curves*, Int. Journal of Fatigue, **26**, 4, 339–347, 2004.
10. G. Socha, *Experimental investigations of fatigue cracks nucleation, growth and coalescence in structural steel*, Int. Journal of Fatigue, **25**, 2, 139–147, 2003.
11. G. Socha, *Influence of Recovery on Plastic Anisotropy of Metals*, Engrg. Trans., **45**, 2, 181–189, 1997.
12. W. Prager, *The theory of plasticity: a survey of recent achievements*, Proc. Inst. Mech. Engrs., 169, 41, 1955,
13. H. Ziegler, *A modification of Prager's hardening rule*, Quarterly of Applied Mathematics, **17**, 1, 1959.
14. W. Szczepiński, *On deformation-induced plastic anisotropy of sheet metals*, Arch. Mech., **45**, 1, 3–38, 1993.
15. A. Menzel, M. Ekh, K. Runesson and P. Steinmann, *A framework for multiplicative elastoplasticity with kinematic hardening coupled to anisotropic damage*, Int. Journ. of Plasticity, **21**, 3, 397–434, 2005.
16. G. Johansson, M. Ekh and K. Runesson, *Computational modeling of inelastic large ratcheting strains*, Int. Journ. of Plasticity, **21**, 5, 955–980, 2005.
17. M. Brünig and S. Ricci, *Nonlocal continuum theory of anisotropically damaged metals*, Int. Journ. of Plasticity, **21**, 7, 1346–1382, 2005.
18. De-Guang Shang, Wei-Xing Yao, *A nonlinear damage cumulative model for uniaxial fatigue*, Int. J. Fatigue, **21**, 187–194, 1999.
19. N. Bonora, D. Gentile, A. Pirondi and G. Newaz, *Ductile damage evolution under triaxial state of stress: theory and experiments*, Int. Journ. of Plasticity, **21**, 5, 955–980, 2005.

20. A. Pirondi, N. Bonora, D. Steglich, W. Brocks and D. Hellmann, *Simulation of failure under cyclic plastic loading by damage models*, Int. Journ. of Plasticity, **22**, 11, 2146–2170, 2006.

21. V. Moorthy, B.K. Choudhary, S. Vaidyanathan, T. Jayakumar, K. Bhanu Sankara Rao, Bladev Raj, *An assessment of low cycle fatigue damage using magnetic Barkhausen emission in 9Cr-1Mo ferritic steel*, Int. J. Fatigue, **21**, 263–269, 1999.

22. G. La rosa, A. Risitano, *Thermographic methodology for rapid determination of the fatigue limit of materials and mechanical components*, Int. J. Fatigue, **22**, 65–73, 2000.

23. N.G.H. Meyendorf, H. Rosner, V. Kramb, S. Sathish, *Thermo-acoustic fatigue characterization*, Ultrasonics, **40**, 427–434, 2002.

24. Y. Nakai, S. Fukuhara, K. Ohnisji, *Observation of fatigue damage in structural steel by scanning atomic force microscopy*, Int. J. Fatigue, **19**, 1, S223–S236, 1997.

Received May 5, 2007; revised version August 14, 2007.

ENGINEERING TRANSACTIONS • *Engng. Trans.* • **56**, 3, 247–268, 2008
Polish Academy of Sciences • Institute of Fundamental Technological Research

MODELLING OF THE ELECTROHYDRAULIC FULL ACTIVE VEHICLE SUSPENSION

J. K o n i e c z n y

Department of Process Control
AGH – University of Science and Technology
Kraków, Poland

The study investigates various models of vehicle suspensions. A quarter-vehicle full active suspension is chosen for further analysis. A mathematical model, governed by nonlinear differential equations, is proposed that takes into account dynamic properties of an electrohydraulic actuator. The mathematical model being implemented, it was expressed in terms of the state variables. In part two, the physical model was implemented and parametric identification procedure was applied. Phenomenological model simulation data are compared with results of experimental testing of a full, active vehicle suspension. The final section is focused on static and dynamic properties of an open-loop system (without a controller) determined on the basis of obtained models.

Key words: electrohydraulic actuator, full active, suspension, servovalve, model.

Notations

$\mathbf{A}$	state matrix,
$\mathbf{B}$	input matrix,
$\mathbf{B}_v$	input matrix corresponding to input v,
$\mathbf{B}_w$	input matrix corresponding to the excitation w,
$\mathbf{C}$	output matrix,
$\mathbf{D}$	feedforward matrix,
$\mathbf{I}$	identity matrix,
$\mathbf{x}$	state vector,
A_a	effective piston area; $A_a = 0.765786\ 10^{-3}$ m^2,
b_1	coefficient of viscous damping in the first DOF; $b_1 = 72$ Ns/m,
b_2	coefficient of viscous damping in the second DOF; $b_2 = 1161.2$ Ns/m,
C_d	flow discharge coefficient; $C_d = 0.611$ [–],
C_{tm}	leakage coefficient; $C_{tm} = 15 \cdot 10^{-12}$ m^5/Ns,
d	spool valve diameter; $d = 5 \cdot 10^{-3}$ m,
e	control error,
E	fluid bulk modulus; $E = 1.4 \cdot 10^9$ Pa,
f_{0i}	$i-$th natural frequency,
f_0	natural frequency,
F_l	leakage force,
F_p	force associated with flow,
f_s	actuator force,

F_{sc} fluid compressibility force,
h cylinder stroke; $h = 0.06$ m,
$\mathrm{Im}(\lambda)$ imaginary part of eigenvalue λ,
k_1 stiffness coefficient in the first DOF; $k_1 = 37412$ N/m (predicted value $k_1 = 44800$ N/m),
k_2 stiffness coefficient in the second DOF; $k_2 = 8652$ N/m (predicted value $k_2 = 8000$ N/m),
k_{sv} voltage to position conversion factor; $k_{sv} = 0.025 \cdot 10^{-3}$ m/V,
k_z stiffness coefficient of the suspension,
l spool valve perimeter; $l = 15,708 \cdot 10^{-3}$ m,
m_1 unsprung mass; $m_1 = 11.5$ kg,
m_2 sprung mass; $m_2 = 86$ kg,
P_d pressure in the lower chamber,
P_g pressure in the upper chamber,
P_r pressure difference,
P_z actuator supply pressure adjustable in the range 1–16 MPa; during the tests $P_z = 12$ MPa,
Q_l volumetric rate of leakage flow,
Q_z instantaneous flow rate between the unit and actuator,
R_1 flow cross-section; $R_1 = u_1 l$,
$\mathrm{Re}(\lambda)$ real part of eigenvalue λ,
u_1 spool displacement,
$u_{1\,\max}$ spool stroke; $u_{1\,\max} = 0.5 \cdot 10^{-3}$ m,
v servovalve control voltage,
V_p volume of hydraulic hose; $V_p = 80.0398 \cdot 10^{-6}$ m^3,
V_t total volume of actuator cylinder chambers; $V_t = 45.9458 \cdot 10^{-6}$ m^3,
w applied disturbance (displacement of an arbitrary contact point between suspension and road surface),
y output expressed in the space of state,
z displacement of the suspension in the vertical,
z_1 displacement of unsprung mass,
z_2 displacement of sprung mass,
α hydraulic coefficient; $\alpha = 44.4495$ N/m^5,
β_i angle between the i-th eigenvector and the real axis,
λ_i i-th eigenvalue of $\mathbf{A}$,
ρ fluid density; $\rho = 880$ Ns^2/m^4,
τ spool valve time constant; $\tau = 2.32 \cdot 10^{-3}$ s for $P_z = 12$ MPa,
ξ_i i-th damping ratio,
Φ nonlinear part of equation governing the actuator dynamics.

1. Introduction

Modelling of vehicle suspension is of key importance at the design stage. When active control systems are to be applied, the mathematical description allows the study of an open-loop system and helps in the synthesis of a control system. Accuracy of a mathematical model can be verified experimentally, by comparing the simulation and laboratory data. For that purpose, however, a physical model is required. This model is particularly useful whilst verifying the control algorithm for an actuator. This study refers to the synthesis and

verification of a mathematical model of an active suspension, with no control systems. Hence we consider an open-loop model, with no feedback. The model takes into account the properties of an electrohydraulic active actuator.

Vehicle suspension is a group of elements connecting the wheels with the rest of the vehicle, and is most difficult to design. Forces generated on the wheel-road surface interface are conveyed to the car body via the suspension. Its main function is to ensure the adequate comfort of the ride, vehicle stability and handling. The key elements include springs and dampers.

Springs enable the vertical movement of the suspension. The available spring types are: rubber springs, coil springs, leaf springs, pneumatic springs, gas-oil elastic elements, torsion bar. A vehicle equipped with springs only, is susceptible to oscillations when encountering an obstacle. When damping elements are used, the up and down movements of the vehicle are limited, depending on the oscillation velocity. Shock absorbers come in the form of oil-filled telescopic cylinders that resist sudden movements.

Suspension systems can be broadly classified into three subgroups: dependent, independent and semi-independent suspension systems. Passenger cars, where the ride comfort is a priority, are provided with independent suspensions only.

An interesting solution of an independent suspension in passenger cars is the McPherson strut-type suspension with simplicity of design as the major benefit. One sub-assembly operates during the ride, springing and damping of the road wheel vibration. A coil spring concentric with the shock absorber acts as an elastic element in this suspension.

There is a compact and separate unit for each wheel, hence an actuator can be employed instead of a shock absorber.

1.1. Suspension model analysis

In terms of physical representation, there are the following vehicle models with independent suspensions:

1) full 3D model,
2) half vehicle 2D model,
3) quarter vehicle 1D model.

In the full model the vehicle mass is represented by a lumped, sprung mass and four unsprung masses, each representing a wheel. Elements of the suspension placed between unsprung masses and the sprung mass are represented by springs and dampers, featuring reduced stiffness coefficient and viscous damping. Tires are modelled as springs with reduced stiffness ratio. Most tire models take into account the damping, J.A. Levitt [9] analyses the influence of a small

but nonzero relative damping term in the tire model ($\xi \approx 0.02$–0.05). Further damping reduces the vibration acceleration in the vertical direction by nearly 30%. The considered structure has 7 DOFs and enables the modelling of suspension's vertical displacement, pitch and roll of the vehicle body, and four vertical displacements of each of the wheels. Actually the model describes the behaviour of the system in all three planes. In active systems it is utilised to the synthesis of a master controller driving the whole suspension.

A half-vehicle model with 4 DOFs is frequently employed, too. The model takes into account longitudinal rolling, vertical displacements of the suspension and displacements in the vertical direction of the front and rear wheels. This model might also represent a half-suspension in the lateral direction, taking into account pitching, vertical displacements of the suspension and displacements in the vertical direction of the right and left wheel. No matter which plane, it will always be a 2D model with 4 DOFs. In the case of active suspensions controlling the vibrations of a vehicle represented by a quarter-car model, the synthesis of the controller should take into account the swaying effect (pitching or rolling).

A quarter-vehicle model featuring 2 DOFs is shown in Fig. 1.

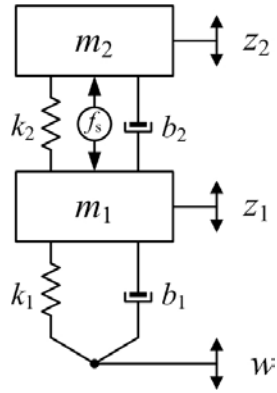

FIG. 1. Quarter-vehicle full active suspension.

Similarly to previous models, this model utilises the reduced stiffness coefficient of the suspension k_2 and the tire k_1 and the reduced viscous damping: of the suspension b_2 and the tire b_1. The mass m_2 is a reduced mass applying the load along one axis. It is a sprung mass and, as mentioned previously, the main function of the suspension is to maximally reduce its vibrations. The mass m_1 is called unsprung, representing chiefly the mass of a wheel and elements of the suspension. Variables z_2, z_1 and w stand for vertical displacements in the neighbourhood of the equilibrium point of the sprung and unsprung mass, and a given contact point between the tire and the road surface. This structure is

widely used in testing the control algorithms and actuators for the purpose of synthesis of active systems.

For clarity and comparability of research data, a quarter-vehicle model is chosen for further analyses. Besides, this structure enables the data verification in the existing laboratory setup. The model in Fig. 1 is provided with an actuator generating an active force f_s.

One can envisage several ways of placing an actuator in single-axis vibration isolation systems, yet the only structures to be employed in passenger cars with independent suspensions are full and slow active structures. Their major advantage is that they go on working (though in a limited degree) when an active system should fail. The main difference lies in that actuators in full active systems be designed such that their failure should not make them more rigid. In the case of slow active systems, an actuator failure should make it more rigid.

Full active suspensions, referred to as broadband or parallel structures, require an actuator operating in a wide frequency range (from 0 to 10–15 Hz). Broadband mode of the operation of the active system leads to major energy consumption. Its main advantage, on the other hand, is that no extensions of the suspension strut are required.

Slow active suspensions, known as narrow-band or limited-band, enables the actuator operation in the range of the first natural frequency of the suspension (from 0 to 3–4 Hz). It appears that this should reduce the external power demand in relation to parallel systems. The main drawback of suspension systems complete with an actuator mounted serially behind the spring is that the height of the suspension column has to be doubled. In order to retain the same stroke of the slow and full active suspensions, the stroke of the spring and actuator must be equal to the designed stroke of the suspension. Another disadvantage is that such suspensions are most sensitive to variations of the sprung mass, which might lead to unstable operation of the system when a spring is applied with a small stiffness coefficient. On account of low-frequency range of actuator operation, this structure is widely used to eliminate vibrations due to pitching (during braking or accelerating) and rolling (for example whilst cornering) [16].

That is why most active systems in vehicle suspensions have a parallel structure and this structure is analysed in this study. Physical implementation of such suspension consists in replacing a shock absorber by an actuator.

1.2. Actuators in vehicle suspensions

Electro-fluid actuators are widely employed as active force generators in concept of the active vehicle suspensions. In widespread use are hydraulic cylinders controlled by servovalves and electro-pneumatic elements utilising the compressibility of gas, which adds an extra elastic element to the system. Pneumatic

elements act as actuators in systems with ON/OFF controllers (rigid suspension – separated pneumatic chamber, soft suspension – added pneumatic chamber). Of particular interest are systems with linear electromagnetic motor. However, such actuators utilise permanent magnets and as it is necessary to generate sufficient force to lift the vehicle, their mass has to be very large. Another factor that precludes their widespread use is high cost associated with small-scale production of such elements.

This study explores electro-hydraulic actuators as they are most popular, at the same time satisfying the specified requirements in terms of force and stroke. Another reason why this particular actuator was selected is easy availability of the working medium in mechanical vehicles. The complete actuating system has a number of interacting hydraulic, electro-hydraulic and electronic assemblies. The main components include: a hydraulic feeder, a filtering unit, accumulator, servovalve, protecting and correcting elements, a hydraulic cylinder and control unit.

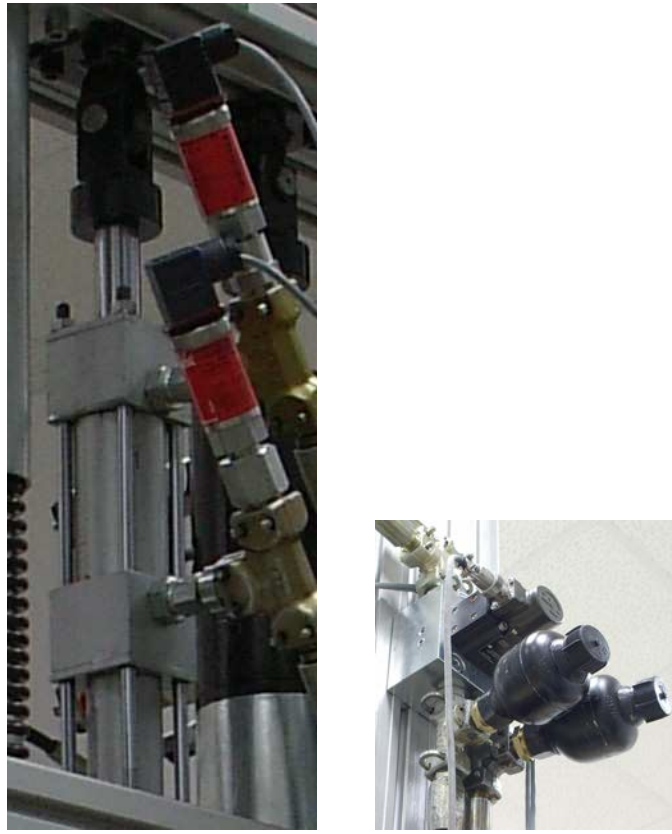

FIG. 2. Hydraulic cylinder with a control servovalve considered in the present study.

A servovalve is an electrohydraulic proportional divider controlling the hydraulic cylinder, it interacts with the control unit and, apart from the cylinder itself, becomes the key element that determines the dynamics of the whole electrohydraulic actuator assembly. A hydraulic cylinder with the servovalve considered in this study are shown in Fig. 2.

The measurement and control circuit comprising a number of transducers, a digital data processing unit, A/D and D/A modules and signal conditioning modules ought to ensure the adequate rate of signal processing and acquisition, if necessary.

The magnitude of force and displacements to be generated depends chiefly on geometric parameters of the hydraulic cylinder. The main function of the cylinder is to transmit mechanical energy to the suspension system in accordance with the selected control algorithm.

Protecting and correcting elements are of major importance too, as they prevent rapid pressure surges and associated hazards, which might lead to the system failure.

Dynamic properties of an active vibration reduction system depend not only on the actuators; the control system is another component that regulates the system dynamics (and hence the vibration isolation performance) and ensures a correct operation of the actuator.

2. Synthesis of a mathematical model

2.1. Mathematical model of an actuator

A hydraulic cylinder controlled by an electro-hydraulic servovalve is placed in parallel to the springs and a viscous damper, between the unsprung and sprung masses. It generates an active force f_s, whose main function is to minimise the displacement of the sprung mass m_2 with respect to an external reference system. The applied double-action cylinder with a two-sided rod is a special design. To minimise the resistance due to friction between its mobile elements, specially chosen sealing systems are applied in the rod and pilot sleeves. It is controlled by a double-stage four-way flow-control servovalve, 4WS2EM-type (601X/20 Rexroth). The servovalve is made in the standard version with mechanical feedback and zero overlap. Equations of actuator dynamics are derived on the basis of a diagram shown in Fig. 3.

Spool position control u_1 allows the liquid stream to be supplied from the source to one of the chambers in the cylinder and removed from the other chamber to the oil reservoir. The pressure difference P_r in chambers causes the working fluid to flow. Multiplying this pressure difference by the effective piston area A_a yields the actuator force f_s.

In order that the model should be expressed in the simplest terms at the same time retaining the vital properties of a real object, certain assumptions have to be made:

- the investigated system has lumped parameters,
- due to the presence of a large reservoir of the working fluid and the applied methodology, the effects of temperature on dynamic properties of an active system are neglected,
- temperature of the medium supplied to the system equals that of the medium inside the system,
- on account of the applied sealing strategy, the resistance force in a cylinder, associated with dry friction, is neglected,
- the flow in the system is turbulent, and continuity of the stream of working medium is maintained,
- conduits connecting the elements of the system are stiff and short and pressure loss of the flowing medium is negligible.

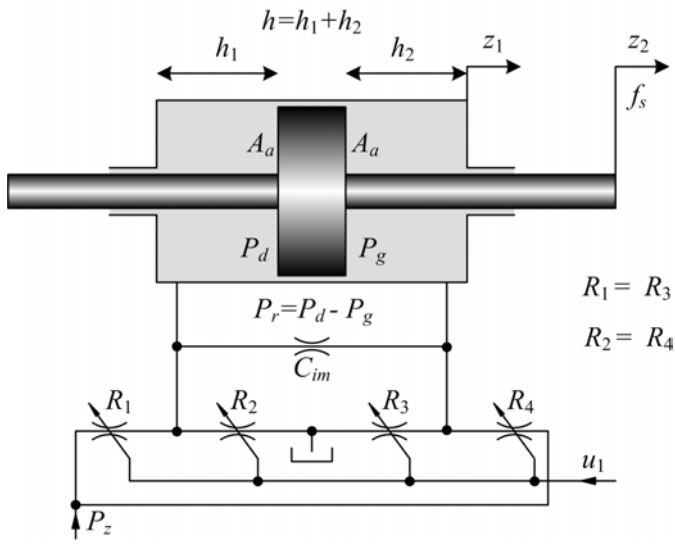

FIG. 3. Schematic diagram of active hydraulic element.

The dynamics of the system is written as an equation of force equilibrium

$$f_s = F_p - F_{sc} - F_l, \tag{2.1}$$

where: F_p – force associated with flow, F_{sc} – force of fluid compressibility, F_l – leakage force.

To derive the equation of state of a full active quarter-vehicle model complete with an actuator, the Eq. (2.1) is differentiated in the time domain yielding the derivatives of force components

$$\dot{f}_s = \dot{F}_p - \dot{F}_{sc} - \dot{F}_l \,. \tag{2.2}$$

Force of compressibility is obtained directly from the following equation [11]:

$$\frac{F_{sc}}{z_2 - z_1} = \frac{4EA_a^2}{V_t + V_p} \tag{2.3}$$

where: $z_2 - z_1$ – piston displacement relative to the cylinder, E – fluid bulk modulus, V_t – total volume of actuator cylinder chambers, V_p – volume of hydraulic hose.

A coefficient $\alpha = \dfrac{4E}{V_t + V_p}$ is used to describe hydraulic parameters. Accordingly, we get

$$\frac{F_{sc}}{z_2 - z_1} = \alpha A_a^2 \,. \tag{2.4}$$

Differentiating Eq. (2.4) with respect to time yields a formula expressing the derivative of the fluid compressibility force

$$\dot{F}_{sc} = \alpha A_a^2 \left(\dot{z}_2 - \dot{z}_1\right). \tag{2.5}$$

The equation of flow is written as

$$A_a \left(\dot{z}_2 - \dot{z}_1\right) = Q_l \,, \tag{2.6}$$

where Q_l – volumetric flow, governed by the formula

$$Q_l = C_{tm} P_r \,, \tag{2.7}$$

where C_{tm} – leakage coefficient.

Directly from Eq. (2.6) and using Eq. (2.5) and (2.7), we get

$$\dot{F}_l = \alpha A_a C_{tm} P_r \,. \tag{2.8}$$

The equation of flow between a symmetrical cylinder and a four-way servovalve is given by formula (2.9) [15]

$$A_a \left(\dot{z}_2 - \dot{z}_1\right) = R_1 C_d \sqrt{\frac{P_z - \operatorname{sign}\left(u_1\right) P_r}{\rho}} \,, \tag{2.9}$$

where: u_1 – spool displacement, R_1 – flow cross-section, $R_1 = u_1 l$ (l – spool circumference equal πd, d – spool valve diameter), C_d – flow discharge coefficient, for turbulent flow $C_d = \pi/\pi + 2 = 0.611$, P_z – supply pressure, ρ – fluid density.

Multiplying both sides of Eq. (2.9) by the derivative of force F_p and making use of Eq. (2.5), we get

$$\dot{F}_p = u_1 l \alpha A_a C_d \sqrt{\frac{P_z - \text{sign}\,(u_1)\, P_r}{\rho}}\,. \tag{2.10}$$

Substituting Eqs. (2.5), (2.8), (2.10) into Eq. (2.2) expressing the derivative of the control force, yields

$$\dot{f}_s = u_1 l \alpha A_a C_d \sqrt{\frac{P_z - \text{sign}\,(u_1)\, P_r}{\rho}} - \alpha A_a^2 \left(\dot{z}_2 - \dot{z}_1\right) - \alpha A_a C_{tm} P_r\,. \tag{2.11}$$

Quantities u_1, P_r, $\dot{z}_2$ $\dot{z}_1$ are time-dependent, other coefficients have constant values given in the Nomenclature section.

A relationship is also provided between the control force and the pressure difference, expressed by the formula

$$f_s = P_r A_a\,. \tag{2.12}$$

Spool position u_1 is controlled by the current level in coils of the servovalve motor. Hence, the spool dynamics can be approximated by a differential equation of the first order

$$\tau \dot{u}_1 + u_1 = k_{sv} v\,, \tag{2.13}$$

where: τ – time constant of the servovalve, k_{sv} – voltage-to-position conversion factor, v – servovalve control voltage.

This approximation appears to be sufficiently accurate for frequencies up to 50 Hz [3, 7, 14].

Equations (2.11)–(2.13) underlie the mathematical model of a vehicle suspension, complete with a electro-hydraulic actuator shown in the space of state.

2.2. Quarter-car model

Figure 1 shows a parallel quarter-car model of a vehicle, with lumped parameters. This is a 2 DOF model. The first DOF associated with mass m_1 applies to the part representing the wheel and tire. The mass of the wheel is unsprung. The second DOF – associated with the mass m_2 – applies to the car body mass with passengers. This mass is referred to as sprung. The main function of the analysed system is to minimise the vibrations of the mass m_2, is spite of disturbances caused by road roughness.

The model uses the following designations:
v – input – servovalve control voltage, which directly controls force f_s,
w – input – can be treated as disturbance due to road irregularities,
z_2 – displacement of the sprung mass.

Equations of motion of the unsprung mass m_1 and sprung mass m_2 in the neighbourhood of a equilibrium point are written as Eqs. (2.14) and (2.15):

$$m_1\ddot{z}_1 + b_2(\dot{z}_1 - \dot{z}_2) + b_1(\dot{z}_1 - \dot{w}) + k_2(z_1 - z_2) + k_1(z_1 - w) = -f_s \tag{2.14}$$

$$m_2\ddot{z}_2 + b_2(\dot{z}_2 - \dot{z}_1) + k_2(z_2 - z_1) = f_s\,. \tag{2.15}$$

On account of the available capacity of the laboratory facilities, the maximal mass to be mounted is taken to be $m_2 = 86$ kg. The unsprung mass is taken as small as possible: $m_1 = 11.5$ kg, comprising a light aluminium platform (for the purpose of assembly), guiding and fixing elements.

The ratio of unsprung to the sprung mass is roughly 0.13. Parameters of passive elements were chosen such that natural frequencies of damped vibrations should coincide with those of a real system – around 1.5 Hz and 11 Hz [2, 5, 8, 13, 17].

2.3. Phenomenological model of a open-loop system

Underlying the synthesis of a phenomenological model are the physical laws governing the kinematics of a suspension, and the equation of force and flow equilibrium in a hydraulic actuator.

The model of a full active suspension is expressed in the form of state and output equations. To derive the equation of state, recall Eqs. (2.11), (2.13)–(2.15).

State variables are expressed in the form of Eq. (2.16):

$$\begin{aligned} &x_1 = z_2, \quad x_2 = \dot{z}_2, \quad x_3 = z_2 - z_1, \quad x_5 = P_r = \frac{f_s}{A_a}, \quad x_6 = u_1\,, \\ &x_4 = \int\left[-\left(\frac{k_2}{m_2} + \frac{k_2}{m_1}\right)\cdot(z_2 - z_1) + \frac{k_1}{m_1}\cdot(z_1 - w) + \left(\frac{A_a}{m_2} + \frac{A_a}{m_1}\right)\cdot\frac{f_s}{A_a}\right]\mathrm{d}t\,. \end{aligned} \tag{2.16}$$

The first three variables of state are the displacement and velocity of the sprung mass and displacement of the sprung mass in relation to the unsprung mass. These parameters are measurable and adequately describe the system dynamics, hence they can be well used as feedback signals. State variable x_4 is derived after transformations of Eqs. (2.14), (2.15). This part is not utilised to derive other state variables. Variables x_5, x_6 describe the actuator dynamics,

representing the pressure difference in the chambers and spool displacement obtained from Eq. (2.13).

A nonlinear part Φ (Eq. (2.18)) is isolated from Eq. (2.11) such that matrices $\mathbf{A}$ and $\mathbf{B}$ in the state equations should contain linear terms only.

For thus defined variables, the state equations are written as:

$$\begin{bmatrix} \dot{x}_1 \\ \dot{x}_2 \\ \dot{x}_3 \\ \dot{x}_4 \\ \dot{x}_5 \\ \dot{x}_6 \end{bmatrix} = \mathbf{A} \cdot \begin{bmatrix} x_1 \\ x_2 \\ x_3 \\ x_4 \\ x_5 \\ x_6 \end{bmatrix} + \mathbf{B} \cdot \begin{bmatrix} v \\ w \end{bmatrix} + \mathbf{A}_\Phi \cdot \Phi, \qquad y = \mathbf{C} \cdot \begin{bmatrix} x_1 \\ x_2 \\ x_3 \\ x_4 \\ x_5 \\ x_6 \end{bmatrix} \tag{2.17}$$

where:

$$\mathbf{A} = \begin{bmatrix} 0 & 1 & 0 & 0 & 0 & 0 \\ -\dfrac{b_1 \cdot b_2}{m_1 \cdot m_2} & 0 & \dfrac{b_2}{m_2} \cdot \left(\dfrac{b_1}{m_1} + \dfrac{b_2}{m_1} + \dfrac{b_2}{m_2} \right) - \dfrac{k_2}{m_2} & -\dfrac{b_2}{m_2} & \dfrac{A_a}{m_2} & 0 \\ \dfrac{b_1}{m_1} & 0 & -\left(\dfrac{b_1}{m_1} + \dfrac{b_2}{m_1} + \dfrac{b_2}{m_2} \right) & 1 & 0 & 0 \\ \dfrac{k_1}{m_1} & 0 & -\left(\dfrac{k_1}{m_1} + \dfrac{k_2}{m_1} + \dfrac{k_2}{m_2} \right) & 0 & \dfrac{A_a}{m_1} + \dfrac{A_a}{m_2} & 0 \\ -A_a \alpha \dfrac{b_1}{m_1} & 0 & A_a \alpha \left(\dfrac{b_2}{m_2} + \dfrac{b_2}{m_1} + \dfrac{b_1}{m_1} \right) & -A_a \alpha & -C_{tm} \alpha & 0 \\ 0 & 0 & 0 & 0 & 0 & -\dfrac{1}{\tau} \end{bmatrix},$$

$$\mathbf{B} = \begin{bmatrix} 0 & 0 \\ 0 & \dfrac{b_1 \cdot b_2}{m_1 \cdot m_2} \\ 0 & -\dfrac{b_1}{m_1} \\ 0 & -\dfrac{k_1}{m_1} \\ 0 & A_a \alpha \dfrac{b_1}{m_1} \\ \dfrac{k_{sv}}{\tau} & 0 \end{bmatrix}, \quad \mathbf{C} = \begin{bmatrix} 1 & 0 & 0 & 0 & 0 & 0 \end{bmatrix}, \quad \mathbf{A}_\Phi = \begin{bmatrix} 0 & 0 & 0 & 0 & 1 & 0 \end{bmatrix}^T,$$

$$\Phi = \alpha l C_d x_6 \sqrt{\frac{P_z - \operatorname{sign}(x_6)\, x_5}{\rho}}\,. \tag{2.18}$$

Both v and w are inputs, yet the displacement w is treated as disturbance while v is the control voltage. Accordingly, the matrix $\mathbf{B}$ can be transformed:

$$\mathbf{B}_v = \mathbf{B} \cdot \begin{bmatrix} 1 \\ 0 \end{bmatrix}, \qquad \mathbf{B}_w = \mathbf{B} \cdot \begin{bmatrix} 0 \\ 1 \end{bmatrix}. \tag{2.19}$$

The equations of state will be rewritten as:

$$\begin{aligned} \dot{\mathbf{x}} &= \mathbf{A}\mathbf{x} + \mathbf{B}_v v + \mathbf{B}_w w + \mathbf{A}_\Phi \Phi, \\ y &= \mathbf{C}\mathbf{x}, \end{aligned} \tag{2.20}$$

where v and w are scalar quantities.

2.4. Linearising of the phenomenological model

The nonlinear model is approximated with the linear one in the neighbourhood of its working point. The method was applied whereby the nonlinear part of the equation of state 2.20 was expanded in the Taylor series. The working point is taken as the spool mid-position and the pressure difference (x_{6_0}, x_{5_0}) equal to zero, as in the static state the spool mid-position is associated with pressure equilibrium in the cylinder chambers. Thus the assumed working point does not cause the state variables to be shifted, since the value of the function at the working point is zero.

In the low frequency range of operation of the vibration control system (up to 20 Hz) and hence of the servovalve, an assumption is made that the negative value of the spool position x_6 corresponds to a negative pressure difference in the chambers, the positive value of the spool position is associated with the positive pressure difference. Assuming that the **sign** function is given as

$$\text{sign } x = \begin{cases} -1 & \text{for} \quad x < 0 \\ 0 & \text{for} \quad x = 0 \\ 1 & \text{for} \quad x > 0 \end{cases}$$

Equation (2.18) can be rewritten as

$$\Phi = \alpha l C_d x_6 \sqrt{\frac{P_z - |x_5|}{\rho}}. \tag{2.21}$$

It is readily apparent that the function Φ is continuous at the specified working point and can be thus linearised. Accordingly, Eq. (2.21) can be expressed as

$$\Delta\Phi = \left[\frac{\partial \Phi\,(x_5, x_6)}{\partial x_5}\right]_{x_{5_0}} \cdot \Delta x_5 + \left[\frac{\partial \Phi\,(x_5, x_6)}{\partial x6}\right]_{x_{6_0}} \cdot \Delta x_6\,. \tag{2.22}$$

The calculations were performed:

$$\left[\frac{\partial \Phi(x_5, x_6)}{\partial x_5}\right]_{x_{5_0}} = \left[-\frac{1}{2}\alpha l C_d x_6 \frac{1}{\sqrt{\dfrac{P_z - |x_5|}{\rho}}} \cdot \frac{\operatorname{sign}(x_5)}{\rho}\right]_{x_{5_0}} = 0,$$

$$\left[\frac{\partial \Phi(x_5, x_6)}{\partial x_6}\right]_{x_{6_0}} = \left[\alpha l C_d \sqrt{\frac{P_z - |x_5|}{\rho}}\right]_{x_{6_0}} = \alpha l C_d \sqrt{\frac{P_z}{\rho}}.$$

The continuity condition of the partial derivative of the function Φ at the working point was checked. Hence, substituting into Eq. (2.22) yields a linearised form of Eq. (2.18)

$$\Phi = \alpha l C_d \sqrt{P_z/\rho}\,(x_6 - x_{6_0}) = \alpha l C_d \sqrt{P_z/\rho}\, x_6\,. \tag{2.23}$$

Alternatively, a numerical procedure can be applied to linearise Eq. (2.18). Knowing the applicable range of the function of state variables x_5, x_6, one can generate input data vectors x_5, x_6 and an output vector Φ, basing on a nonlinear equation. The numerical data are then written as an equation of linear regression of two input variables, which allows the nonlinear function Φ to be approximated with a linear equation in the predetermined range of state variables. This problem was solved using the Matlab package. Regression coefficients were found, hence Eq. (2.18) can be replaced by function (2.24) that captures state variables in the interval $x_5 = \pm 7$ MPa and $x_6 = \pm 0.25$ mm:

$$\Phi = -341.2 \cdot x_5 + 4.666 \cdot 10^{13} \cdot x_6\,. \tag{2.24}$$

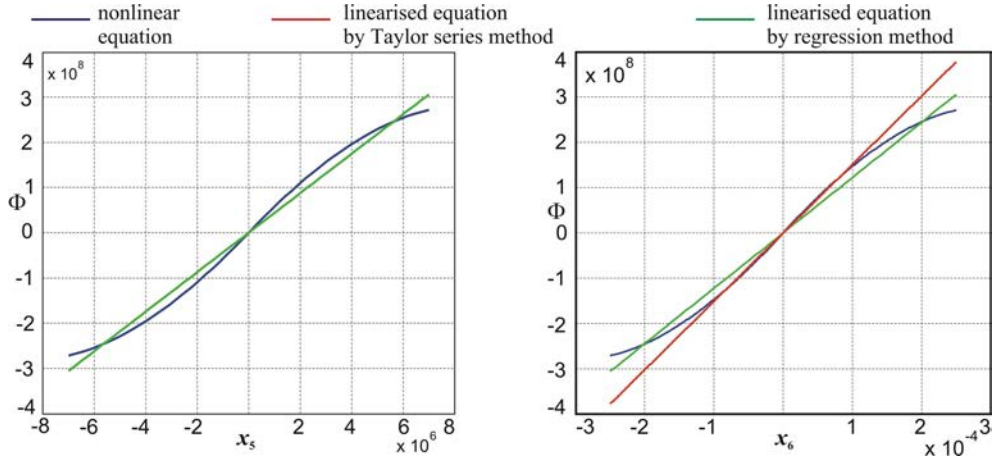

FIG. 4. Comparison of plots $\Phi(x_5)$ and $\Phi(x_6)$ obtained basing on nonlinear equation and equations linearised by the two methods.

Figure 4 shows representation of a nonlinear Eq. (2.18) by linearised Eqs. (2.23), (2.24). In order to establish how linearisation should affect the dynamic properties of the object's model, amplitude-frequency characteristics were obtained: $20\log_{10}(z_2/v)$ and $20\log_{10}(z_2/w)$ (Fig. 5).

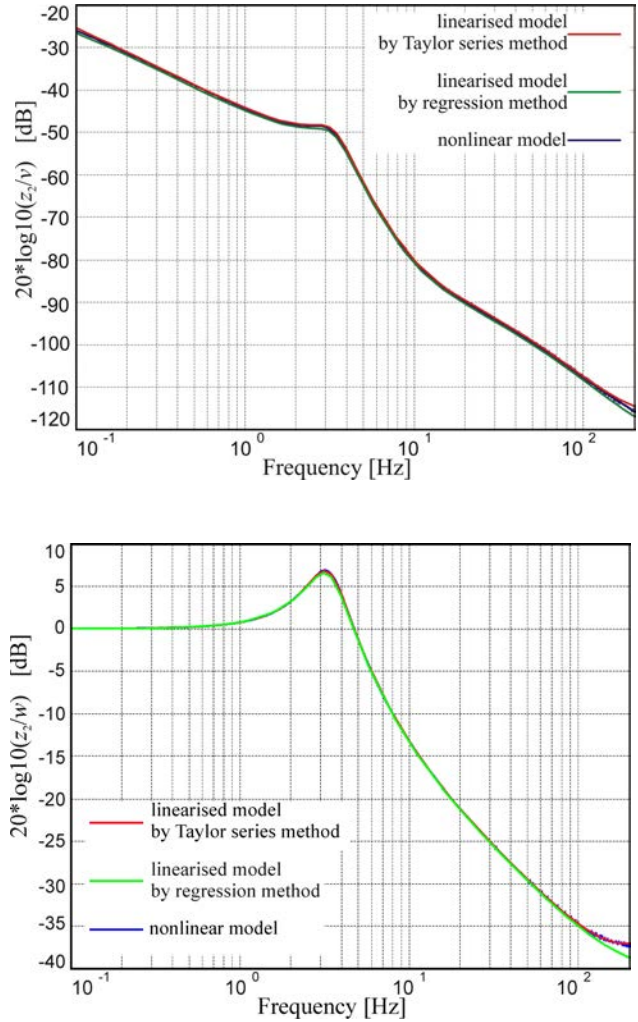

FIG. 5. Comparison of amplitude-frequency characteristics of sprung mass displacement relative to inputs to the nonlinear model and linearised model.

These confirm that representation of a nonlinear model by a linear one is correct throughout the whole investigated frequency range.

Underlying the mathematical model are relationships defining the properties of open-loop models, so the model can be expressed in a linear form. Synthesis

of this model allows for finding physical relationships describing the model of a structure. State variables were selected that well portray the dynamic properties of the investigated structure. Comparison of response times of the phenomenological model and that obtained in the procedure of identification against response times of a laboratory, the physical model enables us to verify the adequacy of identification procedure.

3. Identification of the parametric model

The identification method consists in finding the coefficients in the first-order differential equations governing the system dynamics. The multi-dimensional linear regression method is applied. During the laboratory tests the physical model of a parallel structure was subjected to random excitations, fed to both inputs. The registered parameters include: preset kinematic excitation w, preset control voltage to the servovalve v, outputs: displacement of the sprung mass z_2, displacement of the unsprung mass z_1, pressures in the cylinder chambers P_d, P_g, actuator supply pressure P_z, instantaneous flow rates Q_z between the supplying unit and actuator. The acquired registered signals were pre-processed, which involved re-scaling, trend removal and elimination of high-frequency components. Derivatives of the acquired signals were obtained, too.

Basing on the created phenomenological model and other models available in the literature on the subject [5–7, 17–20], the following physical variables are selected as state vectors that describe the investigated object: $x_1 = z_2$, $x_2 = \dot{z}_2$, $x_3 = z_1$, $x_4 = \dot{z}_1$, $x_5 = P_r = P_d - P_g$. The sixth variable of state is the derivative of work performed by the unit supplying the actuator $x_6 = P_z Q_z$. Hence, x_6 becomes the measure of power absorbed from the unit. Thus the defined variables form a matrix $\mathbf{X}$, containing measured time series of state variables and time series of control variables v, w. The vector of parameters is estimated using the least square method, given by Eq. (3.1)

$$\hat{\boldsymbol{\beta}} = \left(\mathbf{X}^T\mathbf{X}\right)^{-1}\mathbf{X}^T\dot{x}_n\,, \tag{3.1}$$

where $n = 1, 2, ..., 6$.

The procedure of identification of the parameters vector utilises a dedicated computer program developed in Matlab. The parametric model of a quarter-vehicle suspension obtained from identification is governed by the equations:

$$\begin{aligned} \dot{x} &= \mathbf{A}x + \mathbf{B}\begin{bmatrix} v \\ w \end{bmatrix}, \\ y &= \mathbf{C}x, \end{aligned} \tag{3.2}$$

where

$$\mathbf{A} = \begin{bmatrix} 0 & 1 & 0 & 0 & 0 & 0 \\ -231 & -46 & 23 & 40 & 2504 & -401800 \\ 0 & 0 & 0 & 1 & 0 & 0 \\ 305 & 50 & -1248 & -77 & -3493 & 596600 \\ 2 & -1 & -6 & 1 & -53 & 10220 \\ 0 & 0 & 0 & 0 & 0 & -1 \end{bmatrix}, \quad \mathbf{B} = \begin{bmatrix} 0 & 0 \\ 4442 & 212 \\ 0 & 0 \\ -6879 & 949 \\ 47 & 4 \\ 0 & 0 \end{bmatrix},$$

$$\mathbf{C} = \begin{bmatrix} 1 & 0 & 0 & 0 & 0 & 0 \end{bmatrix}.$$

3.1. Model verification in the laboratory setup

The mathematical model was verified in the laboratory setup. The duly implemented of the suspension was subjected to kinematic excitations of square wave-form. Sine signal of frequency linearly increasing in time from 0.063 to 40 Hz was fed to the other input (voltage driving the actuator servovalve). The transition from the initial to the final frequency lasted 40 s. Input signals of different amplitudes were applied in the experiments, both input and output signals (displacement of sprung mass) were acquired. Figure 6 shows the time histories collected for the amplitude of excitations ±10 mm, control voltage amplitude ±3 V and response times of the phenomenological model and that estimated for the predetermined displacement w and voltage v.

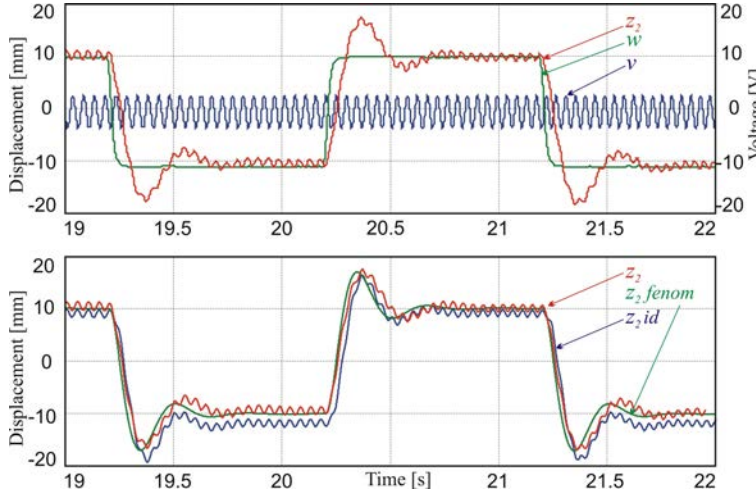

FIG. 6. Comparison of time responses of the: laboratory, phenomenological and estimated model for the set value of the displacement w and voltage v.

Both the phenomenological and estimated models well emulate the shape of the output signal from the object. The phenomenological model performance in

the high frequency range seems to be inferior. This model could be optimised through the tuning of parameters such as servovalve amplification gain, leakage between the chambers and geometric parameters of the spool. Since the model was used only to verify the estimated model and to find the process variables that control the object's dynamics, the test results are taken as satisfactory. The estimated model agrees better with the laboratory model and it takes into account the power consumed by the actuator. On account of above advantage, this model was selected for the synthesis of the control system.

Similar correspondence is obtained when simultaneous random excitations are applied on the inputs w, v. Utmost care must be taken to ensure that these signals should be non-correlated.

4. Dynamic properties of the open loop model

Dynamic properties of the open loop model of a full active structure can be determined on the basis of the model obtained from identification. Similarly to the synthesis of a phenomenological model, the control matrix $\mathbf{B}$ in the identified model has two components: $\mathbf{B}_v$, $\mathbf{B}_w$, corresponding to two inputs to the system: control input v and excitation w. Equation (3.2) can be rewritten as:

$$\begin{aligned} \dot{\mathbf{x}} &= \mathbf{A}\mathbf{x} + \mathbf{B}_v v + \mathbf{B}_w w, \\ y &= \mathbf{C}\mathbf{x}. \end{aligned} \tag{4.1}$$

Figure 7 shows a block diagram of quarter-vehicle suspension model associated with Eq. (4.1).

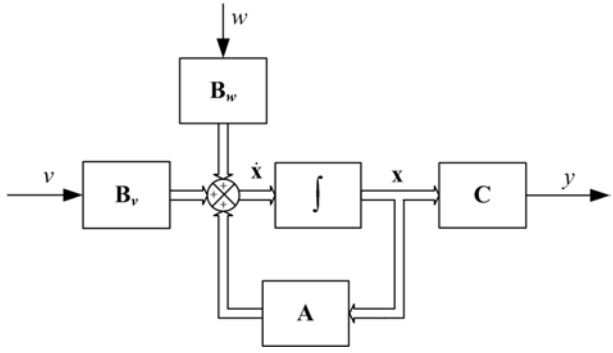

Fig. 7. Block diagram of the vehicle suspension model.

Characteristic equation for the matrix $\mathbf{A}$ is derived from the formula

$$\begin{aligned} &|s\mathbf{I} - \mathbf{A}| = 0\,, \\ &s^6 + 177s^5 + 15713s^4 + 300095s^3 + 6612388s^2 + 14887015s + 8559185 = 0\,. \end{aligned} \tag{4.2}$$

Solving Eq. (4.2) yields the eigenvalues of the matrix **A**:

$$\lambda_1 = -1, \qquad \lambda_2 = -1.439,$$
$$\lambda_3 = -7.495 + j20.570, \qquad \lambda_4 = -7.495 - j20.570,$$
$$\lambda_5 = -79.786 + j77.775, \qquad \lambda_6 = -79.786 - j77.775.$$

Eigenvalues placement on the complex plane is shown in Fig. 8.

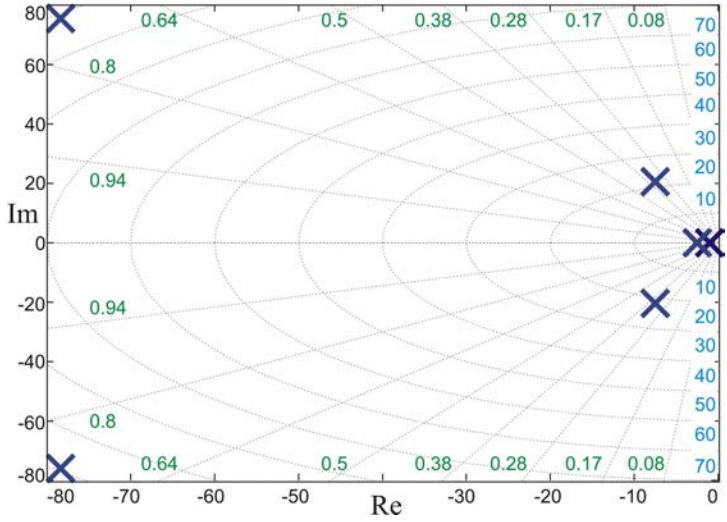

FIG. 8. Eigenvalues placement on the complex plane.

For each eigenvalue the natural frequency f_0 and the damping ratios coefficient ξ are derived from Eqs. (4.3) and (4.4):

$$f_{0i} = \frac{|\lambda_i|}{2\pi} = \frac{\sqrt{\mathrm{Re}^2(\lambda_i) + \mathrm{Im}^2(\lambda_i)}}{2\pi}, \tag{4.3}$$

$$\xi_i = \cos(\beta_i), \tag{4.4}$$

where β_i denotes the angle between the eigenvector and the real axis in the coordinate system. It is obtained from the formula $\beta_i = \mathrm{arctg}\left(\dfrac{\mathrm{Im}(\lambda_i)}{\mathrm{Re}(\lambda_i)}\right)$. Natural frequencies and damping ratios coefficients computed for the eigenvalues of the matrix **A** are:

$$f_{01} = 0.15915 \text{ Hz}, \qquad \xi_1 = 1,$$
$$f_{02} = 0.22894 \text{ Hz}, \qquad \xi_2 = 1,$$
$$f_{03} = f_{04} = 3.4843 \text{ Hz}, \qquad \xi_3 = \xi_4 = 0.34234,$$
$$f_{05} = f_{06} = 17.733 \text{ Hz}, \qquad \xi_5 = \xi_6 = 0.71607.$$

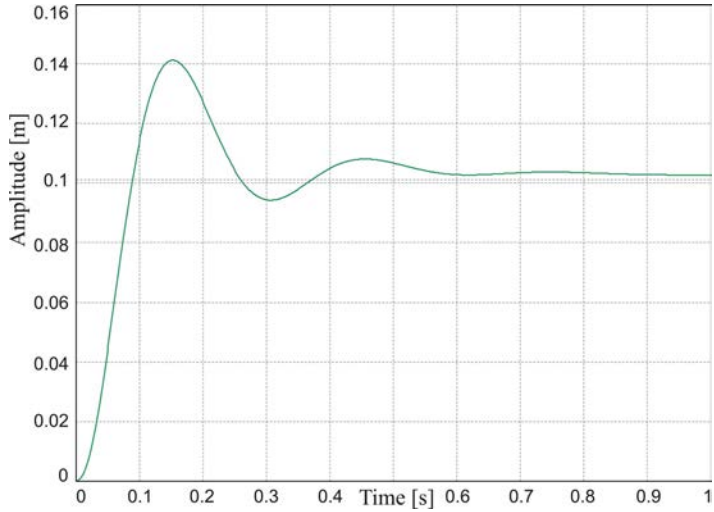

FIG. 9. Suspension step response (0.1 m) without controller.

Figure 9 shows the response of an open-loop system to a step of 0.1 m, Fig. 10 shows the amplitude-frequency characteristics in relation to the excitation w. This is an equivalent of the transfer function defined as the ratio of vibration amplitudes at the output $y = z_2$ to that at the input w, expressed in dB, for the frequency range 0.1–100 Hz.

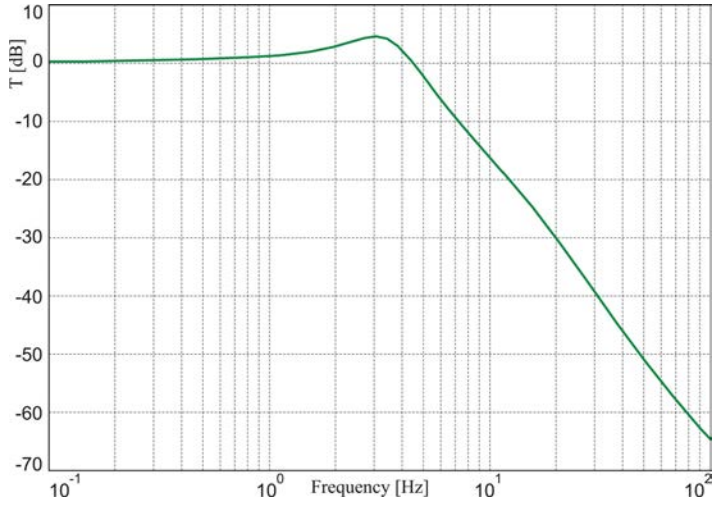

FIG. 10. Vibration displacement transmissibility in the function of frequency.

Characteristics (Figs. 9, 10) are based on the simulations of the identified model under the actuator control voltage equal to zero ($v = 0$). The designed

controller should reduce the vibration amplification in the neighbourhood of resonance frequency $f_0 = 3.4843$ Hz and reduce their displacement transmissibility in the whole frequency range.

From the standpoint of vibration control performance, the transmissibility characteristics is the key measure of quality of the vibration control system. The amplitude-frequency characteristic of the output z_2 in relation to the input v (servovalve control) agrees well with that obtained for the phenomenological model shown in Fig. 5.

5. Conclusions

Properties of actuators generating active force in vibration reduction systems in vehicles are neglected in most models used for the synthesis of control systems. These properties are often assumed to be those of a proportional element. However, taking them into account in a suspension model allows us to evaluate nonlinear features introduced by this very element. In the case of an electrohydraulic actuator, linearisation of the suspension model (in the effective range of state vector variations) does not bring about any major changes that would preclude its use. Both the phenomenological model and that obtained from identification correctly portray the static and dynamic properties of the investigated object. The estimated model agrees better with the laboratory model, furthermore it enables us to evaluate the power consumption by the actuator. The component of the state vector in this model is defined as the power absorbed by an actuator from the supply source. In this approach, power consumption by an actuator and vibration isolation performance can be determined already at the stage of design of the control system. It is a well-established fact that high energy consumption in active vibration control system is the key reason why these systems are rarely employed, so the model proposed by the author might be used in synthesis of a system with lower demands for external power.

References

1. J. Bajkowski, W. Grzesikiewicz, L. Orłowski, *Model matematyczny oraz badania eksperymentalne elementów zawieszenia szybkobieżnego pojazdu gąsienicowego*, Zeszyty Naukowe P.P., Wyd. Polit. Poznańska, **54**, 23–30, 2002.
2. D. A. Crolla, M. B. A. Abdel–Hady, *Active suspension control; performance comparisons using control laws applied to a full vehicle model*, Vehicle System Dynamics, **20**, 107–120 1991.
3. M. D. Donahue, *Implementation of an Active Suspension, Preview Controller for Improved Ride Comfort*, University of California – Berkeley 2001.
4. J. Grajnert, *Izolacja drgań w maszynach i pojazdach*, Wydawnictwo Politechniki Wrocławskiej – Wrocław 1997, ISSN 1425-0993.

5. C. H. Hansen, S. D. Snyder, *Active control of noise and vibration*, E & FN SPON: Chapman and Hall, London 1997.

6. D. Hrovat, *Survey of advanced suspension developments and related optimal control applications*, Automatica, **33**, 10, 1781–1817, 1997.

7. R. Johansson, A. Rantzer, *Nonlinear and Hybrid systems in automotive control*, Springer, 2003.

8. D. Karnopp, *Vehicle stability*, Marcel Dekker, New York 2004.

9. J. A. Levitt, N. G. Zorka, *Influence of tire damping in quarter car active suspension models*, Journal of Dynamic Systems, Measurement and Control: Transactions of the ASME, **113**, 134–137, 1991.

10. R. Palej, *Dynamika i stateczność aktywnych pneumatycznych układów wibroizolacji*, Seria Mechanika – Monografia 218 Wydawnictwo Politechniki Krakowskiej, Kraków 1997, PL ISSN 0860-097X.

11. A. Pizoń, *Hydrauliczne i elektrohydrauliczne układy sterowania i regulacji*, WNT, Warszawa 1987.

12. J. Pluta, J. Konieczny, R. Korzeniowski, *Badanie pneumatycznych układów redukcji drgań mechanicznych*, PNEUMA'2000: XII Krajowa Konferencja Pneuma' 2000 Kielce 2000, Wydawnictwo Politechniki Świętokrzystkiej – Zeszyty Naukowe Elektryka, **39**, 269–278, PL ISSN 0239-4960.

13. R. Rajamani, *Vehicle dynamics and control*, Springer, 2006.

14. Mannesmann Rexroth Catalogue.

15. J. T. Viersma, *Analysis, synthesis and design of hydraulics servosystems and pipelines*, Amsterdam, Elsevier Scientific Publishing Company, 1980.

16. G. R. Wendel, G. L. Stecklein, *A regenerative active suspension system. Vehicle Dynamics and Electronic Controlled Suspensions*, SAE Special Publication Number 861, 129–135, 1991.

17. S. Yildirim, *Vibration control of suspension using a proposed neural network*, Journal of Sound and Vibration, **277**, 1059–1069, 2004.

18. F. Yu, D. A. Crolla, *An optimal self-tuning controller for an active suspension*, Vehicle System Dynamics, **29**, 51–65, 1998.

19. F. Yu, D. A. Crolla, *State observer design for an adaptive vehicle suspension*, Vehicle System Dynamics, **30**, 457–471, 1998.

20. A. Zaremba, *Optimal active suspension design using constrained optimization*, Journal of Sound and Vibration, **207**, 3, 351–364, 1997.

Received July 19, 2007; revised version January 17, 2008.

ENGINEERING TRANSACTIONS • *Engng. Trans.* • **56**, 3, 269–305, 2008
Polish Academy of Sciences • Institute of Fundamental Technological Research

THEORETICAL FOUNDATIONS OF THE HYPOTHESES OF MATERIAL EFFORT

WŁODZIMIERZ BURZYŃSKI (1900–1970)

Czasopismo Techniczne, 1929, **47**, 1–41, Lwów

(*Translated from the original paper in Polish: "Teoretyczne podstawy hipotez wytężenia" by Anna Stręk; scientific editor Ryszard B. Pęcherski*)

This year in June, the Swiss Association of Material Testing for Technology (*Schweiz. Verband für die Materialprüfungen der Technik)* arranged two interesting lectures about material effort and buckling. Even the sole course of the discussion speaks for topical interest of both problems; it is enough to say that it proceeded for over five hours in a tightly filled Auditorium I of the Zurich Polytechnic (*Eidgenössische Technische Hochschule*). The chairman was Prof. Dr. Eng. h.c. M. Roš, the director of the Confederate Material Testing Laboratory (*Eidgenössische Materialprüfungsanstalt – EMPA*).

Personally, I was more interested in the first lecture "Theoretical foundations of the investigations carried out at *EMPA* to elucidate the question of risk of fracture" (*Die theoretische Grundlagen zu den Versuchen der EMPA zur Klärung der Frage der Bruchgefahr*), delivered by a scientist associated with the said laboratory, Eng. A. Eichinger. We can find the content of the lecture in the Chapters I and IV, published respectively in *EMPA Bericht*: No. 28 from 1928 and No 34. from 1929. The whole content can be summarized in the following way. *Critical material effort of a large number of plastic metals obeys quantitatively the Huber-von Mises-Hencky hypothesis. The behaviour of all other materials is relatively best explained, even though not precisely, by Mohr's hypothesis. The idea inherent in the Huber-Hencky theory had until now a hypothetical character; only EMPA has managed – but still with the conservation of Mohr's main idea – to conduct a clear (plausible), convincing and exact proof of rightness of the hypothesis. As a result, the theory of constant critical energy of distortion is nothing else but a generalization of Mohr's concept of an envelope.*

It cannot be denied that the four-year-long series of fine experiments on elucidating the enigma of material effort, conducted with great expenditure of work

and money, has a considerable significance. However, it cannot be denied also that the interpretation of the obtained results, used by *EMPA*, leaves much to be desired. The idea inherent in the Mohr theory is outdated and what even worse – erroneous; there exists a general hypothesis which in the right way and with satisfactory exactness comprises the results of all, without exception, experiments done by the Laboratories in Zürich and Göttingen as well as by many other groups interested in the discussed problem. Similarly, the theoretical efforts of the researches in *EMPA* went the wrong way. The pride of *EMPA*, the meticulous conversion of the Huber-Hencky theory to the area of Mohr's concept, underlined by Roš and Eichinger on nearly every page of the said bulletin, contains a series of errors in the principal matter.

In reply to Eng. Eichinger's lecture I addressed the meeting and in an over one-hour-long speech I tried to explain my view on this question. In the speech I kept, above all, to the outline marked by the title of the preceding speaker's lecture. In the first place then, I explained the theoretical side of the hypotheses of material effort, leaving the experimental aspect of the matter in the background. Referring to the present state of affairs, I limited myself, of necessity, to discuss problems of local and static material effort only.

Foreign countries do not know most of the critical arguments known in Poland, as I had learned on the occasion of delivering a similar lecture in Göttingen. The hypotheses of material effort are treated there – to a certain degree even rightly – only as hypotheses; all novelties in this field, are often studied in laboratories straightaway, without prior insight into elementary theoretical details. Owing to this fact, every couple of years there arises the need for a new general hypothesis, since the old one fails. In such state of affairs only the calculus of probability can tell, by examining all the existing typical groupings of components, how many new and useless theories we will be seeing.

Coming back to the said lecture, I have to admit with satisfaction that it met with a great interest, which reflected at least in Professor Roš's request for a written copy of it; surely, a relevant article will soon appear in German in print, edited by *EMPA*[1)]. Before it happens though, it will be good to acquaint Polish readers with this topical question. The present article extends the mentioned speech by 25%.

Questions of applied mechanics seldom have such a rich history to their credit as the theories of material effort do[2)]. The question started in Galileo[3)] and Leibniz[4)] times, it outlived Coulomb[5)] and Navier[6)] as well as de Saint Venant[7)] and Rankine[8)], Clebsch[9)] and Beltrami[10)], and went through the hands of many later, distinguished scholars and in the present day – the time of competition between reliability and economics – it is, next to the problem of buckling, the most topical scientific issue in the theory of elasticity as well as

in the very popular plasticity and, finally, in the strength of materials. Rarely can one meet with so many different views and inconsistencies as in this field. The hypotheses of material effort were first transferred from their birthplace – the domain of stress – to the ground of strain theories wherefrom, after not very good results, they were moved to their last resort – the energy-based approach, in the state of which they have been remaining till the present day; however, their mathematical form does not guarantee any general reliable theory and clearly does not satisfy the needs and interest of practice. But even though, such divergence of views has never before produced so much benefit as in this field. A thorough review of the existing material allows one to criticize it, to judge its bad and good parts, reject the first and use the latter; in consequence, it leads to a general hypothesis which has a very good chance of success. For a better understanding of its sense and, in case of need, quality, I will give at first a brief list of parameters of calculation of the discussed matter and also a critical draft of the existing hypotheses.

The material effort of a certain point of a body is a physical state closely related to the state of stress of this point, or its strain. The value of the material effort is described, irrespectively of the choice of a coordinate system, by six components of the state of strain ε_x, ε_y, ε_z, $\frac{1}{2}\gamma_x$, $\frac{1}{2}\gamma_y$, $\frac{1}{2}\gamma_z$ or equivalently – by six components of the state of stress[11)] σ_x, σ_y, σ_z, τ_x, τ_y, τ_z. The effects of material effort, especially the manner of passing through the characteristic limits (the proportional limit, the limit of elasticity, the yield point and the ultimate strength), the pace of passing from one limit to the next and changes of behaviour in-between, depend on individual properties of the body. Material efforts of two points subjected to two different states of strain or stress are equal when their physical effects are equal; the function

$$f\left(\varepsilon_x,\, \varepsilon_y,\, \varepsilon_z,\, \frac{1}{2}\gamma_x,\, \frac{1}{2}\gamma_y,\, \frac{1}{2}\gamma_z\right) = a \tag{1}$$

or equivalently

$$g\left(\sigma_x,\, \sigma_y,\, \sigma_z,\, \tau_x,\, \tau_y,\, \tau_z\right) = b, \tag{2}$$

expresses mathematically the consistency of the effects.

We assume that the sets of critical components (as we are going to call them hereafter), which cause equal material effort, change in a continuous manner; we demand the same from the above equations. It is basically guaranteed by the continuity of the material considered; in case of its lack, even the simplest considerations fail in the area of strain as well as of stress.

The highlighted above independence of the material effort of a certain point upon the chosen frame of reference at this point, allows one to simplify the

functions f and g. The mechanics of continuum allows, to one's considerable advantage, replace a set of six arbitrary components by the three principal ones. Their values ε_1, ε_2, ε_3 or σ_1, σ_2, σ_3 result from the cubic equation:

$$\varepsilon^3 - 3\pi_1\varepsilon^2 + 3\left(\pi_1^2 - \frac{1}{2}\pi_2^2\right)\varepsilon - \pi_3^3 = 0 \tag{3}$$

or accordingly

$$\sigma^3 - 3\omega_1\sigma^2 + 3\left(\omega_1^2 - \frac{1}{2}\omega_2^2\right)\sigma - \omega_3^3 = 0, \tag{4}$$

where the homogeneous expressions

$$\begin{aligned} \pi_1 &= \frac{1}{3}\left(\varepsilon_x + \varepsilon_y + \varepsilon_z\right), \\ \pi_2^2 &= \frac{1}{9}\left[\left(\varepsilon_y - \varepsilon_z\right)^2 + \left(\varepsilon_z - \varepsilon_x\right)^2 + \left(\varepsilon_x - \varepsilon_y\right)^2 + \frac{3}{2}\left(\gamma_x^2 + \gamma_y^2 + \gamma_z^2\right)\right], \\ \pi_3^3 &= \varepsilon_x\varepsilon_y\varepsilon_z + \frac{1}{4}\gamma_x\gamma_y\gamma_z - \frac{1}{4}\left(\varepsilon_x\gamma_x^2 + \varepsilon_y\gamma_y^2 + \varepsilon_z\gamma_z^2\right), \end{aligned} \tag{5}$$

or accordingly

$$\begin{aligned} \omega_1 &= \frac{1}{3}\left(\sigma_x + \sigma_y + \sigma_z\right), \\ \omega_2^2 &= \frac{1}{9}\left[\left(\sigma_y - \sigma_z\right)^2 + \left(\sigma_z - \sigma_x\right)^2 + \left(\sigma_x - \sigma_y\right)^2 + \frac{3}{2}\left(\tau_x^2 + \tau_y^2 + \tau_z^2\right)\right], \\ \omega_3^3 &= \sigma_x\sigma_y\sigma_z + \frac{1}{2}\tau_x\tau_y\tau_z - \left(\sigma_x\tau_x^2 + \sigma_y\tau_y^2 + \sigma_z\tau_z^2\right) \end{aligned} \tag{6}$$

are evidently independent of the choice of the six groups of components. They are also mutually independent invariants of the state of stress or strain. The simplest way to calculate their values is to reject the shear (tangent) components and replace the normal components with the principal ones.

If we know the principal components, we can easily define the components ε, $\frac{1}{2}\gamma$ or σ, τ, for the directions ϕ, χ, ψ referred to the orthogonal coordinate system (ε_1, ε_2, ε_3) or (σ_1, σ_2, σ_3), by the formulae:

$$\begin{aligned} \varepsilon &= \varepsilon_1\cos^2\phi + \varepsilon_2\cos^2\chi + \varepsilon_3\cos^2\psi, \\ \left(\frac{1}{2}\gamma\right)^2 &= \left(\varepsilon_2 - \varepsilon_3\right)^2\cos^2\chi\cos^2\psi + \left(\varepsilon_3 - \varepsilon_1\right)^2\cos^2\psi\cos^2\phi \\ &\quad + \left(\varepsilon_1 - \varepsilon_2\right)^2\cos^2\phi\cos^2\chi \end{aligned} \tag{7}$$

or

$$\begin{aligned}\sigma &= \sigma_1 \cos^2\phi + \sigma_2 \cos^2\chi + \sigma_3 \cos^2\psi,\\ \tau^2 &= (\sigma_2-\sigma_3)^2 \cos^2\chi\cos^2\psi + (\sigma_3-\sigma_1)^2 \cos^2\psi\cos^2\phi\\ &\qquad + (\sigma_1-\sigma_2)^2 \cos^2\phi\cos^2\chi\,.\end{aligned} \tag{8}$$

There is only one condition demanded for the existence of these formulae – the material continuity. The orientations $\phi = \psi = \frac{\pi}{4}$, $\chi = \frac{\pi}{2}$, and $\phi = \chi = \psi = \arccos\frac{1}{\sqrt{3}}$ are worthy of consideration. We obtain successively

$$\begin{aligned}\varepsilon &= \varepsilon_{II} = \frac{\varepsilon_1+\varepsilon_3}{2},\\ \frac{1}{2}\gamma &= \frac{1}{2}\gamma_{II} = \frac{\varepsilon_1-\varepsilon_3}{2},\end{aligned} \tag{9}$$

or

$$\begin{aligned}\sigma &= \sigma_{II} = \frac{\sigma_1+\sigma_3}{2},\\ \tau &= \tau_{II} = \frac{\sigma_1-\sigma_3}{2},\end{aligned} \tag{10}$$

for them; moreover:

$$\begin{aligned}\varepsilon &= \frac{1}{3}(\varepsilon_1+\varepsilon_2+\varepsilon_3) = \pi_1,\\ \frac{1}{2}\gamma &= \frac{1}{3}\sqrt{(\varepsilon_2-\varepsilon_3)^2+(\varepsilon_3-\varepsilon_1)^2+(\varepsilon_1-\varepsilon_2)^2} = \pi_2,\end{aligned} \tag{11}$$

or

$$\begin{aligned}\sigma &= \frac{1}{3}(\sigma_1+\sigma_2+\sigma_3) = \omega_1,\\ \tau &= \frac{1}{3}\sqrt{(\sigma_2-\sigma_3)^2+(\sigma_3-\sigma_1)^2+(\sigma_1-\sigma_2)^2} = \omega_2.\end{aligned} \tag{12}$$

For arbitrary directions the formulae for ε, $\frac{1}{2}\gamma$ or σ, τ can be represented in a very fair, developed by MOHR[12)] and well-known graphical form of circles for strains and stresses. A system of three circles for strains is homothetic to a system of three circles for stresses; it occurs not only in elastic regions but also in plastic ones.

The following facts deserve notice: the sum of circumferences of three principal circles, on the assumption that $\varepsilon_1 > \varepsilon_2 > \varepsilon_3$ or $\sigma_1 > \sigma_2 > \sigma_3$, is equal to

$$U_\varepsilon = 2\pi(\varepsilon_1-\varepsilon_3) = 2\pi\gamma_{II} \quad \text{or} \quad U_\sigma = 2\pi(\sigma_1-\sigma_3) = 2\pi\tau_{II}. \tag{13}$$

Similarly, the total area of these circles is equal to

$$F_\varepsilon = \frac{\pi}{4}\left[(\varepsilon_2-\varepsilon_3)^2+(\varepsilon_3-\varepsilon_1)^2+(\varepsilon_1-\varepsilon_2)^2\right] = \frac{9\pi}{4}\pi_2^2,$$

(14) or

$$F_\sigma = \frac{\pi}{4}\left[(\sigma_2-\sigma_3)^2+(\sigma_3-\sigma_1)^2+(\sigma_1-\sigma_2)^2\right] = \frac{9\pi}{4}\omega_2^2.$$

When the principal components are used, the critical material effort is defined by the functions

$$f(\varepsilon_1,\varepsilon_2,\varepsilon_3) = a \tag{15}$$

or

$$g(\sigma_1,\sigma_2,\sigma_3) = b. \tag{16}$$

The functions f and g in the earlier introduced, general forms as well as in the above particular ones are mutually dependent, since there exist close correlations between the components of strain and the components of stress.

Nowadays we hear more and more often that the study of material effort has to be necessarily based on investigation of the critical values of strain as well as stress; this opinion is quite right; however, only from the experimental point of view, since a properly constructed hypothesis serves its turn equally well on the ground of strain as on the ground of stress. In the first case, function f plays the role of the third equation, which in a correlation with an a priori assumed double proportion $\varepsilon_1 : \varepsilon_2 : \varepsilon_3$ allows one to calculate the critical values ε_1, ε_2, ε_3. On the other hand, the function g plays equivalently the unique role for a sequential ratio $\sigma_1 : \sigma_2 : \sigma_3$. On this occasion we have additionally defined a mathematical role of hypotheses of material effort: they are supposed to enable one to calculate correctly the limit (allowable, critical) values of components for their assumed ratio. If only a so-called inhomogeneity of matter could be defined precisely each time, the inhomogeneity would not constitute much difficulty in the interpretation of experimental results and in additional correction of the theories of material effort. However, this is not true in the real terms; facing this fact we have to assume that technically important materials are perfectly homogenous and that the hypotheses of material effort are developed for such materials. It partly explains the deviations between experiment and theory. The lack of uniformity of a strain state, or a state of stress, during laboratory tests, becomes an equally important factor; to obtain uniformity is practically impossible.

In this way, the interpretation of the experimental results presents immense difficulties for the theory; hence, we are being forced to mingle two notions:

the total and the local material effort. All theoretical calculations are based on the material effort of a point (e.g. an outer fibre of a beam in the intersection where a maximum bending moment occurs), while all the experimental data come from the material effort of a certain volume of continuum. This is the next cause of the deviations between the theory and the experiments. However, the most important factor is unquestionably the isotropy – or the quasi-isotropy (in the meaning established by VOIGT[13]) – of materials. We are compelled to decide against a great number of all the various types of anisotropy (defined by 21 elastic constants in a general case; however, still in a quite narrow range). We assume, of necessity, that the investigated materials are isotropic; in a large number of cases we cannot guarantee the latter or determine the corresponding deviations in a precise manner (vibrating of concrete, rolling of steel, internal stresses – to some extent, repeated loading and so on).

The isotropy is expressed in a particularly simple, though highly restricted in its application case: the linear Hooke's law:

$$\begin{aligned} \sigma_{x,y,z} &= 2G\left(\varepsilon_{x,y,z} + \frac{\mu e}{1-2\mu}\right), \\ \tau_{x,y,z} &= G\gamma_{x,y,z} \end{aligned} \tag{17}$$

or

$$\begin{aligned} \varepsilon_{x,y,z} &= \frac{1}{E}\left[(1+\mu)\,\sigma_{x,y,z} - \mu s\right], \\ \gamma_{x,y,z} &= \frac{1}{G}\tau_{x,y,z}, \end{aligned} \tag{18}$$

where E, G, μ are commonly known elastic constants; additionally: $e = 3\pi_1$, $s = 3\omega_1$. The usage of the principal components eliminates the shear ones; for the normal components the indices *1, 2, 3* should be used instead of the x, y, z.

The relation between the components of both states has a secondary character; the energy of strain, or elasticity, of an assumed unit of volume

$$\Phi = \Phi_v + \Phi_f \tag{19}$$

has the primary significance in this aspect, though still with the identical restrictions. The first term Φ_v stands for the energy due to the change of volume, the other term Φ_f – for the energy due to the change of shape; they are shortly expressed by:

$$\begin{aligned} \Phi_v &= \frac{3}{2}\frac{E}{1-2\mu}\pi_1^2 = \frac{3}{2}\frac{1-2\mu}{E}\omega_1^2, \\ \Phi_f &= 3G\pi_2^2 = \frac{3}{4G}\omega_2^2. \end{aligned} \tag{20}$$

Here, the components of one state are partial derivatives of the energy Φ with respect to the components of the other state. The energy Φ expressed in such way has an approximate character, since it consists of the first terms of a general expansion in power series. Basing on the Stickelberg theorem on the structure of an rational integer function, which is independent of the choice of a reference system, we can easily give a general expression for the energy Φ. This is, in general, a series formed from the terms: π_1, π_1^2, π_2^2; π_1^3, $\pi_1\pi_2^2$, π_3^3; π_1^4, $\pi_1^2\pi_2^2$, $\pi_1\pi_3^3$, π_2^4;.... and an appropriate number of elastic constants m as coefficients. A similar series can be formed from the three invariants ω_1, ω_2^2, ω_3^3. In the above expansion, the free term and the term of the first grade is disregarded due to the commonly known reasons. The terms π_3^3; π_1^4, $\pi_1\pi_3^3$, π_2^4;.... are disregarded owing to the unique dependence between the components of strain and stress states; then the invariant π_3^3, does not play any essential role in the theory of elasticity.

The described above decomposition of the energy Φ into the two parts Φ_v and Φ_f, done by STOKES[14] for the first time and a little later by HELMHOLTZ[15], is in this particular case right; however, in general, a linear superposition does not simply lead to a superposition of squares. There arises a thought that this particular feature generally characterizes isotropic bodies (enabling the possibility of transition from solids to liquids). Supposing then the possibility of splitting the energy into the two characteristic parts also in the case considered here, we see that in the general expansion the mixed terms, namely π_1, π_1^2, $\pi_1^2\pi_2^2$,...., are disregarded. Finally, we obtain the result (19), where

$$\begin{aligned} \Phi_v &= m_{2v}\pi_1^2 + m_{3v}\pi_1^3 + m_{4v}\pi_1^4 + \dots, \\ \Phi_f &= m_{2f}\pi_2^2 + m_{4f}\pi_2^4 + \dots. \end{aligned} \tag{22}$$

The series written above are of course convergent; their sums indeed present the energies Φ_v and Φ_f.

We obtain the components of the state of stress by differentiating Φ with respect to the components of the strain state. Using them, and even in a general case, that is without reducing the energy terms, one can easily prove that the invariants of one state are functions of the invariants of the other state. In general then, we have

$$\pi_i = \pi_i(\omega_1, \omega_2, \omega_3) \quad \text{and in reverse} \quad \omega_i = \omega_i(\pi_1, \pi_2, \pi_3), \tag{24}$$

where $i = 1, 2, 3$.

In this way we have finished reviewing the theoretical means used in developing the hypotheses of material effort. Let us now look closely at the arduous way they had to go. The whole effort and wit of the authors of the hypotheses of material effort were focused on producing from the six components of strain or

stress states a single mathematical expression that would experimentally characterize itself with constancy or at least possibly simple, definable variability. That moment there arose an idea that one handles three components more easily than six. Basing on this, the principal components were introduced. This smooth simplification caused a new necessity: to introduce the inconvenient inequality $\varepsilon_1 \geq \varepsilon_2 \geq \varepsilon_3$, or $\sigma_1 \geq \sigma_2 \geq \sigma_3$. We do not realize in general what a great disadvantage in hypotheses of material effort this inequality presents. Let us suppose that one uses such a hypothesis in a certain particular case. The theory of elasticity or the science of strength of materials provides us with the solution of the particular problem by giving six components as functions of spatial coordinates; external loads and dimensions of the investigated element play the role of parameters while the elastic constants are coefficients. We obtain the three principal components from the cubic Eqs. (3) or (4); since, in general, these components are different and real, the solution must be obtained with the use of transcendental functions: in such a solution all the details of calculation are lost. Finally, to crown it all, one has to fix the order $\varepsilon_1 > \varepsilon_2 > \varepsilon_3$ or $\sigma_1 > \sigma_2 > \sigma_3$, which is simply impossible; the hypothesis is of no general use. That these details escape the common notice is due to the fact that we have accustomed ourselves to simplifying some problems to their two-dimensional form, where the above difficulties cancel to a considerable degree.

In search for a possibly simple combination of components defining the material effort, primitive means were initially used. In this way the hypothesis of a constant tension σ_1 disregarded the two remaining principal stresses σ_2 and σ_3 and, respectively, the hypothesis of a constant elongation ε_1 neglected the two principal strains ε_2 and ε_3. Astonishing! The stress hypothesis was quickly denied acceptance in favour of the strain hypothesis; an exact physical justification was being seen in the expression: a system of stresses which causes the greatest elongation is a measure of critical material effort (18). If the stress hypothesis had been put into the following words: a system of strains which causes the greatest tension (17) is a measure of critical material effort, such hypothesis would certainly linger till nowadays in various textbooks and almanacs, just like its rival. But still they are both asymmetrical and both of them are erroneous. Later corrections, that is lower limits introduced with the help of constant pressure σ_3 or constant contraction ε_3, are not worthy much more. A properly constructed hypothesis should express itself with the same groupings of components on both grounds; while here the equalities $\varepsilon_1 = a_1$, $\varepsilon_3 = a_3$ are not corresponded by $\sigma_1 = b_1$, $\sigma_3 = b_3$ and the same in the reverse way (17), (18). All attempts of further resort in this direction failed; the dubious worth of BACH'S coefficient α_0 is at present widely known[16)].

Employing single components did not cause the desired result, so the use of simple sets of groupings of strains or stresses was introduced. The hypothesis of

constant shear stress τ_{II} (10) (COULOMB[5], GUEST[17])has indisputably a fundamental significance in the development of the study of material effort[18]; only very precise experiments proved its very good, though approximate character. It is the effect of the mathematical form of the hypothesis; one should pay careful attention to the fact that the equality $\tau_{II} = b$ corresponds to by the equality $\frac{1}{2}\gamma_{II} = a$ and the same in the reverse direction (17), (18). The substance of the hypothesis is then independent of the choice of the units of measurement. Its minor errors are caused by the absence of the intermediate component. That these errors did not go far beyond the practical limit is only due to the fact that the range of application of this hypothesis is very narrow; *viz.* it refers only to materials whose behaviour in critical tension k_t and compression k_c is expressed by the equality $k_t = k_c = k$.

The matter with the DUGUET[19] and MOHR[20] theory presents itself a bit worse. This hypothesis in the general form:

$$g(\sigma_{II}, \tau_{II}) = b \tag{25}$$

makes a clear progress in the development of the study of material effort. A generalisation inherent in the theory (25) can be even to a certain degree well explained, since the stresses σ_{II} and τ_{II} belong to the same orientation; on a pictorial scheme the three stress circles move along the σ axis and change their total perimeter (13) in a continuous manner. But this interpretation fails in the ground of strain, since, even though τ_{II} corresponds with the magnitude $\frac{1}{2}\gamma_{II}$, the stress σ_{II} is not corresponded by ε_{II} but by (in a linear approximation): $\varepsilon_{II} + \dfrac{\mu e}{1-2\mu} = \dfrac{\varepsilon_1 + 2\mu\varepsilon_2 + \varepsilon_3}{2(1-2\mu)}$ (17). It is similar in a reversed procedure. The hypothesis is then asymmetrical; in the ground of stress it expresses itself differently than in the ground of strain.

As for the details, one should take both perspectives – from Duguet's position and from Mohr's position. The first one was calculating, the other one was drawing – both nearly in the same time; the stranger it seems then, that the first one was forgotten so quickly. Duguet puts Coulomb's premises into a mathematical form; he assumes that the critical effects occur as a result of overcoming friction (of the coefficient $f = \tan\beta$) and cohesion d, namely, in such a two-dimensional orientation ξ, η, ζ for which the left-hand side of the equation $\tau + f\sigma = d$ reaches its maximum; σ and τ are defined by the formulae (8). I am not sure if it is commonly known that the intermediate stress σ_2 is cancelled from Duguet's calculation only due to a mathematical coincidence, since the critical orientation turned out to be the direction $\xi = \frac{\pi}{4} - \frac{\beta}{2}$, $\eta = \frac{\pi}{2}$, $\zeta = \frac{\pi}{4} + \frac{\beta}{2}$. Mohr proceeds inversely and incorrectly; he assumes in advance and without appropriate justification, the independence of material effort of the intermediate stress σ_2 and, disregarding the two stress circles, he surrounds the series of circles (σ_1, σ_3) by

an envelope and in consequence, with the help of the consideration of not the material effort itself but the geometrical features of the pictorial scheme of the stress circles, he comes to the same critical orientation and the same scheme of envelope as the one (but not called this name) found by Duguet. These details have been overlooked in the literature; Mohr's unquestionably justified authority weighed here more than his theory of material effort.

This theory is then unfit for a general use for the reasons explained above (the inconvenient inequality) and incorrect due to the proved asymmetry. Also experiments do not support it completely; envelopes for different groupings of components do not and cannot mutually cover; the influence of the intermediate stress σ_2 cannot be omitted. And even if such a particular envelope existed, it would not suit characterizing material effort in this case; the experimental details as well as the mathematical arguments and to some extent – even the hypothesis itself, demand and prove that Mohr's envelope does not surround all possible critical circles, since some of them are hidden inside the envelope without touching it.

This detail in the case of existence of the said envelope does not prove fundamentally the incorrectness of the Duguet-Mohr theory; it only indicates that the coordinate system (σ, τ) is inadequate for expressing the substance of this hypothesis. The appropriate system for this hypothesis would be the system (σ_{II}, τ_{II}), in which all the critical states find their place in the form of the points (σ_{II}, τ_{II}). This subtlety has also escaped notice, which can be proved by the graphical schemes found in the immense number in various publications and drawn exactly due to Mohr's recipe. Meanwhile, it is clear that it is easier to put the point in the system (σ_{II}, τ_{II}) than to draw a circle with the center coordinates $(\sigma_{II}, 0)$ and the radius τ_{II} in the system (σ, τ). As for the angles – a simple relation $\sin\beta = \tan\alpha$ between the slope of the tangent $\beta = \arctan f$ in the system (σ, τ) and α in the system (σ_{II}, τ_{II}) (α, β measured from the negative sense of the axis of abscissae) has also escaped notice. The whole misunderstanding lies in the fact that it is commonly assumed that the envelope is the essence of Mohr's hypothesis while it is untrue: the essence of the hypothesis is the assumption of existence of the function (25).

There is no need for proving that every hypothesis can be graphically illustrated by a single-parameter set of envelopes; it is enough to make this parameter (c) dependent on the value σ_2 in the following way:

$$\sigma_2 = \frac{1+c}{2}\sigma_1 + \frac{1-c}{2}\sigma_3 = \sigma_{II} + c\tau_{II}, \tag{26}$$

where c is limited by the inequality $-1 \leq c \leq 1$; each c corresponds one envelope. This can be clearly seen in the illustrations to experiments on brittle materials for which, due to technical difficulties, laboratories apply the two extreme cases

$c = -1$, $c = 1$, or rarely $c = 0$. These envelopes – as I have mentioned – are not identical. In this way, the general incorrectness of all hypotheses which disregard the intermediate stress σ_2, and in particular the Duguet-Mohr one, is being stated.

The attempt at mathematical justification of the theory of material effort made by Duguet, close to correctness and the only one known in the literature, failed. This attempt shows clearly that there exist no *theories* of material effort, there are only *hypotheses* of material effort. In this field one must not prove but should only verify.

With passing of time, the failures, which I have presented, have forced one to a considerable carefulness in formulating hypotheses. The generality of the hypothesis discussed above is already a proof of this fact. HERTZ[21)] went even further. He suggested namely to represent each of the three components by a point in the coordinate system (σ_1, σ_2, σ_3) and to obtain the equation of the surface constructed in this manner as the desired function. If we look closely at Hertz's concept, we see that there is a lot of – let us say – practical sense in it, but nothing more. Hertz did not know really what to think about the material effort. HAIGH[22)], an Englishman, took up Hertz's suggestion (independently of him, it seems) and developed it with reference to all hypotheses known by himself; we did not witness any significant progress in the field of material effort due to this fact.

In the meantime, the needs of theory and practice were insistently demanding some plausible hypothesis. Sometimes this pressure caused desperate actions. BECKER[23)], an American, overlapped (in the exact meaning of this word) the hypothesis $\tau_{II} = b$ on the hypothesis $\varepsilon_1 = a_1$, $\varepsilon_3 = a_3$. Then, he multiplied the first one by 1.2 (Bach's 1.3 reminds itself) and, finally, in the system (σ_1, σ_3) he obtained for plane states a decagon whose outline agreed with the experiments. WESTERGAARD[24)] drew this outline along the line $\sigma_1 = \sigma_2 = \sigma_3$ and has obtained in the Hertz-Haigh system a prism deceptively similar to the Huber-Mises-Hencky cylinder; their cross-sections differed only by 8 per cent. To use such hypothesis is simply impossible.

The hypothesis developed in the doctor's dissertation (TH Stuttgart) by SANDEL[25)] is more demanding in this aspect; it is a classic example of ... a false theory. According to this hypothesis, in case when $\kappa = \frac{k_c}{k_t} > 3$ (and we know technical materials for which κ reaches even the value 20), the three following states should be considered to be equal in terms of material effort $\sigma_1 = -\infty$, $\sigma_2 = -\infty$, $\sigma_3 = -\infty$; $\sigma_1 = 0$, $\sigma_2 = -\infty$, $\sigma_3 = -\infty$; $\sigma_1 = +\infty$, $\sigma_2 = -\infty$, $\sigma_3 = -\infty$; it is completely sufficient to demonstrate the value of this theory. However, the example of Sandels hypothesis is very worthy. His theory relates linearly maximum shear strain $\frac{1}{2}\gamma_{II}$ with a volumetric strain $e = 3\pi_1$; it is then symmetrical since in terms of stress the above expressions (18) correspond to

magnitudes τ_{II} and $s = 3\omega_1$ constructed in an analogous way. Where to search for the cause of the incorrectness? The answer is simple: the magnitudes $\frac{1}{2}\gamma_{II}$ and π_1 are not connected (9), (11); similarly to τ_{II} and ω_1 (10), (12). Since the first ones are the tangent components of the orientation $\phi = \frac{\pi}{4} = \psi$, $\chi = \frac{\pi}{2}$, the other ones express the normal components of the orientation $\phi = \chi = \psi = \arccos\frac{1}{\sqrt{3}}$, that is of a totally different one. It is – as we see – a case opposite to the Duguet-Mohr's one, where the referred expressions were used, but moving from one system of units (*variables – ed. note*) to the other induced the asymmetric results. A correctly constructed hypothesis should satisfy both conditions.

I have noticed with surprise (*EMPA Diskussionsbericht Nr. 28*) that Sandel, without explaining reasons, abandoned the theory he had been previously working on and privately informed about the development of a new one about the constant "resultant" strain $\varepsilon_1^2 + \varepsilon_2^2 + \varepsilon_3^2 = a^2$. This hypothesis has a much narrower range of application, namely only for the cases where $\kappa = 1$; it does not lead then to so many distinct contradictions as the former one. However, it is still incorrect: the sum of squares of principal components does not have any known significance. The hypothesis is asymmetrical: the expression $\varepsilon_1^2 + \varepsilon_2^2 + \varepsilon_3^2$ corresponds, according to Hooke's law (18), to a more extent expression in stress components: $\sigma_1^2 + \sigma_2^2 + \sigma_3^2 + \dfrac{2\mu\,(1-2\mu)}{1+3\mu-\mu^2}\,(\sigma_2\sigma_3 + \sigma_3\sigma_1 + \sigma_1\sigma_2)$, which reduces to the symmetrical hypothesis expressed in stress components only for the theoretical value $\mu = \frac{1}{2}$, possible in materials with $\kappa = 1$ only in plastic regions. One cannot develop every couple of years any new, completely different hypotheses without exposing oneself to suspicion that one has recognized the former one as incorrect.

It will not be irrelevant here to state a certain general remark induced by the review of all the known hypotheses: all theories involving Poisson's ratio μ in their mathematical form are more or less incorrect. For, elastic constants have nothing in common with the material effort or, more precisely: it is not the material effort that depends on them, but they depend on the material effort. If we are considering the dimensions of a bar in tension, we do not think of the constant E or μ, but of the allowable stress $\sigma_1 = k_t$; if we are designing a twisted shaft, we do not ask about the constant G or μ but about the admissible effort, whose measure is $\tau_{II} = k_s$. It must be similar in a general three-axial case. Calibrating the empirical facts by the constant μ completely misses the point and is only an unfortunate burden to the form of the theory of material effort. It is a detail which, apart from other facts, speaks against Sandel's new concept.

A great step forward in the development of the hypotheses was assuming by Beltrami[8], Huber[26] and Haigh[22] the energy $\Phi = \dfrac{3}{2}\dfrac{1-2\mu}{E}\omega_1^2 + \dfrac{3}{4G}\omega_2^2$ (19), (20), (21) as a measure of critical material effort. The energy-based theories have

a lot of characteristics of being probable. Material effort is a directionless magnitude (*by the assumption of material isotropy – ed. note*) – a scalar, and energy is also a scalar. The energy is the expression of independence of the state of strain, or stress, of our fancy of choosing directions of reference; material effort is also independent of the choice of a coordinate system. A change of units of calculation (*variables - ed. note*) does not reflect on the shape of the theories, since we also have: $\Phi = \frac{3}{2}\frac{E}{1-2\mu}\pi_1^2 + 3G\pi_2^2$ (19), (20), (21). The hypothesis expresses itself in the most general way by six components; conversion to principal components consists in deleting the tangent ones. The inequality, which was used in other hypotheses precluding their further discussion and application, here cancels out from the calculation completely. The magnitudes π_1, π_2 or equivalently ω_1, ω_2, are not in conflict with each other; they hold distinct positions on the field of strain as well as stress (11), (12).

It was difficult at first to find any better means. And, in spite of all, there was a great need to find such, since the new hypothesis – even in the narrow range of its application – did not satisfy our demands for exactness. If we look closer at the essence of this failure, we see that there is only one reason for this failure. The hypothesis was burdened with the presence of Poisson's ratio μ; as I have mentioned above, it is a rather general cause of the incorrectness of a considerable number of hypotheses.

There exists in the literature a faint, probably unconscious, attempt to remove this constant. From WEHAGE'S[27] theory (1905) it follows that he considers the expression $\sigma_1^2+\sigma_2^2+\sigma_3^2 = b^2$ as a measure of material effort; it is nothing else but Beltrami's hypothesis for $\mu = 0$. Sandel's new approach then consists only in replacing the units σ with ε. One can advance identical critical arguments against Wehage's theory.

Only HUBER[26] (1904) gave the matter a favorable turn by taking under consideration the decomposition of energy introduced by STOKES[12] and HELMHOLTZ[13]. His hypothesis, set in a letter to FÖPPL[28], contains an unusual idea. This hypothesis has all the advantages of the theory discussed before and apart from that, it gives a certain generalization by introducing two critical regions: $\omega_1 \geq 0$ and $\omega_1 \leq 0$. Unfortunately, the range of the hypothesis still remains narrow: $1 \leq \kappa \leq 1.225$, owing to the incomplete omission of the constant μ. Apart from that, the hypothesis comes from one region to the other one in a discontinuous manner.

According to the above reasons, only the second part of the Huber hypothesis $\Phi_f = \frac{3}{4G}\omega_2^2 = b^2$, and without the restrictions concerning ω_1, has been accepted in the literature. Tests in the first place and HENCKY'S papers[29] from the field of theory of plasticity in the second case contributed to this fact. MISES'S[30] (1913) solely graphical argument of a sphere as a surface of critical states in the system

of tangent principal components had a considerably smaller influence. Based on erroneous mathematical and logical premises, Roš and Eichinger's efforts to present the hypothesis as a general expansion of Mohr's idea have completely no meaning. It is enough to say that the referred proof describes the strain state of a body with the help of only three, and moreover – tangent components, and that it neglects difference between a vector and a tensor (by introducing a geometrical summation of components of strain state without regard to their respective two-dimensional orientation) and that, finally, as a consequence of the above mistakes, it describes isotropy by the material constants characterizing material that depend on the direction. On the other hand, among experiments, one should put Roš and Eichinger's[31)] tests on the first place. From a whole series of facts stated in *EMPA*, one fact demands a special attention; Roš proved empirically the mathematical equality $\Phi_f = \frac{3}{4G}\omega_2^2 = 3G\pi_2^2$ (21) in the meaning that one can use ω_2 equally well as π_2 as a measure of material effort of plastic materials $\kappa = 1$. It clearly confirms my supposition that the change of variables should not reflect in any way on the form of a hypothesis.

Huber-Hencky's theory discredited a whole series of other hypotheses at one go. Final accounts with a very near Coulomb-Guest's theory were made easier to settle by Roš[31)], Ensslin, Lode[32)] and many other researchers' great experiments. Presently, no one doubts its truthfulness for plastic metals characterized by $\kappa = 1$. In this area the question of material effort has been definitely solved. If further, verifying tests are being performed, it is only due to extend the interval of its validity with respect to the types of stress states, namely to possibly advance the two border limits: hydrostatic uniform tension on the one hand and the corresponding pressure on the other.

However, the matter has not been settled in general; there remain all the materials $\kappa > 1$, that is a great majority of technically important materials. There were attempts to solve this difficult task, yet still simplified by a large amount of the existing material. A careful reader guesses at once what such a theory should look like in its general shape. It should relate to Huber-Hencky theory like the Duguet-Mohr hypothesis relates to Coulomb-Guest hypothesis. One should be a generalization of the other; from the more general one, there should follow a more specific one as a particular case.

Unfortunately, this direction has not been exactly followed. Schleicher[33)] (and Mises at the same time, it seems) picked up Huber's general idea; instead of – as primarily Huber had done – dividing the critical groupings into the two regions $\omega_1 \geq 0$ and $\omega_1 \leq 0$, he made a division into an infinitely large number of infinitesimally small areas, he fixed a different measure of material effort in each of them and moved on to a limit in a purely mathematical sense. To get rid of the suspicion of the deciding meaning of the energy – based idea or maybe to attain originality, he did not introduce into the calculation the essential com-

ponents of Huber's general theory, that is Φ_v and Φ_f, but $\omega_1 = \sqrt{\frac{2E\Phi_v}{3(1-2\mu)}}$ and $\sigma_0 = \sqrt{2E\Phi}$, which are still in a close relation to the latter. And this was the critical mistake of his theory $g(\omega_1, \sigma_0) = b$, since in this manner it lost the influence of the energy of distortion Φ_f and shut itself the way to transition to Huber-Hencky hypothesis in a specific case $\kappa = 1$. This hypothesis flashed up for a moment and then vanished dumped by... its author (*Bauingenieur, 1928*); for, on the occasion of calibration of elementary experiments on shear, the hypothesis demanded for concrete $\mu = 2.8$ or 5.4, which was too far beyond the possibility $0 \leq \mu \leq 0.5$. The number μ led the hypothesis to catastrophe. The curve $g(\omega_1, \sigma_0) = b$, assumed by Schleicher to be typical exclusively for plastic materials, can be obtained from his theory for brittle materials, as marble, and inversely. A comprehensive critics of the discussed hypothesis can be found in my article[1)]. One should not be surprised then that Schleicher abandoned his theory, for the sake of the rests of appearances he introduced a new hypothesis only under the name of a different mathematical form. The error lies in the false assumption of the relation between Φ and Φ_f, that is – the relation which is never fulfilled by brittle materials and by plastic ones – only approximately.

The review of the above remarks allows one to judge the mistakes in the existing hypotheses and draw conclusions concerning the correctness of the theoretical construction of hypotheses of local material effort. They can be summarized in the following way:

1. A mathematical form of a hypothesis of material effort should be characterized by continuity and simplicity.
2. The hypothesis should be expressed in general by six components.
3. The choice of units of calculation (*variables – sci. ed. note*) should not influence the substance of the hypothesis.
4. The use of principal components should not be restricted by any numerical sequence of them.
5. Single terms built from the components must have a mechanical sense (from the point of view of continuum mechanics).
6. Sets of such terms must have a distinct and concrete meaning.
7. Such set cannot be calibrated by elastic constants (as e.g. μ).
8. In the particular case of plastic materials of the characteristic $k_t = k_c = k$, that is $\kappa = \frac{k_c}{k_t} = 1$, the hypothesis should transform to the Huber-Hencky's theory.
9. The number of parameters like k_t, k_c, k_s,... should be possibly small.
10. The hypothesis should correspond with the experiments.

I tried to settle a hypothesis that would meet all the requirements listed. It can be generally formulated in the following way:

I. The local material effort of isotropic bodies is expressed by a function created from three invariants of strain state, that is:

$$F(\pi_1, \pi_2, \pi_3) = A. \tag{27}$$

II. The local material effort of isotropic bodies is fully described by three invariants of stress state in the form:

$$G(\omega_1, \omega_2, \omega_3) = B. \tag{28}$$

These two hypotheses, though expressed by different variables, are not different, as it could seem to be after our experience with a great number of previous hypotheses; on account of the relations (24) they are identical.

In the above statements we give, apart from a new, very general hypothesis, also a new way of presenting all hypotheses in the orthogonal reference system (π_1, π_2, π_3) or equivalently $(\omega_1, \omega_2, \omega_3)$. All critical states, e.g. plane states, are referred by points lying on the plane (π_1, π_2) or equivalently (ω_1, ω_2); uniform hydrostatic states find their representation here in points lying on the plane (π_1, π_3) or (ω_1, ω_3). The Huber-Hencky hypothesis is here illustrated by a plane parallel to the plane (π_1, π_3) or (ω_1, ω_3). If particular points (π_1, π_2, π_3) or $(\omega_1, \omega_2, \omega_3)$ in a particular series of experiments generate a surface with two finite curvatures, the hypothesis should remain valid and should be applied in the general form (27) and (28). Though, one should expect that the invariant π_3 or equivalently ω_3, does not play any prominent role in defining the material effort. It would be represented by a cylindrical surface of generators parallel to the direction π_3 or equivalently ω_3, or by simplified equations

$$F(\pi_1, \pi_2) = A, \tag{29}$$

$$G(\omega_1, \omega_2) = B. \tag{30}$$

The simplification implies the following suppositions:

III. Energy of distortion and certain part of energy of volumetric strain, which depends on the strain state and individual characteristics of a body, are measures of the material effort.

As we have mentioned above, the invariant π_3 of necessity cancels out from the energy term. Moving on to the other variables, we can express the Statement III in the following manner:

IV. About material effort decides the function built from the energy of elasticity in general shear and hydrostatic uniform stress, namely – the Eq. (30).

The two seemingly different definitions due to (24) are also convergent here. The statements III and IV have a certain disadvantage; they use the word "energy" taken from the grounds of elasticity. Whereas, the presented hypothesis should be valid in all regions of material effort – of course, at the cost of the appropriate change of numerical parameters characterizing the material in each region. It is, to some extent, a disadvantage common for all the energy-based hypotheses. To avoid the above, we come to the following definition:

V. Critical material effort depends quantitatively on strains of the orientation $\phi = \chi = \psi = \arccos \frac{1}{\sqrt{3}}$ *referred to principal directions.*

As I have mentioned – those are the normal strains π_1 and the tangent ones π_2 (11). In this way we come again to the form (29) without exposing ourselves to the blame for limited validity of the hypothesis.

Statement V demands a small explanation. If we assume that the material effort is really caused by components of a certain direction then, on the assumption of isotropy of the body, it is clear that there can be only one such orientation which is neutral regarding the principal directions and it is the only one assumed above. I lay strong emphasis on the fact that one comes to this orientation exclusively in the way shown here, that is in the way of logical reasoning and assumption. The attempt existing in the literature (Roš and Eichinger) at arithmetical proof of the choice of exactly this direction among all the others, is false from the very foundations; in the science of material effort nothing can be proved, one can only experimentally verify the accuracy of some logical assumptions.

The hypothesis V can be transferred to the ground of stress, namely:

VI. Critical material effort is produced by stresses in the neutral orientation $\phi = \chi = \psi = \arccos \frac{1}{\sqrt{3}}$.

It is mathematically expressed by the Eq. (30). Presently, this orientation is being suspected to be a slip-plane. The above justification is a generalization of the Huber-Hencky theory in the sense of stress (similarly as Duguet-Mohr relates to Coulomb-Guest).

In the literature on material effort there are sometimes graphical proofs of the hypotheses given (Mohr, v. Mises). Let us also present one here:

VII. In critical states, a system of three strain circles moves along the axis of abscissae changing its total area in a continuous manner, due to its position.

As we have proved, this surface it proportional to π_2^2 (14), by introducing π_1 as the coordinate of the position of the complex of circles we come again to (29). Just as well we can agree for the following statement:

VIII. The manner of change of the magnitude of the surface and position of the three stress circles of critical states changes, that is the relation (30) is a measure of material effort.

Both graphical explanations are identical since the system of three strain circles is – independently of the existence of Hooke's law or the quality of the investigated critical state – always homothetic to the complex of stress circles.

In this manner, the discussed hypothesis has been explained in eight different ways; in particular: in a purely mathematical way (the invariants) on the grounds of strain, stress or energy and, finally, in a graphical scheme. All these ways lead to one result, what cannot be said about all the other hypotheses, known to us. The presented theory belongs to all the hitherto known groups and at the same time to none.

The above hypothesis in the incomplete form II and in the complete ones IV and VI. As well as VIII (with a great number of details, not given here due to the space restrictions) I have developed in 1927 and published in my dissertation *"A study on hypotheses of material effort"* (issued by Academy of Technical Sciences – Lwów, Jan. 7, 1928)[1)]. After myself, on the basis of an erroneous assumption, SCHLEICHER[33)] (Bauingenieur, 1928) derived the form IV from his primary hypothesis. Generalization of the so-called degree of reliability given by him can be found also in my work.

The presented theory satisfies all the recently listed conditions. The actual presence of uniformity of material and state of strain (stress) and additionally – the isotropy of a body, are guarantee of the laboratory success of the theory. If the above conditions are not fulfilled, the theory has in the highlighted sense only an approximate meaning; and speaking precisely – the verifying tests have an approximate sense in this case. But even then the author's hypothesis will differ from the presently launched Duguet-Mohr theory – and will differ significantly, since it will satisfy in an exact manner a whole series of remaining conditions, which cannot be stated with respect to the competitive theory.

Apart from this, deviations from the experiments here can be removed in a relatively simple way. I performed such an attempt in the work referred above; it has led to – as it will turn out – most favorable results. However, before I shall speak about this, it will not be irrelevant to discuss first some practical details concerning the conditions 9 and 10, which have been not discussed as yet.

The question of the number of constant parameters in the mathematical form of the hypothesis has not been discussed comprehensively in the literature as yet. One cannot precisely state what number of the simplest facts like:
(i) uniaxial tension $\sigma_1 = k_t, \sigma_2 = 0, \sigma_3 = 0$,
(ii) uniaxial compression $\sigma_1 = 0, \sigma_2 = 0, \sigma_3 = k_c$,
(iii) simple shear $\sigma_1 = k_s, \sigma_2 = 0, \sigma_3 = -k_s$

and so forth, the construction of the functions of material effort should be based on. This matter should be elucidated. In all publications known to myself one can see a silent suggestion of two parameters. It reveals itself evidently in the efforts to state the relation $k_s = f(k_t, k_c)$. But has a unique relation been found? Is it possible to infer the whole shape of the critical surface exclusively from the traces of coordinate axes? Is it enough to know only the behaviour of a body in one, the most simple case $\omega_1 > 0$ $(c = -1)$ and in another, equally simple one $\omega_1 < 0$ $(c = 1)$? Should not one of the critical states from the range $\omega_1 = 0$ $(c = 0)$ be also taken under consideration?

The answer can be delivered by a whole series of not too complicated experiments on various materials conducted only for the three first states (i), (ii) and (iii). The following, rather general formulae

$$k_s = s_a \frac{k_t + k_c}{2\sqrt{3}}, \qquad k_s = s_g \sqrt{\frac{k_t k_c}{3}}, \qquad k_s = s_b \frac{2}{\sqrt{3}} \frac{k_t k_c}{k_t + k_c}$$

or other, similar to these, could be used as the basis of an arithmetical verification. It is worthy of notice that the harmonic formula results mainly from linear hypotheses and the geometrical one - from square hypotheses; the arithmetical one has the least prospects for success. It is obvious that the numerical coefficient s cannot be kept absolutely constant. Maybe in can be put in the form of a function $s = s(\kappa)$; but if it would be unique, it is hard to say. However, in general, it seems that developing the hypotheses with two constants is incorrect; they can have an approximate meaning, limited to a certain range. Three constant stress parameters in general could be a starting point.

(*Sci. ed. note: In the doctoral dissertation of Burzyński, op. cit.*[2)] *pp. 111–114, the discussed above statements of material effort hypothesis are formulated in an equivalent way as an energy-based hypothesis, called by the Author the hypothesis of variable volumetric – distortional limit energy, expressed by the following equation:*

$$\Phi_f + \eta(p)\,\Phi_v = K, \tag{N1}$$

where $\eta = w + \frac{\delta}{p}$, $0 \le \eta \le 1$, $p \equiv \omega_1$, *is a certain material function accounting for a particular material properties and the diminishing pressure sensitivity, while* K *is a limit material constant. The core of Burzyński's formulation of the energy-based material effort hypothesis is the exchange of three material parameters* w, δ, K *appearing in (N1) with the discussed above three material constants:* k_t, k_c, k_s, *or with the triplet* k_t, k_c, ν, *accomplished by means of the replacements:*

$$\frac{1-2\mu}{1+\mu} w = \frac{1-2\nu}{1+\nu}, \quad \frac{1-2\mu}{1+\mu}\delta = \frac{3(k_c - k_r)}{1+\nu}, \quad \nu = \frac{k_c k_r}{2k_s^2} - 1,$$

$$12GK = \frac{3k_c k_r}{1+\nu}, \quad \sigma_f^2 = 12G\Phi_f,$$

what results in the following formula:

$$\frac{1+\nu}{3}\sigma_f^2 + 3\,(1-2\nu)\,p^2 + 3\,(k_c - k_r)\,p - k_c k_r = 0, \tag{N2}$$

where ν is the so-called "plasticity coefficient" describing the degree of material ductility. For hard and brittle materials $\nu < \frac{1}{2}$, for hard but ductile materials $\nu = \frac{1}{2}$ and for soft (plastic) materials $\nu > \frac{1}{2}$, and it is assumed that $0 \le \nu \le 1$. Consequently, Equation (N2) can be transformed as follows:

$$\frac{1+\nu}{3}\sigma_f^2 + 3\,(1-2\nu)\left(p+\sigma'\right)^2 = k'^2, \tag{N3}$$

where $\sigma' = \dfrac{k_c - k_t}{2\,(1-2\nu)}$, $k'^2 = k_c k_t + \dfrac{3}{4}\dfrac{(k_c - k_t)^2}{1-2\nu}$.

Generally it is assumed that $k_s \ge \dfrac{2}{\sqrt{3}}\dfrac{k_t k_c}{k_t + k_c}$, *due to this the required transition:* $k_t = k_c = k$, $\sqrt{3}\,k_s = k$ *is provided. Equation (N3) describes in the plane* $(p,\, \sigma_f)$ *curves of the second degree. In particular:*

(i) for $\nu < \frac{1}{2}$, *i.e. if* $k_s \ge \sqrt{\dfrac{k_s k_r}{3}}$, $1 - 2\nu > 0$ *and* $k'^2 > 0$ *we get an ellipse,*

(ii) for $\nu < \frac{1}{2}$ *and* $\frac{k_c}{k_t} > 1$ *equation (N3) describes a parabola of the second degree, while for* $\frac{k_c}{k_t} = 1$ *two lines parallel to the axis p are obtained,*

(iii) for $\nu > \frac{1}{2}$, *i.e. if* $\dfrac{2}{\sqrt{3}}\dfrac{k_c k_t}{k_c + k_t} < k_s < \sqrt{\dfrac{k_c k_t}{3}}$ *we have* $1 - 2\nu < 0$ *and* $k'^2 < 0$, *Equation (N3) describes a hyperbola, only one branch of which has a physical meaning.*

(iv) in particular for $k_s = \dfrac{2}{\sqrt{3}}\dfrac{k_c k_t}{k_c + k_t}$, *the hyperbola degenerates into two straight lines intersecting on the axis p.).*

The author's theory can be adjusted to experiments in general by means of three parameters, in specific cases – by two, and finally – by one parameter. This cannot be said about the Duguet-Mohr theory, since, if we assume that one of the arbitrarily chosen experimental envelopes can also be represented by three parameters, we have to express all the remaining envelopes with the help of the shape set in such way. Although experiments indicate that these are homothetic curves, they at the same time prove that they are translated and rotated; then, there are at least two additional parameters (due to the symmetry of envelopes, the translation occurs only along the σ axis) required for calibration. Meanwhile, the same experiments teach that the author's theory uses none or only one additional parameter. In this way, the point 9 would speak in favor of the new hypothesis.

A couple of words about uniformity of material. A simple experiment on compression demands for brittle materials 4–6 tests, since particular results differ from each other sometimes even by 20 per cent. What to say then about complex experiments, in which the ratio $\sigma_1 : \sigma_2 : \sigma_3$ assumes an arbitrary value? Can we regard a datum resulting from one such test as reliable? Besides, can one succeed in repeating this test? For, most often in laboratory devices, due to technical difficulties, the directions σ_1, σ_2, σ_3 are not associated and the preservation of the assumed ratio $\sigma_1 : \sigma_2 : \sigma_3$ cannot be simply realized. And there are a lot of such measurements, either for the reason of the mentioned difficulties or for the reason of economy. What absolute value do the resulting numbers have?

And what about the uniformity of the state of stress? Again, the simple experiment of uniaxial compression teaches that realization of a uniform distribution of stresses in a whole body is simply impossible. However, it seemed until now that the state obtained in these conditions was at least axially symmetrical. Whereas, we learn (a private conversation with prof. Roš) that it is out of the question: careful measurements on a compressed rectangular prism show that to obtain equal stresses along four edges of a specimen, an external resultant must be placed eccentrically. Material heterogeneity causes inhomogeneity of the stress state. And if the material does not hold any flaw, a large influence is found on the side of the technical devices. It is commonly known that different machines are used for different types of stress states. Each of them causes certain experimental deviation, while moving from one device to another the deviations change not only their values but, what is worse, maybe even their signs. However what in the theory of compensation would be an advantage, here is absolutely none, since the corresponding series of points on a graph are not distributed in an arbitrary manner. One series of them goes in a continuous manner along one curve, and another series – along another curve, and so forth. And can the results of experiments be assumed as exactly certain?

Finally – the isotropy. This is absolutely out of the question, there is in fact no isotropy. So perhaps quasi-isotropy, mathematically established in Voigt's beautiful work? It could be generally taken under consideration if the dimensions of crystalline structures would be small in comparison to the dimensions of a body. Then, due to the immense quantity of them, the disorder in orientations of particular individual ones would not distinguish any direction. To obtain such a situation, the dimensions of specimens would have to be adequately large in comparison to the dimensions of crystalline structures; but, in this manner we would give way to heterogeneity of the material and additionally we would demand very precise technical devices. And still, experimental results are dependent on the size of the investigated body, which is a kind of a proof of the above. If only the anisotropy could be theoretically defined, just like for all the known crystals! Unfortunately, in the technical materials used these are impalpable in-

fluences. And again we have to ask ourselves – how big are the deviations that our measurements are burdened with?

One must always take into account the most unfavourable possibilities. Let us assume that all the briefly described effects do not mutually cancel – on the contrary: let us assume that they sum up, that they exist. The theoretical hypothesis can be in this case corrected – as I have mentioned – by one additional parameter, which unfortunately quite considerably ruins the previous harmony; we are forced in advance to assume the inequality $\sigma_1 \geq \sigma_2 \geq \sigma_3$. The correction can be introduced in two ways, namely IV or VI and still with the same result. The first is more arduous one for it requires longer considerations of energy of isotropic bodies; here we will confine ourselves to use the second manner only.

We assume that presence of the calculated deviations will make the material effort dependent on stresses of orientation slightly different from the one used till now $\phi = \chi = \psi = \arccos\frac{1}{\sqrt{3}}$, and in particular that it will distinguish one of the principal cases e.g. σ_2. For this purpose, assuming generally: $\phi^* = \arccos\sqrt{\frac{\lambda}{1+\lambda}} = \psi^*$, $\chi^* = \arccos\sqrt{\frac{1-\lambda}{1+\lambda}}$, we obtain from formulae (8) the expressions for components of this direction

$$
\begin{aligned}
\sigma &= \frac{\lambda\sigma_1 + (1-\lambda)\,\sigma_2 + \lambda\sigma_3}{1+\lambda} = \omega_1^* \\
\tau &= \frac{\sqrt{\lambda}}{1+\lambda}\sqrt{(1-\lambda)\,(\sigma_2-\sigma_3)^2 + \lambda\,(\sigma_3-\sigma_1)^2 + (1-\lambda)\,(\sigma_1-\sigma_2)^2} = \omega_2^*.
\end{aligned}
\tag{31}
$$

The corrected hypothesis presently reads:

$$
G\,(\omega_1^*, \omega_2^*) = B. \tag{32}
$$

The additional parameter λ is limited by the theoretical inequality $0 \geq \lambda \geq 1$. The lower limit $\lambda = 0$ is – as it seems – of no significance, the upper limit $\lambda = 1$ reduces the expressions (31) to formulae (10) and in consequence of the theory (32) we obtain the hypothesis (25). The Duguet-Mohr theory is then comprised in the correction (32) as a specific case. We obtain a correct theory for isotropic bodies for a middle case $\lambda = \frac{1}{2}$. Experiments seem to teach that deviations which have been discussed, require a correction inherent generally in a narrower interval $\frac{1}{2} \leq \lambda \leq 1$. The values $\lambda > 1$ are theoretically impossible; their presence could be explained only by basic numerical incorrectness of the experimentally indicated stresses; this fact is possible in the case of presence of primary stresses (*internal stresses – sci. ed. note*).

The bigger is the influence of inhomogeneity of material and stress state, of experimental devices and of anisotropy is, the more λ deviates from values of

the range: 0.5 to 1.0 – that is the more the author's hypothesis (32) gets closer to the Duguet-Mohr theory (25). Experimental results do not confirm the latter one; but even though, there exists presently a tendency to apply this theory – due to the absence of any better one. It is a wrong opinion. Let us suppose for example that the parameter $\lambda = 0.75$, lying in the middle between 0.5 and 1.0 is needed for the adjustment. In this case, the deviations of tests from the theories of the author (without correcting λ) and Duguet and Mohr have practically the same value; they are both from the experimental point of view to the same degree wrong and they both – apparently – have equal rights to be used as an approximate application. However, while one will be still able to raise, apart from the approximate character, a whole series of critical arguments comprised in the points 1–8 against the hypothesis (25), there will be only the argument of approximation speaking against the hypothesis (29) or (30); and it will still meet the theoretical application and simplicity requirements. These arguments have such a dominant significance that they settle the matter in favor of the author's hypothesis (29) or (30), even when $\lambda > 0.75$. And regarding a complete adjustment of the theory to the research results, it can be performed – as I have mentioned – in the discussed hypothesis by means of one additional parameter λ in Duguet-Mohr theory there are required at least two of them. This argument also speaks strongly against the theory of envelopes.

As I have highlighted in the introduction, the aim of this paper is, above all, to define the theoretical foundations of hypotheses of the material effort. For this reason I confine the illustration of the point (10) only to a couple of interesting experiments.

Beautiful tests on Carrara marble indisputably belong to this account. They deserve attention even for the sole reason that they were conducted in different laboratories and by different researchers. For the reason of the already marked difficulties, these tests were hitherto conducted for two extreme types of loading (26): $\sigma_1 < \sigma_2 = \sigma_3 \ \ (c = -1)$ or $\sigma_1 = \sigma_2 > \sigma_3 \ \ (c = 1)$. (Results from BÖKER[34)] tests on twist performed on solid samples should be regarded as uncertain.) Figures 1 and 2 present in the systems (σ_{II}, τ_{II})or (ω_1^*, ω_2^*) the results of these experiments, conducted on three different sorts of marble by Kármán, Böker and Roš and Eichinger. The hollow circular points $(c = -1)$ lie due to the Duguet-Mohr theory on a curve which is here always above the curve of solid circular points. The corresponding corrections $\lambda = 0.73,\ 0.87,\ 0.75$ (obtained not by means of fitting, but from brief considerations) get both of the two different types of experiments to a one common, gently bent curve in the author's system. It is possible that the value of the parameter λ is dependent on the crystalline structure of a material; however, in this case λ should be common for all the cited experiments. One should suspect rather that accidental effects, mentioned earlier, decide on the value of this parameter.

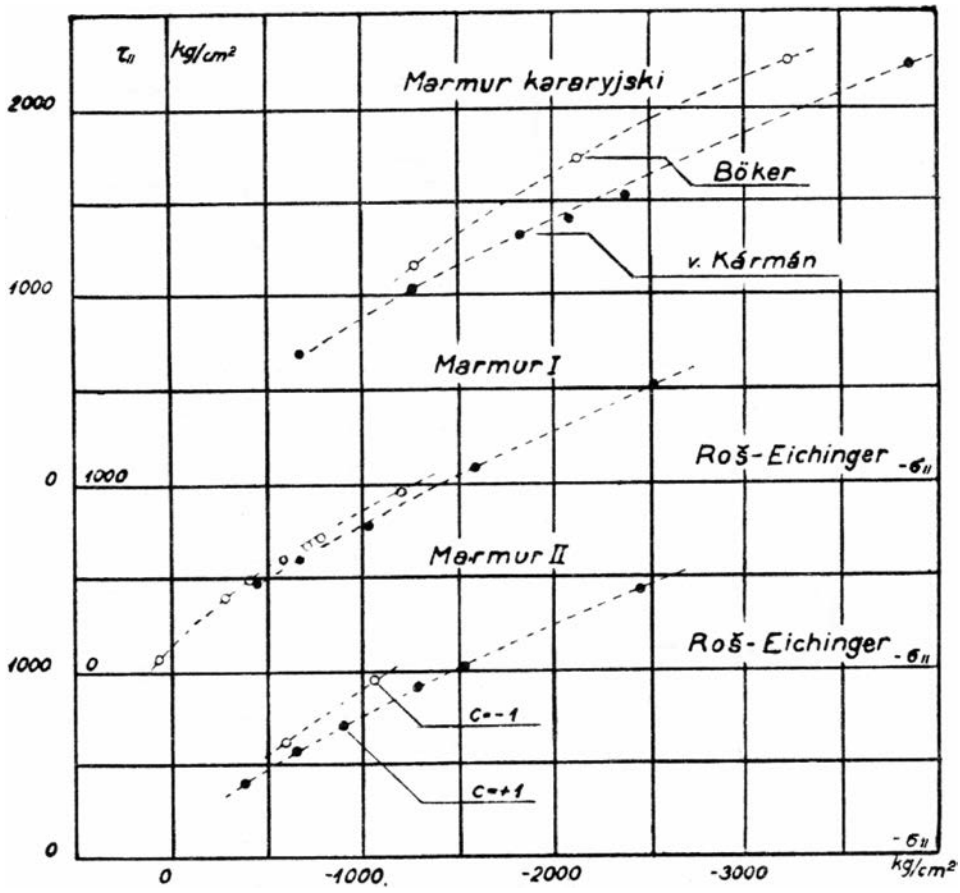

FIG. 1. The results of the tests on Carrara marble (*marmur kararyjski*), in the system (σ_{II}, τ_{II}) corresponding to the Duguet-Mohr theory, performed on three different sorts of marble (*marmur*) by Kármán, Böker and Roš and Eichinger[35)].

Experiments, also performed by Roš and Eichinger, on china, pure cement and cement mortar, cannot be used for a comprehensive discussion or comparison of hypotheses for the reason of very small number of tests (two or three pairs of points $c = \pm 1$).

Further experiments with artificial resin, though, deserve notice. It is an exceptionally uniform and certainly isotropic material. Unfortunately, we may suppose that it is burdened to a considerable degree with primary stresses (*i.e. internal stresses – sci. ed. note*), like all artificial preparations of this kind. We are confirmed with this supposition by the fact that it was required to assume $\lambda > 1$, namely $\lambda \cong 1.32$ to adjust the experimental results to author's theory (32). Results of the experiments are shown in Figs. 3 and 4, that is in the system (σ_{II}, τ_{II}) corresponding to the Duguet-Mohr theory and the author's corrected

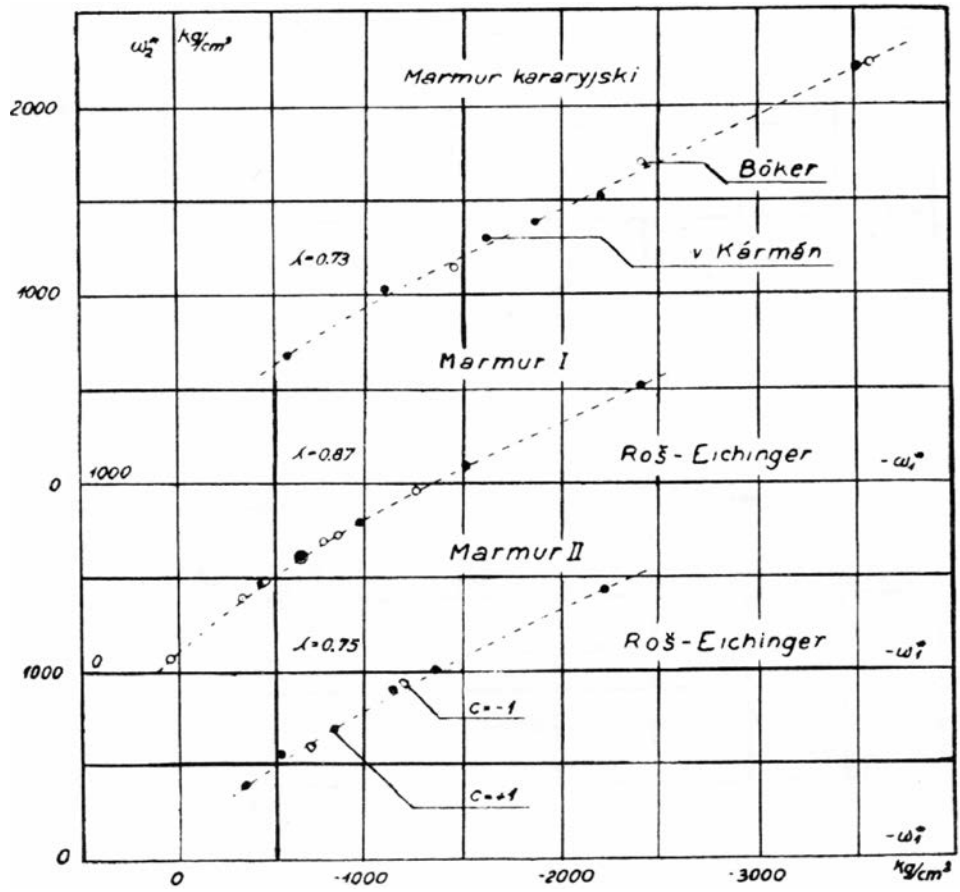

FIG. 2. The results of the tests on Carrara marble (*marmur kararyjski)*, in the author's corrected system (ω_1^*, ω_2^*), performed on three different sorts of marble (*marmur*) by Kármán, Böker and Roš and Eichinger[35)].

system (ω_1^*, ω_2^*). As we can see, we have to do here with a completely opposite case; the points $c = -1$ go beneath the points $c = 1$ by Mohr, while in the author's illustration these differences vanish.

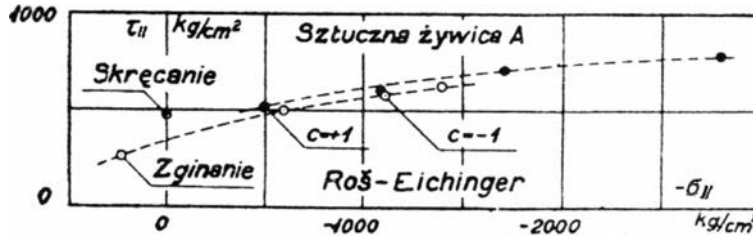

FIG. 3. The results of the experiments with artificial resin (*sztuczna żywica*) in the system (σ_{II}, τ_{II}) corresponding to the Duguet-Mohr theory[35)].

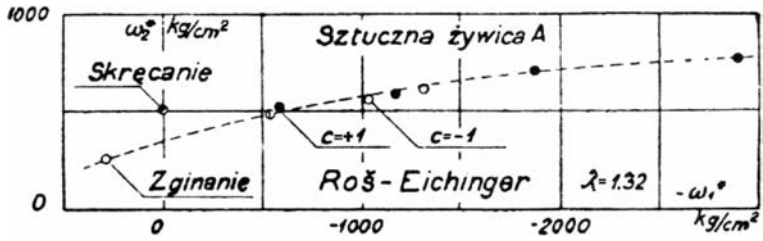

FIG. 4. The results of the experiments with artificial resin (*sztuczna żywica*) in the author's corrected system (ω_1^*, ω_2^*)[35].

From the experiments on 'brittle' metals we take into consideration the experiments by *EMPA* on cast iron (*Elektroguss EK50*) and (*Maschinenguss HS50*). They are in a much more general tone than the ones cited hitherto, for they take into account the three following types of stress states: $c \cong -1.0,\ 0.0,\ 0.3,\ 0.8$C (as shown in Fig. 5 and Fig. 6). But unfortunately there are on the average only three points for each of these types, which is not quite enough for a relatively broad interval of stresses. And in particular it is difficult to recognize what correction λ should be assumed. For this reason it has been disregarded (or more precisely: the theoretical value $\lambda = 0.5$ has been kept) and the results have been

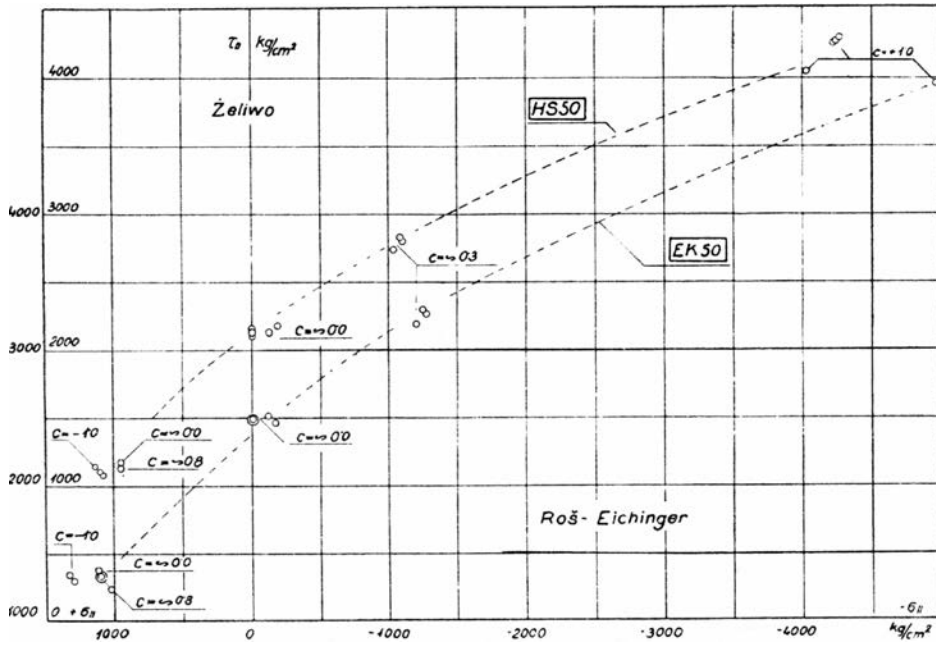

FIG. 5. The results of the experiments on "brittle" metals: experiments by *EMPA* on the cast iron (*żeliwo*) – (*Elektroguss EK50*) and (*Maschinenguss HS50*) in the system (σ_{II}, τ_{II}) corresponding to the Duguet-Mohr theory[35].

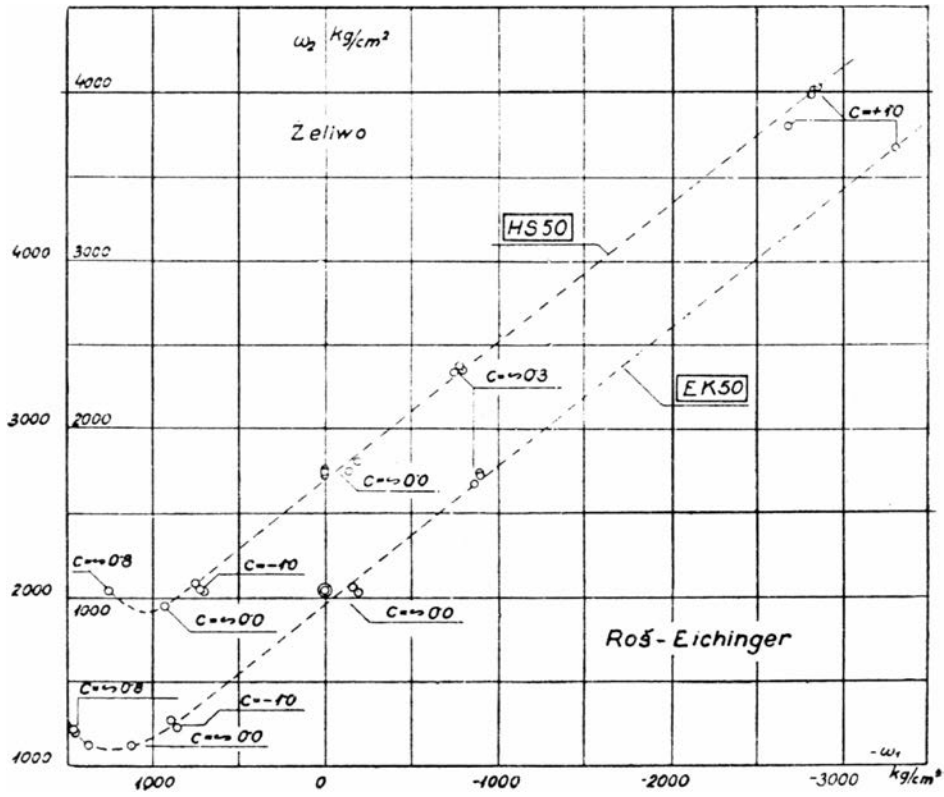

FIG. 6. The results of the experiments on "brittle" metals: experiments by *EMPA* on the cast iron (*żeliwo*) – (*Elektroguss EK50*) and (*Maschinenguss HS50*) in the author's corrected system (ω_1^*, ω_2^*)[35].

presented in the theoretical system (ω_1, ω_2). However, even this is enough to recognize the superiority of the invariants theory over the one of envelopes. First of all it can be clearly seen that experimental points in the system (σ_{II}, τ_{II}) (Fig. 5) are spread more widely than in the system (ω_1, ω_2) (Fig. 6). Apart from this, it is worthy of notice that in the second system almost all experimental results lie on straight line, while by Duguet and Mohr they lie along a curve or more precisely – curves, since here, as well as in general, one curve is out of the question. In other words, the relation $k_s = \dfrac{2}{\sqrt{3}} \dfrac{k_t k_c}{k_t + k_c}$ is precisely fulfilled for cast iron. Finally, it would be good to underline one more detail, namely grouping of points in the area $\sigma_{II} > 0$ or $\omega_1 > 0$. Evidently there is a confusion in this matter in the Duguet-Mohr theory; it is not known how to lead the assumed curve. Whereas the author's theory sorts the data in a clear manner due to the value c and arranges it in a clear continuous curve; in other words, it estimates the influence of the medium stress σ_2 (*cf. Eq. (26) – sci. ed. note*), which cannot be said about the competitive theory.

Finally, let us add a couple of remarks concerning tests on plastic materials. The author's theory transforms then into the Huber-Hencky theory or other, similar to it if we assume $\lambda \neq 0.5$; in other words, the veracity of the hypothesis of energy of distortion is supported by correctness of the theory of invariants; and possible shortcomings of the energy-based theory can be removed in the theory (32) by means of the parameter λ.

As it is known, the Huber-Hencky theory refers only to plastic materials of a characteristic $k_t = k_c = k$. In this case we can use instead of the systems (σ_{II}, τ_{II}) and (ω_1, ω_2), a common one. In general there is namely:

$$\begin{aligned} \omega_1 &= \sigma_{II} + \frac{c}{3}\tau_{II}\,, \\ \omega_2 &= \frac{\sqrt{2\,(c^2+3)}}{3}\tau_{II}\,. \end{aligned} \tag{33}$$

The dependence of τ_{II} on σ_{II} disappears in the case of the discussed materials in the Coulomb-Guest theory $\tau_{II} = \frac{k}{2}$ (that is – the simplified Duguet-Mohr theory); the Huber-Hencky theory $\omega_2 = \frac{\sqrt{2}}{3}k$ is totally independent of the influence of ω_1. Regarding this fact and (33), at the same time we can write both hypotheses in the form of equations:

$$\begin{aligned} \tau_{II} &= \frac{1}{2}\,, \\ \frac{\tau_{II}}{k} &= \frac{1}{\sqrt{c^2+3}}\,. \end{aligned} \tag{34}$$

A corresponding author's correction, that is (32), can be analogically presented in the form:

$$\frac{\tau_{II}}{k} = \frac{1}{\sqrt{2\,(1+\lambda) + 2c^2\,(1-\lambda)}}. \tag{35}$$

The Eqs. (34) and (35) can be easily presented in the system $\left(c, \frac{\tau_{II}}{k}\right)$. Let us notice at the same moment that for the abscissa $c = \pm 1$ we obtain one and the same ordinate, namely $\frac{\tau_{II}}{k} = 0.5$, from all the three equations.

In the contemporary literature, the Roš and Eichinger experiments on Siemens-Martin's cast steel are considered to be the foundations of the Huber-Hencky theory. The numerical values of stress in the moment of going beyond the upper yield point confirm this hypothesis most exactly and it was taken under consideration. The results of these experiments are presented in Fig. 7; we have assumed $k = 2615$ kg/cm^2 as the mean value of all measurements of k_t and k_c. The experimental data indeed fall symmetrically according to

Huber-Hencky curve, disregarding the line resulting from the Coulomb-Guest theory (Duguet-Mohr). The experiments on annealed cast steel conducted by Roš and Eichinger to reinforce the hypothesis of energy of distortion have, unfortunately, hardly any value; 25 among the 32 tests were performed for $c = \pm 1$, and 3 of the remaining 7 tests are in favor of the Coulomb-Guest theory, while 4 – support the Huber-Hencky theory. The same Fig. 6 explains it clearly.

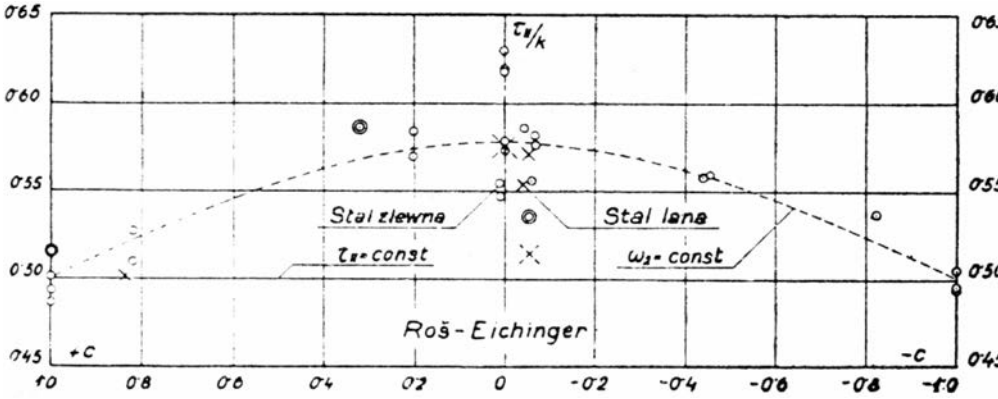

FIG. 7. The Roš and Eichinger experiments on Siemens-Martin cast steel (*stal lana*) , with assumed $k = 2615$ kg/cm^2 as the mean value of all measurements of k_t and k_c, and the experiments on annealed cast steel (*stal zlewna*)[35].

As for the selection of types of critical stress states, Lode experiments on cast iron, nickel and copper look very well in this respect; they are presented in Fig. 8; the parameter c runs here through many more values than those by Roš and Eichinger. Unfortunately, one and the same specimen was used several times in these experiments which, of course, were reflected in the results and, owing to this reason, these are less suitable for stating validity of the Huber-Hencky theory. The experiments can be best calibrated by the parameter $c = 0.6$, numerically very close to the theoretical value $c = 0.5$, supporting in this way the author's theory.

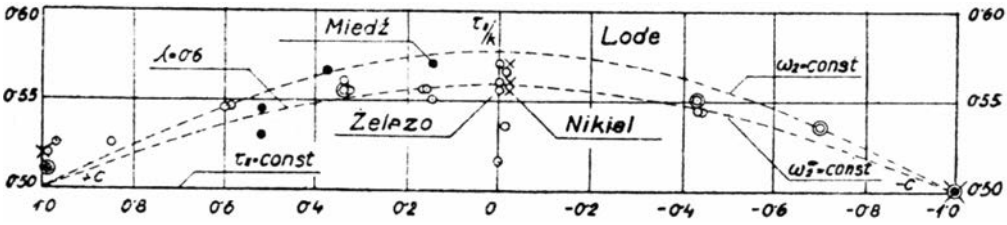

FIG. 8. The results of the Lode experiments on cast iron (*żeliwo*), nickel (*nikiel*) and copper (*miedź*)[35].

Roš and Eichinger tests on aluminum, copper and tombac cannot automatically confirm the validity of the hypothesis of distortion energy, because it has been found that $k_t \neq k_c$ for these materials. Apart from this, the mentioned experiments were conducted only for three simple states: (i), (ii) and (iii), so they are off the general, comparative considerations.

The experimental results state, as it turns out, that the author's theory with the correction λ is suitable for mathematical adjusting all former experiments; it performs this adjustment in a unique way. The parameter λ gets closer to the limit $\lambda = 0.5$ as the qualitative conditions of tests and in particular of the material itself get better. Disregarding the defects of material and all accidental sources of errors, we have to assume $\lambda = 0.5$ in (32) and in this way to accept the theory in its fundamental form (27) and (28) or (29) and (30), which shows the advantages alien to Duguet-Mohr theory. The assumption $\lambda = 0.5$ is more admissible since because brittle materials, for which the experience shows experimental value $\lambda > 0.5$, find their application in technology in dimensions much larger than those used in laboratories. In these conditions secondary effects such as inhomogeneity, incomplete isotropy, etc., lose to one's advantage their disturbing character following in the consequence the author's theory.

Some final remarks should be devoted to the so-called slip surfaces. This matter does not have any fundamental meaning for the material effort; it is only a certain side-effect, which gains significance in specific fields (problems of theory of plasticity, expert opinions in construction disasters, partially a problem of equilibrium of slopes, etc.)

Measurement of the angle ϑ between two planes of slip is a riddle, which – I honestly admit – I do not understand. This measurement should be made – strictly speaking – in one body point; since it is impossible, finite dimensions are being used. However, there is a non-uniform stress state in the range of these; so the slip does not occur on a plane but on a surface and moreover, on a non-cylindrical one. Why then slip planes are being considered, and why two of them and not three or four? What is regarded as the discussed angle in a measurement?

Without engaging closer in understanding and probability of the discussed problems and considering only the numerical results, we can state anyway that the Duguet-Mohr theory does not correspond with the measured data; the acute angle

$$\vartheta = \frac{\pi}{2} - \beta, \tag{36}$$

that is the angle between a tangent to an envelope and the axis τ, is a bit too small in the range of states $c > 0$ (in fact $c = 1$), and immeasurably large when

$c < 0$ ($c = -1$ in current tests). At the same time we see that the argument of impossibility of existence of an envelope which envelopes all circles of critical states, succeeds also at this place; since for the hydrostatic – let us say – tension, this angle obviously has to be indefinite; the referred point cannot have any definite tangent – hence, it cannot lie on the envelope of the remaining states.

More precise determination of the angle ϑ according to Mohr's recipe is impossible with the use of other hypotheses; indeed, as I have mentioned, each of them can be represented by a group of envelopes depending on the parameter $c\,(\sigma_2)$, but exactly for this reason there arises a serious problem, namely – can one in this case measure that angle from the tangent to the axis τ, or should it be measured each time to some other direction depending on the numerical value of c? Actions performed currently in laboratories are now being questionable. With reference to the author's theory the following fact can be noted: the angle ϑ calculated from the equation

$$\cos\vartheta = \cot\delta \tag{37}$$

has the same degree of approximation to the laboratory data as the angle ϑ taken from particular envelopes; δ means in the coordinate system (ω_1, ω_2) or $\left(\omega_1^*, \omega_2^*\right)$, the acute angle between a tangent and the direction ω_2 or ω_2^*. In the determination of δ it disappears the ambiguity present by the group of envelopes. I do not consider the angle δcalculated in this way as a fully correct solution, similarly as it happens in Mohr's case.

There still arise doubts and even more serious than the previous ones. The angle δ has a secondary meaning; the orientations of slip surfaces have the primary meaning, since only from these the value δ should be calculated. Mohr's concept was a kind of a stroke of genius assuming the axis σ_2 as the line of intersection of two slip planes (which was also mathematically proved by Duguet on the basis of the hypothesis of internal friction). Mohr prevented his followers from using his theory as a starting point for attempts to generalize or modify his stand. It is obvious that if we reject Mohr's assumption or Duguet's results, we face the difficult riddle. Let us pay attention to the following by the Duguet and Mohr theory: the direction σ_2 has a geometric meaning – it is the axis of symmetry. If this direction would be highlighted so much (and not ignored, as others say), indeed two slip planes should be assumed in the coordinate system of principal directions. Their normals make angles $\pm\left(\frac{\pi}{4} - \frac{\beta}{2}\right)$ and $\pm\left(\frac{\pi}{4} + \frac{\beta}{2}\right)$ with the directions σ_1 and σ_3 or – in other words – planes of the systems $\sigma_1\sigma_2$ or $\sigma_2\sigma_3$ are planes of symmetry with respect to slip. The orientations $\pm\frac{\pi}{4}$, $\frac{\pi}{2}$, $\pm\frac{\pi}{4}$ or $\pm\frac{\pi}{4}$, $\frac{\pi}{2}$, $\mp\frac{\pi}{4}$ have a significant meaning in this theory, since the Duguet-Mohr hypothesis uses the stresses (10) of these very directions. The normals of the slip planes are rotated with respect to the latter by the angle $\frac{\beta}{2}$; the direction σ_2

is then a kind of axis of rotation. Finally, this direction is perpendicular to the components σ_{II}, τ_{II} of the diagonal orientations described above. We see that so many various points of view are connected with the theories of slip planes (25); by Duguet and Mohr they all lead to one result and it is only thanks to the fact of giving σ_2 a privileged though unjustified position.

If we disregard this position – and, of course, we have to do that – each of the points of view described above will lead to different results. If we assume the existence of one arbitrary slip plane, we do not know how to reach the other one at all. Assumption a simultaneous symmetry to two planes of coordinate system fails, because in this way again one of the directions would be privileged. Assuming symmetry with respect to one of the system planes leads to a number of slip planes larger than two due to equivalence of each of the principal directions; but, if we assume only two of them a priori, the question arises how to define their edge of intersection. This question – at least by now – we cannot solve.

However, regardless of this, certain details of the Duguet-Mohr theory can be generalized in reference to one slip orientation. First of all, with respect to the remarks presented on the occasion of explaining our theory, we will assume a plane indifferent to all principal directions i.e. $\phi = \chi = \psi = \arccos\frac{1}{\sqrt{3}}$ (8) or its experimentally corrected form $\phi^* = \psi^* \neq \chi^*$ (31), instead of unreliable plane $\phi = \frac{\pi}{4} = \psi$, $\chi = \frac{\pi}{2}$. We will assume – similarly to Duguet and Mohr – that the slip plane is inclined to the above one by the angle $\frac{\beta}{2}$, but – as it has been mentioned above (36), (37) – there is: $\sin\beta = \cos\vartheta = \cot\delta$. In this assumption we leave the previous meaning of δ, but we lose the previous meaning of ϑ due to introducing the new stress orientation as a starting point for calculation; the angle δ or β is here only a measure of deviation of the slip plane with respect to the one used for calculation. Having calculated this one with the help of δ, taken from a graphical scheme or calculated from the function of material effort $\left(\cot\delta = -\frac{d\omega_2}{d\omega_1}\right)$, we are facing a simple analytical problem, which, unfortunately, can have two solutions, depending on our further considerations.

Assuming that the calculated plane due to material effort has been rotated round the axis σ_2 (as by Mohr) by the angle $\frac{\beta}{2}$, we obtain the following expressions as direction cosines of the searched slip orientation (ξ, η, ζ):

$$
\begin{aligned}
\cos\xi &= \sqrt{\frac{2\lambda}{1+\lambda}}\cos\left(\frac{\pi}{4} - \frac{\beta}{2}\right), \\
\cos\chi &= \sqrt{\frac{1-\lambda}{1+\lambda}}, \\
\cos\zeta &= \sqrt{\frac{2\lambda}{1+\lambda}}\cos\left(\frac{\pi}{4} + \frac{\beta}{2}\right).
\end{aligned}
\tag{38}
$$

from which in particular for $\lambda = 1$ we obtain $\xi = \frac{\pi}{4} - \frac{\beta}{2}$, $\eta = \frac{\pi}{2}$, $\zeta = \frac{\pi}{4} + \frac{\beta}{2}$ as in Duguet-Mohr theory, which fact, of course, was easy to be predicted. The data obtained in this manner satisfy certain elementary experimental demands. Among other things, they e.g. confirm the result that a normal to a slip plane makes a smaller angle with the algebraically greater stress; for, one should remember that the present considerations are valid for the case $\sigma_1 > \sigma_2 > \sigma_3$. However, a serious argument speaks against the above formulae: the direction σ_2 again has played a privileged role.

In view of the above we can act in a different way: namely, let us assume that the calculated plane as the result of process has been rotated by the angle $\frac{\beta}{2}$ round the axis perpendicular to the stresses ω_1^* and ω_2^* (σ_{II} and τ_{II} by Duguet). In this way we will obtain the direction cosines of the desired orientation(ξ, η, ζ):

$$
\begin{aligned}
\cos\xi &= \sqrt{\frac{\lambda}{1+\lambda}}\left[\cos\frac{\beta}{2} + \frac{\sigma_1 - \omega_1^*}{\omega_2^*}\sin\frac{\beta}{2}\right], \\
\cos\eta &= \sqrt{\frac{1-\lambda}{1+\lambda}}\left[\cos\frac{\beta}{2} + \frac{\sigma_2 - \omega_1^*}{\omega_2^*}\sin\frac{\beta}{2}\right], \\
\cos\zeta &= \sqrt{\frac{\lambda}{1+\lambda}}\left[\cos\frac{\beta}{2} + \frac{\sigma_3 - \omega_1^*}{\omega_2^*}\sin\frac{\beta}{2}\right].
\end{aligned}
\tag{39}
$$

The obtained expressions are very probable. The experimental fact of dependence of the position of a slip plane upon an algebraic value of principal components is here clearly confirmed. And here also – as previously – for $\lambda = 1$ we come to orientations described by the Duguet-Mohr hypothesis. Two additional facts deserve notice. The orientation (ξ, η, ζ) depends on material effort in two ways; firstly through the angle β, and secondly directly through the components σ_1, σ_2, σ_3. This seems to be right; for, it can (or rather: has to) happen that in the graph (ω_1^*, ω_2^*) two points belonging to two different types of loadings (e.g. $c = 1$ and $c = -1$) will overlap; then angle β will be common for both of them, but (ξ, η, ζ) will be not. In this way the serious shortcoming of Mohr's relations would be removed. The other fact is the indeterminacy of (ξ, η, ζ) in the case when $\sigma_1 = \sigma_2 = \sigma_3$, since then the numerator and the denominator of the multiplier of $\sin\frac{\beta}{2}$ simultaneously become zero; obviously, it is clear and convincing. Apart from this, the denominator ω_2^* can never be zero, so the given formulae do not contain any contradictions in themselves.

As I have stressed two times, the formulae (38) and (39) have been derived from two important assumptions; the first one consists in assuming the angle δ as the measure of deviation of the slip plane with respect to the plane of stresses which decide on critical material effort; and the other – in the possibility of transition of the defined orientations (ξ, η, ζ) onto the Duguet-Mohr directions

in case when $\lambda = 1$. Both assumptions are of course hypothetical; the first implies the shape of the graphs (ω_1^*, ω_2^*) or – for $\lambda = 0.5$ – the curve (ω_1, ω_2); the other is probable inasmuch as it is based on a general – quoted several times – numerical dependence of the Duguet-Mohr theory (25) on the author's theory (32) provided with the correction λ. As far as I know, the formulae (38) and (39) are the only ones known in the literature attempts of this kind (of course apart from Duguet's calculation or Mohr's graphical solution). I do not attribute any distinct significance to it, anyway, not to the degree as I do in my general theory of material effort (27) and (28) or the simplification (29) and (30). The theory (32) has the meaning of a laboratory correction.

Zürich-Lwów, 1929

Acknowledgement

The preparation of this edition of the Burzyński work was made under the auspices of the Commission of Applied Mechanics of the Kraków Branch of the Polish Academy of Sciences.

Notes from the scientific editor

The original paper in Polish was reprinted in the Selected Papers of Włodzimierz Burzyński: *Dzieła Wybrane*, tom I, Polska Akademia Nauk, PWN Warszawa, 1982, 265–303, prepared by the Editorial Committee of the Polish Academy of Sciences: Eustachy Burka (secretary), Stefan Cieśla, Marian Janusz, Igor Kisiel, Franciszek Misztal, Witold Nowacki, Zbigniew Olesiak (scientific editor), Fryderyk Staub, Robert Szewalski (chairman), Czesław Woźniak, Marek Zakrzewski, Jerzy Zawadzki.

[1] The lecture was published as the paper: *Ueber die Anstrengungshypothesen* von Dr. Ing. Wladimir v. Burzyński, Assistent der Technischen Hochschule Lwów, Polen Schweizerische Bauzeitung, Bd. 94, Nr. 21, 23. November 1929, 259–262; reprinted in Włodzimierz Burzyński: *Dzieła Wybrane*, tom I, Polska Akademia Nauk, PWN Warszawa, 1982, 259–262.

[2] The detailed references of papers given below, quoted in the paper only by names, were taken from the – published in Polish – doctoral dissertation of Włodzimierz Burzyński: *Studjum nad hipotezami wytężenia* (*Study on Material Effort Hypotheses*), under the imprint of the Academy of Technical Sciences, Lwów, 1928, 1–192; reprinted in: Włodzimierz Burzyński: *Dzieła Wybrane*, tom I, Polska Akademia Nauk, PWN Warszawa, 1982, 67–257.

[3] Galileo Galilei, *Discorsi e dimonstrazione matematiche*, Leyden, 1638.

[4] G.W. Leibniz, *Demonstrationes novae de resistentia solidarum*, Acta Erudit., 1684.

[5] C.A. Coulomb, *Essai sur une application des régles de Maximis et Minimis à quelque problémes ...*, Mem. par divers savants, Paris, 1776.

[6] B. Navier, *De la résistance des corps solides*, 1826, 3. éd. par Barré de St. Venant (1864), Historique Nr. XLIV.

[7] B. de Saint Venant, *Leçons de Navier*, Historique Abrégé, 1837.

[8] W.J.M. Rankine, Applied Mechanics, London, 1856.

[9] A. Clebsch, *Theorie der Elastizität fester Körper*, Leipzig, 1862.

[10] E. Beltrami, *Sulle condizioni di resistenza dei corpi elastici*, Opere matematiche, Rend. Ist. Lomb. ser. rol. LXXXI, 1885.

[11] In Author's notation the symbols γ_x, γ_y, γ_z and τ_x, τ_y, τ_z denote shear strains and shear stresses in planes of normals x, y, z respectively.

[12] O. Mohr, *Über die Darstellung des Spannungszustandes und des Deformationszustandes eines Körperelementes*, Zivilingenieur, 1882.

[13] W. Voigt, Annal. Phys. Chem. (Wiedemann) Bde. 31, 1887; 34 u. 35, 1888; 38, 1889; cf. also the summary of Voigt results given by A.E.H. Love, *Treatise of the Theory of Elasticity*, (in German translation by A. Timpe, *Lehrbuch der Elastizität*, Leipzig u. Berlin, 1907); (see also the recent edition: A.E.H. Love, *A Treatise on the Mathematical Theory of Elasticity*, Chapter VI, Dover Publications, New York, first published in 1944 as unabridged and unaltered republication of the fourth (1927) edition of Cambridge University Press – *sci. ed. note*).

[14] Citation given after A.E.H. Love, *Treatise of the Theory of Elasticity* (in German translation by A. Timpe, *Lehrbuch der Elastizität*, Leipzig u. Berlin, 1907); G.G. Stokes, On *the theories of the ... Equilibrium and Motion of Elastic Solids*, Cambridge Phil. Soc. Trans., vol. 8 (1845); reprinted in *Stokes's Math. And Phys. Papers*, vol. 1, Cambridge, 1880, p. 75.

[15] H. v. Helmholtz, *Dynamik continuerlich verbreiteter Massen*, Leipzig, 1902.

[16] C. Bach, *Elastizität u. Festigkeit*, Berlin, 1905.

[17] J. Guest, *Strength of ductile materials under combined stress*, Philosophical Magazine, T. 50, 1900.

[18] In his dissertation (*op. cit. 2*) Burzyński refers in the context of the limit shear stress hypotheses also to the paper of H. Tresca, *Mémoire sur l'ecoulement des corps solides*, Mémoires par divers savants, Paris, XVIII, 1868, XX, 1872.

[19] Ch. Duguet, *Limite d'élasticité et résistance à la rupture*, Statique generale, 1885.

[20] O. Mohr, *Welche Umstände bedingen die Elastizitätsgrenze u. den Bruch eines Materials*, Z. d. V. D. I., 1907.

[21] Citation given after A. Föppl, Mitteilungen aus dem mech.-techn. Laboratorium der k. techn. Hochschule in München, 1896.

[22] B.T. Haigh, *The strain-energy function and the elastic limit*, Engineering, Vol. CIX, 1920.

[23] A.J. Becker, *The Strength and Stiffness of Steel under Biaxial Loading*, Univ. of Illinois Bull., 13, 1916.

[24] H.M. Westergaard, *On the resistance of ductile materials to combined stresses in two or three directions perpendicular to one another*, Journal of Franklin Inst., 189, 627, 1920.

[25] G.D. Sandel, *Über die Festigkeitsbedingungen*, Dissertation, T.H. Stuttgart, 1919.

[26] M.T. Huber, *Właściwa praca odkształcenia jako miara wytężenia materjału*, Czasopismo Techniczne, Lwów, 1904 (see also the recent edition of English translation in the centennial of original Polish publication: *Specific work of strain as a measure of material effort*, Arch. Mech., 56, 173-190, 2004).

[27] H. Wehage, *Die zulässige Anstrengung eines Materials bei Belastung nach mehreren Richtungen*, Z.d.V.D.I., 1905.

[28] A. Föppl, *Vorlesungen über die technische Mechanik*, B.G. Teubner-Verlag, Leipzig, 1920.

[29] H. Hencky, *Über langsame stationäre Strömungen in plastischen Massen mit Rücksicht auf die Vorgänge beim Walzen, Pressen und Ziehen von Metallen*, ZAMM, Bd. 5, 1925.

[30] R. v. Mises, *Mechanik der festen Körper im plastisch-deformablen Zustand*, Göttingen Nachrichten, Math.-phys. Klasse, Z. 4 (1), 582-592, 1913.

[31] M. Roš, A. Eichinger, *Versuche zur Klärung der Frage der Bruchgefahr*, Eidgenössische Materialprüfungsanstalt, Berichte 14, 1926; see also Proc. 2^{nd} Int. Congr. Appl. Mech., Zurich, 1926.

[32] W. Lode, *Versuche über den Einfluss der mittleren Hauptspannung auf die Fliessgrenze*, ZAMM, Bd. 5, 1925.

[33] F. Schleicher, *Der Spannungszustand an der Fliessgrenze (Plastizitätsbedingung)*, ZAMM, Bd. 6, 1926, 199–216; F. Schleichez, *Über die Sicherheit gegen Überschreiten der Fliessgrenze*, Der Bauingenieur, 1928, Heft 15, 253–261.

[34] R. Böker, *Versuche, die Grenzkurve der Umschlingungsversuche und der Druckversuche zur Deckung zu bringen*, Dissertation, Aachen, 1914.

[35] The figure captions from the scientific editor.

Received April 10, 2008; revised version July 15, 2008.

DIRECTIONS FOR THE AUTHORS

The periodical *ENGINEERING TRANSACTIONS (ROZPRAWY INŻYNIERSKIE)* presents original papers which should not be published elsewhere.

As a rule, the volume of a paper should not exceed 40 000 typographic signs, that is about 20 type-written pages, format: 210×297 mm, leaded. The papers should be submitted in two copies and follow the norms outlined by the Editorial Office. The following directions are particularly important:

1. The paper submitted for publication should be written in English.
2. The title of the paper should be as short as possible. The text should be preceded by a brief introduction; it is also desirable that a list of notations used in the paper should be given.
3. Short papers should be divided into section and subsection, long papers into sections, subsections and points. Each section, subsection or point must bear a title.
4. The formula number consists of two figures: the first represents the section number and the other the formula number in that section. Thus the division into subsections does not influence the numbering of formulae. Only such formulae should be numbered to which the author refers throughout the paper. This also applies to the resulting formulae. The formula number should be written on the left-hand side of the formula; round brackets are necessary to avoid any misunderstanding. For instance, if the author refers to the third formula of the set (2.1), a subscript should be added to denote the formula, viz. $(2.1)_3$.
5. All the notations should be written very distinctly. Special care must be taken to distinguish between small and capital letters as precisely as possible. Semi-bold type must be underlined in black pencil. Explanations should be given on the margin of the manuscript in case of special type face.
6. Vectors are to be denoted by semi-bold type, transforms of the corresponding functions by tildes symbols. Trigonometric functions are denoted by sin, cos, tg and ctg, inverse functions – by arc sin, arc cos, arc tg and arc ctg; hyperbolic functions are denoted by sh, ch, th and cth, inverse functions – by Arsh, Arch, Arth and Arcth.
7. The figures in square brackets denote reference titles. Items appearing in the reference list should include the initials of the first name of the author and his surname, also the full of the paper (in the language of the original paper); moreover;
   a) In the case of books, the publisher's name, the place and year of publication should be given, e.g., 5. S. Ziemba, *Vibration analysis*, PWN, Warszawa 1970;
   b) In the case of a periodical, the full title of the periodical, consecutive volume number, current issue number, pp. from ... to ..., year of publication should be mentioned; the annual volume number must be marked in semi-bold type as to distinguish it from the current issue number, e.g., 6. M. Sokołowski, *A thermoelastic problem for a strip with discontinuous boundary conditions*, Arch. Mech., **13**, 3, 337–354, 1961.
8. The authors should enclose a summary of the paper. The volume of the summary is to be about 100 words.
9. The authors are kindly requested to enclose the figures prepared on diskettes (format WMF, EMF, GIF, PCX, BitMaP, EPS or PostScript).

Upon receipt of the paper, the Editorial Office forwards it to the reviewer. His opinion is the basis for the Editorial Committee to determine whether the paper can be accepted for publication or not.

Once the paper is printed, 25 copies of reprints free of charge are sent to the author.

The papers submitted for publication in the journal should be written in English. No royalty is paid to the authors.

Please send us, in addition to the typescript, the same text prepared on a diskette (floppy disk) 3 1/2″ as an ASCII file, preferably in the TEX or LATEX.

Editorial Committee
ENGINEERING TRANSACTIONS
(ROZPRAWY INŻYNIERSKIE)

ENGINEERING TRANSACTIONS **Appears since 1952**

Aims and Scope

ENGINEERING TRANSACTIONS promotes research and practise in engineering science and provides a forum for interdisciplinary publications combining mechanics with material science, electronics (mechanotronics), medical science and biotechnologies (biomechanics), environmental science, photonics, information technologies and other engineering applications. The Journal publishes original papers covering a broad area of research activities including experimental and hybrid techniques as well as analytical and numerical approaches. Engineering Transactions is a quarterly issued journal for researchers in academic and industrial communities.

Address of the Editorial Office:
Engineering Transactions
Institute of Fundamental Technological Research
Świętokrzyska 21,
PL 00-049 Warsaw, Poland

Phone: (48-22) 826 60 22, Fax: (48-22) 826 98 15, E-mail: publikac@ippt.gov.pl

Abstracted/indexed in:

Applied Mechanics Reviews, Current Mathematical Publications, Inspec, Mathematical Reviews, MathSci, Zentralblatt für Mathematik.

http://et.ippt.gov.pl/

SUBSCRIPTIONS

Address of the Editorial Office: Engineering Transactions
Institute of Fundamental Technological Research, Świętokrzyska 21
PL 00-049 Warsaw, Poland
Tel.: (48-22) 826 60 22, Fax: (48-22) 826 98 15, E-mail: publikac@ippt.gov.pl

Subscription orders for all journals edited by IFTR may be sent directly to the Editorial Office of the Institute of Fundamental Technological Research

Subscription rates

Annual subscription rate (2008) including postage is US $ 176.
Please transfer the subscription fee to our bank account: Payee: IPPT PAN,
Bank: PKO SA. IV O/Warszawa,
Account no. 05124010531111000004426875.

All journals edited by IFTR are available also through:

- Foreign Trade Enterprise ARS POLONA ul. Obrońców 25, 03-933 Warszawa, Poland, Tel. 4822 509 86 38, 509 86 37
- RUCH S.A. ul. Jana Kazimierza 31/33, 01-248 Warszawa, Poland, Tel. 4822 532 89 00, Fax 4822 532 87 45
- International Publishing Service Sp. z.o.o ul. Noakowskiego 10 lok. 38 00-664 Warszawa, Poland tel./fax: (48-22) 625 16 53, 625 49 55

Warunki prenumeraty

Prenumeratę na wszystkie czasopisma wydawane przez IPPT PAN prowadzi Biblioteka. Bieżące numery można nabyć a także zaprenumerować roczne wydanie Engineering Transactions bezpośrednio w Bibliotece IPPT PAN, Świętokrzyska 21, 00–049 Warszawa, Tel.: (48–22) 826 60 22; Fax: (48–22) 826 98 15.

Cena rocznej prenumeraty z bonifikatą (na rok 2008) dla krajowego odbiorcy wynosi 176 PLN Również można je nabyć, a także zamówić (przesyłka za zaliczeniem pocztowym) we Wzorcowni Ośrodka Rozpowszechniania Wydawnictw Naukowych PAN, 00-818 Warszawa, ul. Twarda 51/55, tel. (48–22) 697 88 35.

Wpłaty na prenumeratę przyjmują także jednostki kolportażowe RUCH S.A. Oddział Krajowej Dystrybucji Prasy, 01-248 Warszawa, ul. Jana Kazimierza 31/33, Konto: PBK.S.A. XIII Oddział Warszawa nr 68124010531111000004430494. Dostawa odbywa się pocztą zwykłą w ramach opłaconej prenumeraty z wyjątkiem zlecenia dostawy pocztą lotniczą, której koszt w pełni pokrywa zleceniodawca. Tel.: (48-22) 620 10 39, fax: (48-22) 620 17 62.

Arkuszy wydawniczych 9.75; Arkuszy drukarskich 7.75
Papier offset. kl. III 70 g. B1
Oddano do druku w sierpniu 2008 r. Druk ukończono we wrześniu 2008 r.
Skład w systemie LaTeX K. Jezierska
Druk i oprawa: Drukarnia Braci Grodzickich, Piaseczno ul. Geodetów 47A